REPORT No. 80

THIN AIRFOILS IN ROTATIONAL FLOW

DONALD R. KOTANSKY

September, 1965

GAS TURBINE LABORATORY
MASSACHUSETTS INSTITUTE OF TECHNOLOGY
CAMBRIDGE · 39 · MASSACHUSETTS

THIN AIRFOILS IN ROTATIONAL FLOW

by

DONALD R. KOTANSKY

Under the Sponsorship of:

General Electric Company
Allison Division of General Motors Corporation

GAS TURBINE LABORATORY

REPORT NO. 80

September 1965

MASSACHUSETTS INSTITUTE OF TECHNOLOGY
Cambridge, Massachusetts

ABSTRACT

The problem of rotational or shear flow about thin airfoils has been investigated theoretically and experimentally.

The theoretical approach is based on the concept of a lifting line in a bounded shear flow whose primary flow velocity profile may be expressed in terms of elementary linear, hyperbolic, and / or circular functions. The solution of the linearized equations of motion is reduced to the solution of a characteristic value problem whose form is dependent on the geometry of the primary flow. The characteristic value problem is solved for four different velocity profiles including that of a monotonic-matched linear profile (a layer of constant vorticity fluid bounded by layers of uniform flow) which serves as a model for the experimental shear flows.

The experimental work includes the measurement of local lift coefficients and spanwise lift distributions on thin symmetrical airfoils in monotonic shear flows for three values of the ratio of airfoil chord to shear layer thickness. The results of the lifting line theory show good agreement with the experimental data within the range of applicability, i.e. within the linear region of the C_L, α relationship and for flow geometries where the distortion (spanwise convection) of the surfaces of constant stagnation pressure is negligible.

The assumption that the local lift coefficient is a function only of the local angle of attack and the two-dimensional characteristic of the airfoil section (a fundamental assumption of lifting line theory) is investigated experimentally through a consideration of local pressure coefficient distributions. An approximate correction to the lifting line theory is suggested for flows in which the distortion of surfaces of constant stagnation pressure cannot be neglected.

ACKNOWLEDGEMENTS

I wish to express my sincere appreciation to my thesis supervisor, Professor William R. Hawthorne, Institute Professor at M. I. T. and Director of the University Engineering Laboratory at Cambridge University, who devoted a great deal of time and effort to see this project through to completion in spite of a busy trans-Atlantic schedule. His sincere interest in this work and in the progress of the investigator was a constant source of inspiration.

A special word of appreciation to Professor Edward S. Taylor, Director of the Gas Turbine Laboratory at M. I. T. who, in addition to providing financial support for the project and the investigator, contributed much to the project and to the author's 'self-education'. The continuing interest and contributions of Professor Erik L. Mollo-Christensen of the Department of Meteorology and Professor Alar Toomre of the Department of Mathematics at M. I. T. who served as members of the author's thesis committee are greatly appreciated.

This work was carried out with the day-to-day interest and advise of the members of the teaching and research staff of the Gas Turbine Laboratory. The technical assistance of Mr. Thorwald Christensen was particularly helpful, and the assistance of a number of undergraduate students, notably O. J. Birkestrand and Shridhar Shrimali is hereby acknowledged.

The manuscript was typed (and sometimes edited) by Mrs. Madelyn Euvrard who surmounted the innumerable equations during a busy summer session and still managed to find the time and energy to organize and prepare the GTL summer picnic.

The programmed computations were carried out with the assistance of the M. I. T. Computation Center's IBM 7094 digital computer.

TABLE OF CONTENTS

NOMENCLATURE

P = $P(x, y, z)$ = pressure

ρ = density

$\overline{V}$ = total velocity vector = $u'\hat{i} + v'\hat{j} + w'\hat{k}$

u' = $u'(x, y, z)$ = total velocity in x direction

v' = $v'(x, y, z)$ = total velocity in y direction

w' = $w'(x, y, z)$ = total velocity in z direction

$\overline{v}$ = perturbation velocity vector = $u\hat{i} + v\hat{j} + w\hat{k}$

u = $u(x, y, z)$ = perturbation velocity in x direction

v = $v(x, y, z)$ = perturbation velocity in y direction

w = $w(x, y, z)$ = perturbation velocity in z direction

U = $U(y)$ primary flow in x direction

U' = $\frac{d}{dy} U(y)$

ϕ = $\phi(x, y, z) = F(y)\, G(x, z)$ = Hawthorne's 'potential' function

F = $F(y)$ = separated function of y, Hawthorne's theory

G = $G(x, z)$ = separated function of x and z, Hawthorne's theory

Y = $Y(y) = F(y)\, U(y)$ = separated function of y, Honda's theory

ψ = $\frac{d}{dy} Y(y) = \frac{d}{dy} (FU)$; stream function

A = $A(x, y, z)$ = 'non-potential' component of u perturbation velocity, Hawthorne's theory

P_{KT} = $P_{KT}(y, z; k)$ = separated function of y and z, von Kármán and Tsien's theory

Λ_{KT} = $\Lambda_{KT}(y, z) = - P_{KT}(y, z; 0)$ = von Kármán and Tsien's potential function

P_H = $P_H(x, z)$ = separated function of x and z, Honda's theory

$\overline{\Omega}$ = total vorticity vector = $\xi\hat{i} + \eta\hat{j} + \zeta\hat{k}$

ξ = x component of vorticity

η = y component of vorticity

ζ = z component of vorticity

ℓ = span of airfoil = width of channel = $2t$

b = shear layer thickness = $2s$

d = depth of channel = $2D$

t = $\ell/2$

s = $b/2$ = shear layer half thickness

D = $d/2$

h = reference dimension in y direction

c = chord of airfoil

L = lift per unit span

α_o = geometrical angle of attack with respect to axis of zero lift

C_L = lift coefficient

C_{Lo} = two dimensional lift coefficient = (constant) α_o

AR = aspect ratio = ℓ/c

λ, k, β = eigenvalues, separation constants

Q = constant in series representation of ϕ

p, q, r = coefficients in general Sturm-Liouville problem, r = weighting function

C_p = pressure coefficient

C_{pp} = pressure coefficient on pressure side of airfoil

C_{ps} = pressure coefficient on suction side of airfoil

Γ = circulation

U_o = reference velocity at $y = 0$

Ω_o = slope of velocity profile at $y = 0$

K = parameter in velocity profile expression

k = constant in series representation of U'

Special Mathematical Symbols

U' = $\frac{d}{dy} U(y)$

ψ = $\frac{d}{dy} Y(y) = \frac{d}{dy} (FU)$

θ_n = $\lambda_n s$

μ = $s/t = b/\ell$; $1/y^*$

$\lambda_{(m/\mu)} = m\pi/\mu\ell$ = degenerate eigenvalue

$y^* = y/(b/2)$

$I(y) = \int_{-b/2}^{b/2} \frac{U'(q)dq}{(y-q)}$

$I_{(p)}(n) = \int_0^{\pi} \cos^p \phi \sin n\phi \, d\phi$

$\alpha(n) = I_{(0)}(n) - 6I_{(2)}(n) + 5I_{(4)}(n)$

$\beta(n) = I_{(2)}(n) - I_{(4)}(n)$

$\gamma(n) = I_{(0)}(n) - 9I_{(2)}(n) + 15I_{(4)}(n) - 7I_{(6)}(n)$

$\delta(n) = I_{(2)}(n) - 2I_{(4)}(n) + I_{(6)}(n)$

Subscripts

LL = lifting line x = 0, z = 0

OL = plane of lifting line x = 0

R = reference

T = Trefftz plane x = + ∞

TR = trailing

TEP = trailing edge-pressure side

TES = trailing edge- suction side

m = integer index

n = summation index, eigenvalue index

o = reference, origin y = 0

0 = (0) region of shear flow

1 = (1) region of shear flow

2 = (2) region of shear flow

THIN AIRFOILS IN ROTATIONAL FLOW

by

Donald R. Kotansky

1. INTRODUCTION

Many problems of aerodynamic design of turbo-machinery arise due to the lack of understanding of the complex three-dimensional flows found in these machines. The design engineer's approach to the problem is guided by extensive literature in the field of fluid mechanics in general and by more specialized information closely related to the turbo-design problem. Much useful information can be found in applications of boundary layer theory, investigations of separation and stall phenomena, studies of skewed boundary layer effects and other problems peculiar to the turbo-machine, but in many cases past experience and 'rules of thumb' are the deciding design factors. The theoretical methods of attack are sometimes limited because serious restrictions or over-simplifications are required to yield solutions at all, and it follows that the practical usefulness of such analyses is sometimes limited.

A somewhat closer approach to the actual situation can sometimes be made by the general theory of secondary flows. Applications of this theory to the problems of flow in turbo-machinery require simplifications, as with other theoretical approaches, but the 'three-dimensionality' of this approach suits it well to some of these problems.

A particular problem of interest in this area is that of the effects of vorticity or 'shear' on the flows about lifting airfoils. Flows of this type are characteristic of axial turbo-machinery since in these machines the velocity profile often develops a gradient of stagnation pressure through the action of viscous forces or the non-uniformity of work distributions. The study of rotational flows about airfoils is not intended to model the actual internal flow in a turbo-machine (where a cascade would be a more appropriate model) but to gain a fundamental understanding of the nature of the three-

dimensional flow involved. Work in this area has been undertaken by previous investigators in various forms, the bulk of this being of an analytical nature on the theory of shear flows in general and not always directly applicable to the airfoil problem. One of the earliest, and perhaps one of the most enlightening contributions to the airfoil problem is the theoretical work of T. von Kármán and H. S. Tsien[1] in which Prandtl's lifting line theory (a three-dimensional theory for a wing of finite span in a uniform flow) was extended to the more general case of a rotational primary flow. The fruits of this work have remained more or less unharvested probably because of the relative simplicity of the lifting line concept as opposed to the more sophisticated approach offered through thin airfoil or lifting surface theories. An important contribution in the realm of thin airfoil theory is that of M. Honda[2] who succeeded in obtaining theoretical results for the case of a thin airfoil in a linear shear flow bounded by two parallel walls. As might be expected, the two approaches are related through the assumption of a known rotational primary flow and the linearization of the equations of motion in accordance with the assumption of small disturbances.

The fundamental motivation for this research may be described through two primary objectives.

1) To synthesize from existing fundamental contributions and additional theoretical work a useful theory that can be applied to the problem of a thin airfoil in a shear flow without exhaustive mathematical complications.

2) To obtain experimental data on the performance of a thin airfoil in a shear flow that can be modeled analytically with a minimum of complications due to real fluid effects, i.e. viscous shear forces, separation, and stall.

A third implied objective is that of reasonable agreement of theory with experiment.

To illustrate the complicated nature of this shear flow problem, the

three-dimensional effects resulting from the rotational flow of a fluid (in this case atmospheric air) about a circular cylinder are shown on the following page. The flow is from left to right, the velocity variation approximately 1.5 to 1 across a shear layer bounded by two uniform layers adjacent to the boundary walls of the duct. The first photograph shows the pronounced vertical displacement of the streamline in the plane of symmetry of the cylinder, and, in addition, the warping of the surfaces of constant stagnation pressure or 'Bernoulli surfaces' in the flow about the cylinder. The second photograph indicates the magnitude of the displacement effect in the neighborhood of the disturbance. The secondary flows in this case are produced by pressure gradients in the essentially inviscid regions of the flow, i.e. away from solid boundaries. The secondary flows are not confined to 'boundary layer regions' although the shear flows required to produce them may have been formed as a result of the action of viscous forces upstream of the region of the disturbance. Of course, there are boundary layer interactions with the secondary flows and significant viscous effects, especially in the case of a cylinder where downstream separation is present. The remainder of this work will be concerned for the most part with small disturbances to parallel shear flows - not of the relative magnitudes indicated in the photographs. The 'large disturbance' in this case indicates the qualitative behaviour of these secondary flows.

The term secondary flow, as usually associated with rotational flows, is here interpreted to consist of those first and higher order corrections to a selected primary flow (which may or may not be rotational) as described mathematically through an appropriate approximation technique. The development of the inviscid theory of secondary flows has followed two general analytical approaches:

1) disturbances are small and the equations of motion may be linearized with respect to a known primary flow

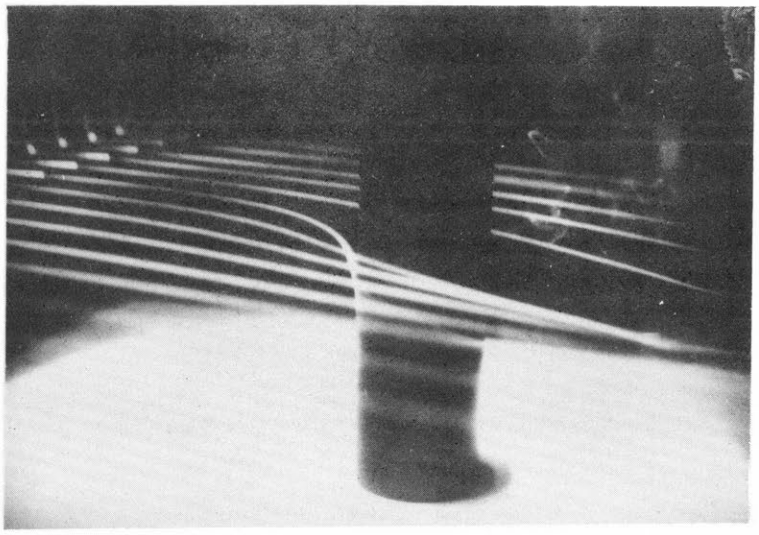

DISTORTION OF BERNOULLI SURFACE

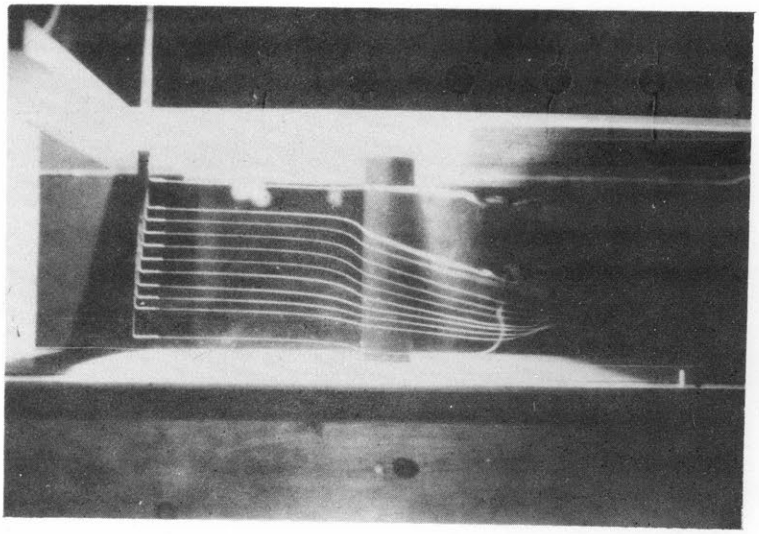

DISPLACEMENT EFFECT

FIGURE I ROTATIONAL FLOW
ABOUT A CYLINDER

2) vorticity is small and is convected by an associated primary flow

Various methods of approximation and means for their solution are discussed in detail by Hawthorne[3].

The general problem of shear flow has received considerable attention in the past, beginning largely with the work of Squire and Winter[4] who derived analytical results for the development of streamwise vorticity when an inviscid fluid with an initial velocity gradient is turned in a bend. Squire and Winter's work was directed at shear flow in cascades through a 'bend' or 'passage' approach.

A theoretical approach to secondary flows was developed by Hawthorne[5] who derived an integral expression for the development of streamwise vorticity along a streamline in a rotational flow. Experimental work on secondary flows in bends was carried out by Eichenberger[6] which showed agreement with Hawthorne's theory. Hawthorne's theory was later applied to a cascade of airfoils[7] and the theory verified experimentally in the work of Hawthorne and Armstrong[8]. An inviscid theory for shear flows about non-lifting struts and airfoils was developed by Hawthorne[9] and the theory investigated experimentally by Ling[10]. In this approach, the amount of distortion of the Bernoulli surfaces is assumed to be negligibly small and the primary flow considered is a two-dimensional potential flow.

Some exact solutions of the incompressible and inviscid equations of motion for rotational flows about bodies have been obtained for the two-dimensional case, but these solutions are somewhat restrictive in that a particular distribution of vorticity or constant vorticity is required in the undisturbed flow. Examples of solutions of this type are given by Tsien[11], James[12], Jones[13], and Murray and Mitchell[14].

It is easy to verify that in a two-dimensional flow with only one component of vorticity that this vorticity ζ is given by

$$\nabla^2\psi = -\zeta \tag{1-1}$$

where ψ is the familiar stream function. From the Helmholtz equation for steady flow

$$(\bar{V} \cdot \nabla)\,\bar{\Omega} = (\bar{\Omega} \cdot \nabla)\,\bar{V} \tag{1-2}$$

we see that in the two-dimensional case, ζ is constant along any streamline. If we then require that the undisturbed flow be of uniform vorticity, i.e. ζ does not change from streamline to streamline, then ζ is everywhere constant, and we require a solution of Poisson's equation.

$$\nabla^2\psi = -\zeta_o \tag{1-3}$$

Let the velocity in the x direction far from the disturbance be expressed by

$$u' = U_o - \zeta_o\, y \tag{1-4}$$

Then ψ_o of the undisturbed flow is given by

$$\psi_o = U_o\, y - \zeta_o\, y^2/2 \tag{1-5}$$

Let $$\psi = \psi_o + \psi_1 \tag{1-6}$$

and substituting in (1-3),

$$\nabla^2\psi_1 = 0 \tag{1-7}$$

Therefore any solution of Laplace's equation and (1-5) will satisfy equation (1-3). Tsien[11] used this method to study the shear flow about Joukowski airfoils.

Another exact solution, but not one of constant vorticity, is that of Murray and Mitchell[14]. With equations (1-1) and (1-2), if it is assumed that ζ, which is constant along a streamline, is a function of ψ, which is also constant along a streamline, then from (1-1)

$$\nabla^2\psi = -f(\psi) \tag{1-8}$$

Murray and Mitchell then assumed $f(\psi) = \pm\, \psi/a^2$, where a is an arbitrary dimension of the disturbance. They then let $\psi = \psi_o + \psi_1$ where ψ_1 vanishes far from the disturbance. The undisturbed stream function ψ_o then resulted in sinusoidal or hyperbolic velocity distributions in the undisturbed flow

depending on the sign of f; the disturbance stream function ψ_1 was determined by the equation

$$\nabla^2\psi_1 = \mp \psi_1/a^2 \qquad (1\text{-}9)$$

The fundamental differences between the above solutions and so-called secondary flow solutions are that no stretching of deformation of the vortex lines appears in the two-dimensional solutions although in a mathematical sense they are not approximations.

The initial work of Hawthorne[5] was extended to the case of compressible flows which introduces the effects of density stratification and instability (see Hawthorne[15]). Smith[16] extended Hawthorne's work on the generation of streamwise vorticity in an incompressible and frictionless fluid to that of a rotating passage for application to flows in rotating turbomachinery. Other theoretical contributions are those of Smith[17], who considers secondary flows in cascades with special application to turbomachinery, and the work of Dean[18], who investigates the behavior of secondary flows in axial compressors. Dean's work was based in part on the experimental work of Van Le[19]. Van Le approached the problem theoretically through the linearization technique which he then applied to cascades with small turning. A rather comprehensive study of secondary flow and associated losses in a compressor cascade is given by Soderberg[20], who confirmed his theoretical work with experimental findings.

Another interesting approach to the theory of secondary flow from the 'convection' standpoint is that of Lighthill[21], who utilized a theory of Darwin[22], concerning the permanent deformation of fluid lines or surfaces in the irrotational flow of a frictionless fluid past an obstacle. Lighthill proposed that vortex lines, which are known to be identified with particular fluid particles, are stretched in the flow about the body in the same manner as Darwin's 'drift' surfaces. Using this concept and the supposition that the vorticity is weak, such that the resulting secondary flows themselves do

not stretch these lines of vorticity to a significant amount, Lighthill studied the flow about cylindrical bodies and a sphere in weakly sheared flow.

Hall[23] analyzed the shear flow about a sphere in a study of the pitot tube displacement effect and showed that the three-dimensional theory predicted the correct order of displacement based on experimental data where it is known that the two-dimensional theory falls short of this. The discrepancy between the two theories is attributed to the inadequacy of the two-dimensional theory to model the physical situation in which the stretching of vortex lines must be taken into consideration. Hall's analysis determines the displacement effect in the plane of symmetry of the flow assuming that the shear is small. The stretching of the vortex lines is determined by successive approximations to include the additional stretching caused by the induced secondary velocities. Lighthill[24] analyzed the displacement effect problem in a later paper through the use of his earlier work (Lighthill[21]) and compares his findings with those of Hall.

Lighthill[25] analyzed the effect of a small disturbance on a weakly sheared flow utilizing the small disturbance-linearization technique. The disturbance in this case was a 'weak' source. Lighthill concludes that the small disturbance approximation is valid far from the disturbance while the convection solution is valid near it.

The results of the above investigation have been applied, for the most part, to the solution of three classes of problems

1) the secondary flows in bends, channels, and cascades
2) the secondary flows about struts and airfoils
3) the pitot tube displacement effect

The last of these refers to the correction necessary for the measurement of total pressure when a pitot tube is inserted in a shear layer.

The theoretical approach followed in this investigation is based on the fundamental analysis of Hawthorne[3] which is dependent on the solution of a

second order partial differential equation of the form

$$\nabla^2\phi(x, y, z) + \left[\frac{U''}{U} - 2\left(\frac{U'}{U}\right)^2\right]\phi(x, y, z) = 0 \qquad (1\text{-}10)$$

The solution of this equation for ϕ is, of course, largely dependent on the distribution of velocity in the primary flow U(y), and, in addition, the geometry of the disturbance, although geometry (especially thickness) is not considered directly in the lifting line approach. The equation for ϕ reduces to the familiar Laplace equation for the case of uniform flow and indicates the existence of potential perturbations in this case. The solution of the equation in the case of a rotational primary flow results in rotational perturbations. In addition to Hawthorne's work, the analysis draws on the work of von Kármán and Tsien[1] and to a lesser degree on that of Honda[2].

The essentials of the resulting analysis, hereafter referred to as the lifting line theory, and a comparison of the theoretical results with selected experimental data are given in Section 2.

Section 3 contains a detailed exposition of the lifting line theory in which the analytical solutions for four different shear velocity profiles are obtained. These velocity profiles are shown in the following sketch.

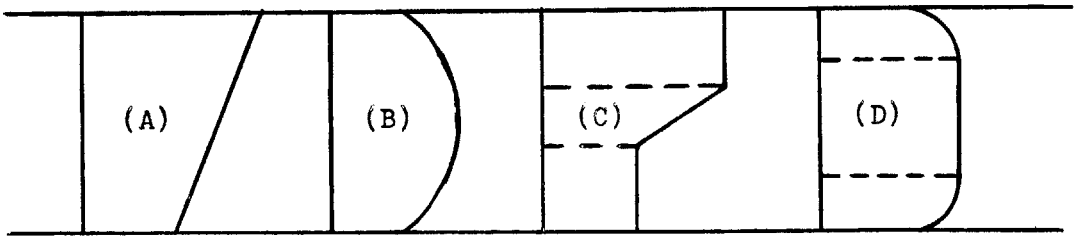

Perhaps the most useful and interesting of these velocity profiles in a practical sense is that of case (D) which is intended to model a region of uniform flow bounded by shear layers representing wall boundary layers. Profile (C) was selected to model the experimental shear layer in which the layer of rotational flow was bounded by two layers of uniform flow.

Section 4 is devoted to what is termed 'a first theoretical approximation' which is related in concept to ordinary lifting line theory. In this

approximation, no attempt is made to satisfy the complete system of linearized equations of motion; the induced secondary flows are determined through a consideration of the strength of the trailing vortex sheet in the 'wake' of the airfoil alone.

Section 5 consists of a presentation of the experimental work which consists largely of measured values of local lift coefficients and spanwise distributions of lift for thin symmetrical airfoils (NACA 0012) in what may be termed monotonic shear flows of the type described above (profile (C)). The tests were performed for three different ratios of airfoil chord to shear layer thickness (c/2s) in a low speed wind tunnel. The artificial shear flows were generated through the use of a honeycomb structure inserted in the tunnel upstream of the test section.

A comparison of theoretical results with experimental data and the discussion of this and other aspects of the work is presented in Section 6. This section also contains the conclusions and recommendations for further study.

The curves indicating the comparison between the lifting line theory, as well as the first theoretical approximation,with the experimental results are presented in Appendix I. Included in the comparison is the data of Mendelsohn and Polhamus[26]. A spectrum of analytical results computed for shear velocity profiles of the types (A), (B), and (D) is presented in Appendix III. Appendix IV is devoted to a discussion of the design of the honeycomb used for the generation of the shear flows in the experimental work.

2. ESSENTIALS OF ANALYSIS

The purpose of this section is to present the lifting line theory in condensed form. A comparison of the results of the theory with experimental data on the predicted and measured distributions of lift on a thin symmetrical airfoil in a monotonic shear flow is included. The analysis is based on the fundamental works of T. von Kármán and H. S. Tsien[1], M. Honda[2], and W. R. Hawthorne[3].

The problem considered is that of a thin airfoil in a steady, frictionless, and incompressible shear flow. The flow is bounded in the spanwise or 'y' direction by parallel walls and provision is made for bounding in the 'z' direction normal to the plane of the airfoil.

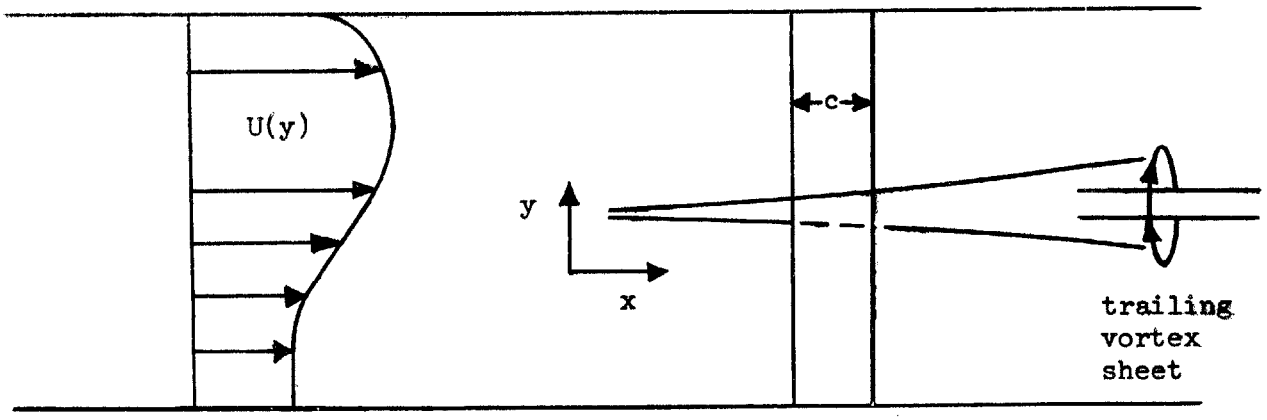

The theory is based on the concept of a lifting line[1] and is restricted here to the case of airfoils of fixed chord and constant geometrical angle of attack.

2.1 Hawthorne's Linearized Theory

Hawthorne[3] has investigated the solution of the linearized equations of motion for small disturbances to a parallel shear flow which is selected as the primary flow U(y). The results of the linearization and the assumption of a particular form to represent the perturbation velocity vector is a second order partial differential equation in $\phi(x, y, z)$ where ϕ represents a type of 'potential' function for rotational flows. The Euler equations of

motion may be expressed in vector form as follows:

$$\left[(U(y)\,\mathbf{i} + \bar{v}) \cdot \nabla\right](U(y)\,\mathbf{i} + \bar{v}) = -\frac{1}{\rho}\nabla P \qquad (2\text{-}1)$$

If U is taken to be of order 1 and the disturbance velocities to be of order δ, the terms of order δ^2 may be assumed negligible, i.e.

$$(\bar{v} \cdot \nabla)\bar{v} \qquad 0 \qquad (\delta^2) \to 0 \qquad (2\text{-}2)$$

Using equation (2-2) and taking the curl of equation (2-1) to eliminate pressure, the following result is obtained

$$\frac{\partial}{\partial x}\left[\nabla x(U\bar{v})\right] = \left[\hat{k}\frac{\partial}{\partial y} - \hat{j}\frac{\partial}{\partial z}\right](U'\,v) \qquad (2\text{-}3)$$

where U' denotes $\frac{d}{dy}(U(y))$. Hawthorne selects the following form for the perturbation velocity vector

$$U\bar{v} = \nabla(U\phi) + \mathbf{i}\,U\,A(x, y, z) \qquad (2\text{-}4)$$

For this choice of $U\bar{v}$, equations (2-3) become simply

$$\frac{\partial A}{\partial x} = -\frac{U'}{U}v \qquad (2\text{-}5)$$

The corresponding perturbation velocity components from (2-4) are

$$u = \frac{\partial \phi}{\partial x} + A \qquad (2\text{-}6)$$

$$v = \frac{\partial \phi}{\partial y} + \frac{U'}{U}\phi \qquad (2\text{-}7)$$

$$w = \frac{\partial \phi}{\partial z} \qquad (2\text{-}8)$$

If equations (2-6) through (2-8) are substituted into the continuity equation

$$\nabla \cdot (U\,\mathbf{i} + \bar{v}) = 0 \qquad (2\text{-}9)$$

we have the desired result (using equation (2-5))

$$\nabla^2\phi + \left[\frac{U''}{U} - 2\left(\frac{U'}{U}\right)^2\right]\phi = 0 \qquad (2\text{-}10)$$

We note that the above results are dependent on the requirement that $|u_i| << |U|$; therefore, the magnitude of U cannot approach zero, nor can there be any stagnation points in the flow about the disturbance. The usefulness of the result (2-10) is evidenced through the ease by which the per-

turbation velocity components may be derived from ϕ and the scalars U and A.

2.2 Von Kármán and Tsien's Lifting Line Theory

In their analysis of the lifting line theory for a wing in a non-uniform flow, von Kármán and Tsien[1] worked with the linearized pressure equation and noted that the fundamental solutions of that equation for the boundary conditions of undisturbed pressure at $x = \pm \infty$ require that P be an even function of x. The relation

$$\phi(x, y, z) = -\frac{1}{\rho U} \int_{-\infty}^{x} P(x, y, z)\, dx$$

which relates Hawthorne's ϕ function to the static pressure indicates, in turn, that ϕ is an odd function of x. We can then conclude from equations (2-7) and (2-8) that the perturbation velocity components v(x, y, z) and w(x, y, z) which are required to vanish at $x = -\infty$ are themselves odd functions of x and we can write the following:

$$v(0, y, z) = 1/2\ v(\infty, y, z) = 1/2\ v_T(y, z) \qquad (2\text{-}11)$$

$$w(0, y, z) = 1/2\ w(\infty, y, z) = 1/2\ w_T(y, z) \qquad (2\text{-}12)$$

The above equations, relating the magnitudes of the perturbation velocities downstream of the disturbance at $x = +\infty$ (the Trefftz plane) to those at the disturbance x = 0 constitute the 'Trefftz plane approximation' for a rotational flow of this type.

2.3 Fundamental Solutions of the ϕ Equation

To facilitate the solution of equation (2-10) the following variables are introduced:

$$\phi(x, y, z) = F(y)\, G(x, z) \qquad (2\text{-}13a)$$

$$\psi(y) = \frac{d}{dy}(FU) \qquad (2\text{-}13b)$$

We then consider a higher order form of equation (2-10)

$$\frac{\partial}{\partial y}\left\{ U\nabla^2\phi + U\phi\left[\frac{U''}{U} - 2\left(\frac{U'}{U}\right)^2\right]\right\} = 0$$

which is, in terms of the v perturbation velocity component,

$$U\nabla^2 v = U''v \tag{2-14}$$

The fundamental solutions of equation (2-14) include those of equation (2-10) plus an additional solution introduced by the additional differentiation. We have from equations (2-7), (2-13a), and (2-13b)

$$v = G(x, z)\,\frac{\psi}{U}$$

Substituting this for v into equation (2-14) and choosing λ^2 as the separation constant for the function G(x, z), we have the following result:

$$\frac{d^2}{dy^2}\left(\frac{\psi}{U}\right) + \left(\frac{\psi}{U}\right)\left[\lambda^2 - \frac{U''}{U}\right] = 0 \tag{2-15}$$

and

$$\nabla^2 G(x, z) = \lambda^2 G(x, z) \tag{2-16}$$

We can now write the solutions of (2-15) for velocity profiles in which $U''/U = \beta^2 = \text{constant}$.

$$\frac{\psi}{U} = C_1 \sin \sigma y + C_2 \cos \sigma y$$

where we define $\sigma = \sqrt{\lambda^2 - \beta^2}$ for real values only. The desired fundamental solutions for F(y) are then, using (2-13b),

$$F(y) = \frac{C_1 \int U \sin \sigma y\, dy}{U} + \frac{C_2 \int U \cos \sigma y\, dy}{U} \tag{2-17}$$

We have eliminated a third solution $F(y) = C_3/U$ in order to satisfy the ϕ equation (2-10). The requirement adopted here that $U''/U = \beta^2$ limits the solution (2-17) to shear velocity profiles expressible as elementary linear, hyperbolic, and circular functions of 'y', but this is not a serious restriction, since a variety of useful shear profiles can be selected satisfying this requirement.

In a lifting line approach to this rotational flow problem, the desired quantity is the w component of velocity at the lifting line. Through the use of the Trefftz plane approximation we are able to consider solutions of equation (2-16) downstream of the disturbance at $x = +\infty$. We then define

$$G_T(z) = -\frac{1}{\rho UF} \lim_{x\to\infty} \int_{-\infty}^{x} P(x, y, z)\, dx$$

and equation (2-16) becomes

$$\frac{d^2}{dz^2} G_T(z) = \lambda^2 G_T(z)$$

whose general solutions are simply

$$G_T(z) = C_1 \cosh \lambda z + C_2 \sinh \lambda z \qquad (2\text{-}18)$$

2.4 General Lifting Line Solution

The general solution for $\phi(x, y, z)$ may be expressed as the infinite sum of the eigensolutions $F_n(y)\, G_n(x, z)$. We now consider the limiting case of $\phi_T(y, z)$ which may be expressed in the following form

$$\phi_T(y, z) = \sum_{n=1}^{\infty} Q(\lambda_n)\, F_n(y)\, G_{Tn}(z) \qquad (2\text{-}19)$$

The $F_n(y)$ are linear combinations of the appropriate fundamental solutions of equation (2-15). The eigenvalues λ_n are determined in accordance with the boundary conditions that $v = 0$ at the boundary walls in the 'y' direction and the requirement that v and P be continuous in y throughout the flow. The functions $G_{Tn}(z)$ in equation (2-19) are of the form given in equation (2-18) with the boundary condition that the w component of velocity be zero at the boundaries in the 'z' direction.

To determine the unique solution, we must relate $\phi_T(y, z)$ to the strength of the disturbance at the lifting line. In accordance with the assumptions of von Kármán and Tsien[1], the spanwise velocities which constitude the trailing vortex sheet at $z = 0^{\pm}$ are equal and opposite. We then relate the strength of the trailing vortex sheet to the spanwise gradient of lift on the lifting line, i.e.

$$\frac{1}{\rho U} \frac{dL(y)}{dy} = v_T(y, 0^+) - v_T(y, 0^-)$$

From this and the relationship between the spanwise velocities, we have the result

$$v_T(y, 0^{\pm}) = \pm \frac{1}{2} \frac{1}{\rho U} \frac{dL(y)}{dy} \qquad (2\text{-}20)$$

We then write L(y) in terms of the usual thin airfoil notation

$$L(y) = \frac{1}{2} \rho U^2 c C_L = \pi \rho c U^2 (\alpha_o + w_{LL}/U) \tag{2-21}$$

where c is the chord of the airfoil, and α_o is the geometrical angle of attack. The relationship between L(y), $U^2(y)$, and the corrected angle of attack $(\alpha_o + w_{LL}/U)$ assumes that the lift on a thin airfoil in a shear flow at a geometrical angle of attack α_o is the same as the lift that would be experienced by the airfoil in a corresponding uniform flow U at an angle of attack $(\alpha_o + w_{LL}/U)$. This is a reasonable assumption in accordance with the small disturbance approximation provided that the secondary flows do not distort the surfaces of constant stagnation pressure to any significant amount. The limit of the applicability of this approximation is, of course, dependent on the specific geometry of the problem considered, but, in a general sense, this effect is related to a parameter $\alpha_o cU'/U$ which will here be assumed sufficiently small to render the distortion of the Bernoulli surfaces negligible.

We can, after manipulation of the above equations, arrive at the following expression for $Q(\lambda_n)$ in equation (2-19):

$$\sum_{n=1}^{\infty} Q^{\pm}(\lambda_n) \frac{1}{U^2} \frac{d}{dy} (UF_n(y)) \left[G_{Tn}(0^{\pm}) \mp \frac{\pi c}{4} \frac{\partial}{\partial z} G_{Tn}(0^{\pm}) \right] = \pm \pi \alpha_o cU'/U \tag{2-22}$$

The solution of equation (2-22) requires the use of the orthogonal properties of the functions $\frac{d}{dy} (F_n U)$ with respect to the weighting function $1/U^2$. It can be established that if U(y) is continuous and the eigenfunctions $F_n(y)$ are determined in accordance with the appropriate boundary conditions, the following result is valid:

$$(\lambda_m^2 - \lambda_n^2) \int_{\ell_1}^{\ell_2} \frac{d}{dy} (F_m U) \frac{d}{dy} (F_n U) U^{-2} \, dy = 0 \tag{2-23}$$

We have purposely allowed for discontinuities in U' and higher derivatives of U in that primary flows in which these derivatives are not continuous may be treated by matching the eigenfunctions $F_n(y)$ in corresponding regions of the flow. The limits of the integral in equation (2-23) are the ordinates

of the bounded region in the 'y' direction.

Using the result (2-23), equation (2-22) may be solved for the constant $Q(\lambda_n)$. For convenience, a change in the two-dimensional lift coefficient C_{Lo} is here denoted by ΔC_{Lo}, and we can write

$$\frac{\Delta C_{Lo}}{C_{Lo}} = \frac{w_{LL}}{U\alpha_o} = \frac{1}{2U\alpha_o}\frac{\partial}{\partial z}\phi_T(y, 0^{\pm}) \tag{2-24}$$

using equations (2-8) and (2-12).

2.5 Solution for Arbitrary U(y)

If we now consider the flow to be bounded in the 'z' direction by parallel walls at $z = \pm D$, the requirement that w vanish at the walls is, from equation (2-8),

$$\frac{d}{dz} G_{Tn}(\pm D) = 0 \tag{2-25}$$

Using this requirement and equation (2-18) we have the result

$$\left[G_{Tn}(0^{\pm}) \mp \frac{\pi c}{4}\frac{\partial}{\partial z} G_{Tn}(0^{\pm}) \right] = 1 + \frac{\pi c \lambda_n}{4} \tanh \lambda_n D \tag{2-26}$$

The final form of the desired solution for $\Delta C_{Lo}/C_{Lo}$ may be written from equations (2-18), (2-19), (2-24), and (2-25)

$$\frac{\Delta C_{Lo}}{C_{Lo}} = \frac{\mp 1}{2U\alpha_o} \sum_{n=1}^{\infty} Q^{\pm}(\lambda_n)\, F_n(y)\, \lambda_n \tanh \lambda_n D \tag{2-27}$$

If equation (2-22) is solved for $Q^{\pm}(\lambda_n)$ using (2-23) and (2-26), and the result is substituted into equation (2-27), the following result is obtained:

$$\frac{\Delta C_{Lo}}{C_{Lo}} = -2 \sum_{n=1}^{\infty} \frac{\int_{\ell_1}^{\ell_2} \frac{U'}{U}\frac{d}{dy}(F_n U)\, dy \left[\frac{F_n(y)}{U(y)}\right]}{\int_{\ell_1}^{\ell_2} \left[\frac{d}{dy}(F_n U)\right]^2 \frac{1}{U^2}\, dy \left[1 + \frac{1}{\frac{\pi\lambda_n c}{4} \tanh \lambda_n D}\right]} \tag{2-28}$$

Equation (2-28) is the general form of the lifting line solution for an arbitrary primary flow U(y). The above result is valid for all velocity profiles in which U(y) is continuous and sufficiently greater than zero. The evaluation of the integrals in equation (2-28) is greatly simplified when

the eigenfunctions are forms of equation (2-17).

The form of equation (2-28) for shear flows unbounded in the 'z' direction is obtained by setting the term $\tanh \lambda_n D = 1$.

2.6 Comparison of Theory with Experiment

The results of the lifting line theory will be compared with experimental measurements of spanwise distributions of lift on a thin symmetrical airfoil in an artificial shear flow. The measurements were performed in a low speed wind tunnel with a 20" x 30" test section. The airfoil used was NACA 0012 with a 3" chord and a span of 30". Trip wires (0.006" diam.) were attached to the airfoil at 10% chord to assure the formation of turbulent boundary layers because of the low Reynolds number of the experiments.

The experimental shear flow was modeled theoretically by a layer of constant vorticity flow between two layers of uniform flow all bounded by the walls of the test section. The velocity variation across the shear layer was from 69 ft/sec to 109 ft/sec in a spanwise distance of approximately 4 inches. The geometry of the flow is indicated in the following sketch:

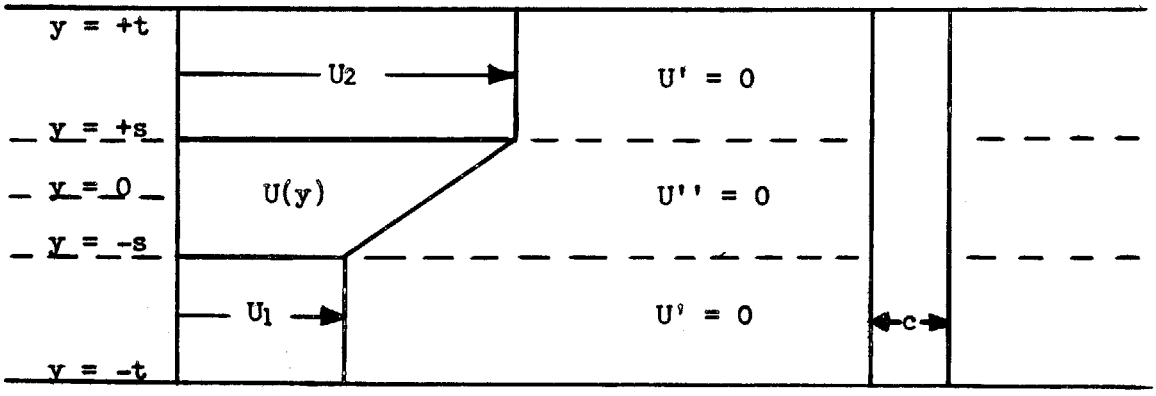

The eigenfunctions, from equation (2-17) with $\beta^2 = 0$ since $U'' = 0$ in this case, are of the following forms:

$$F(y) = C_1 \left[\cos \lambda y - \frac{U' \sin \lambda y}{\lambda U(y)} \right] + C_2 \left[\sin \lambda y + \frac{U' \cos \lambda y}{\lambda U(y)} \right]$$

for the constant vorticity layer, and

$$F(y) = C_1 \cos \lambda y + C_2 \sin \lambda y$$

for the uniform layers where U' = 0. The matching of the above eigenfunctions at the boundaries of the three regions of the flow and the boundary conditions at the walls (y = ±t) constitute a system of six algebraic equations whose solution determines the constants in the eigenfunctions (in terms of an arbitrary constant) and the characteristic equation for the determination of the eigenvalues λ_n. The characteristic equation is of the following form:

$$\theta_n^2 \sin\left(\frac{2\theta_n}{\mu}\right) = \frac{(U_2 - U_1)^2}{4U_2U_1}\left[\theta_n\left(\cos\left(\frac{2\theta_n}{\mu}\right) - \cos 2\theta_n\right) + \sin 2\theta_n \sin^2\left(\frac{1}{\mu} - 1\right)\theta_n\right] \tag{2-29}$$

where $\theta_n = \lambda_n s$ and $\mu = s/t$

The above equation can be shown to have degenerate solutions for which the corresponding eigenfunctions change form, but, in general, this difficulty presents no major problem since in many cases, the degenerate solutions of equation (2-28) are trivial. The number of eigensolutions required for reasonable convergence is dependent on the ratio s/t; no solution of this form exists for the limiting case of s/t = 0.

The integrals in equation (2-28) may be evaluated through the use of the appropriate eigenfunctions and corresponding U(y) for the three regions of the flow. The limits of the integral in the numerator of (2-28) become simply (-s) to (+s) in this case since U' = 0 outside of this region.

The comparison of the theoretical results for the first 30 eigenvalues with the experimental distributions of U^2C_L for two different geometrical angles of attack is presented in Figure 2 on page 20. The theoretical result is obtained by calculating $U^2(1 + \Delta C_{Lo}/C_{Lo})$ from the theoretical model of the shear velocity profile and equation (2-28) and multiplying this by C_{Lo} as determined from experimental data on the performance of the airfoil in a uniform flow. The dotted curves in Figure 2 are theoretical values of U^2 multiplied by the experimental value of C_{Lo} which forms the basis of a crude 'two-dimensional' approximation.

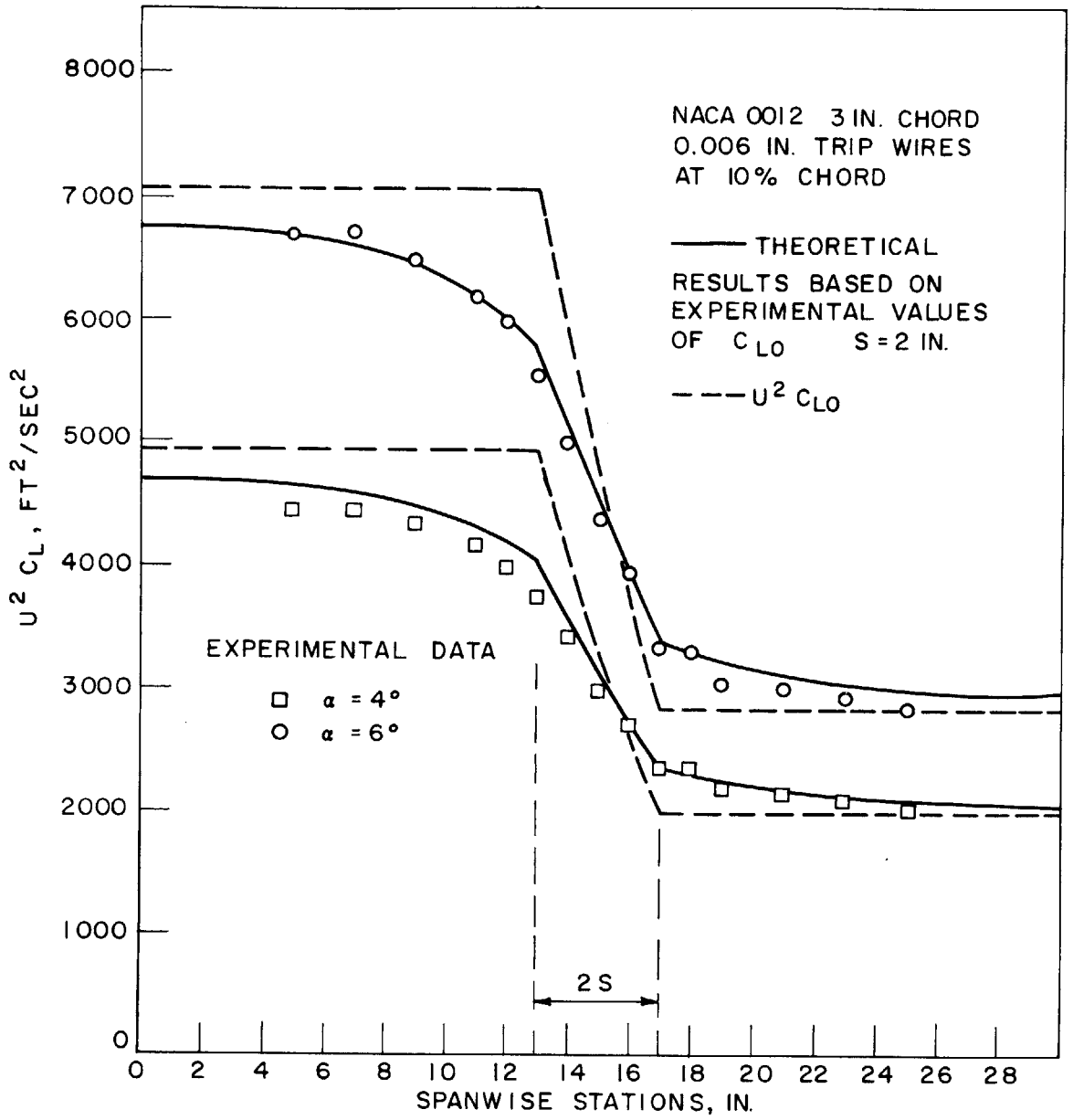

FIGURE 2 COMPARISON OF EXPERIMENTAL AND THEORETICAL DISTRIBUTIONS OF U^2C_L

3. LIFTING LINE THEORY FOR A THIN AIRFOIL IN A STEADY BOUNDED SHEAR FLOW

The following development provides a method of determining the lift on a thin airfoil in a steady shear flow bounded by a rectangular channel. The desired result is achieved through the application of fundamental theoretical results obtained by T. von Kármán and H. S. Tsien[1], M. Honda[2], and W. R. Hawthorne[3]. The fundamental notation is conventional and applies to a major portion of the above works, but in some cases the original notation has been changed to avoid ambiguity.

The geometry of the flow is described in the following sketch:

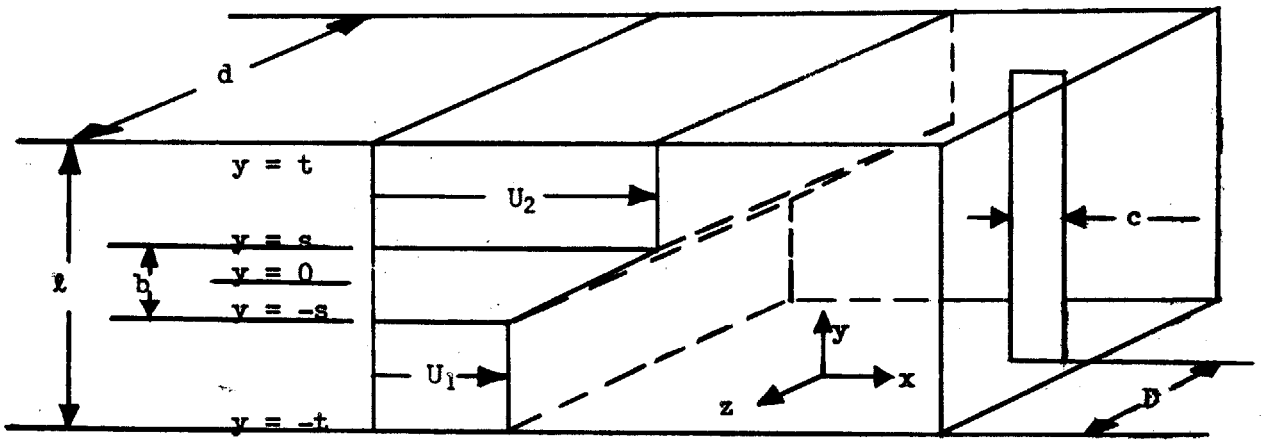

3.1 Hawthorne's Linearized Theory

If we write the vector velocity of a fluid in a Cartesian system in the form

$$\overline{V} = u'\hat{i} + v'\hat{j} + w'\hat{k} \tag{3-1}$$

the Euler equations of motion for a frictionless and incompressible fluid become

$$u' \frac{\partial u'}{\partial x} + v' \frac{\partial u'}{\partial y} + w' \frac{\partial u'}{\partial z} = - \frac{1}{\rho} \frac{\partial P}{\partial x} \tag{3-2}$$

$$u' \frac{\partial v'}{\partial x} + v' \frac{\partial v'}{\partial y} + w' \frac{\partial v'}{\partial z} = - \frac{1}{\rho} \frac{\partial P}{\partial y} \tag{3-3}$$

$$u' \frac{\partial w'}{\partial x} + v' \frac{\partial w'}{\partial y} + w' \frac{\partial w'}{\partial z} = - \frac{1}{\rho} \frac{\partial P}{\partial z} \tag{3-4}$$

and the continuity equation becomes

$$\nabla \circ \overline{V} = \frac{\partial u'}{\partial x} + \frac{\partial v'}{\partial y} + \frac{\partial w'}{\partial z} = 0 \qquad (3\text{-}5)$$

Consider a parallel shear flow far from a small disturbance which is located at the origin of our coordinate system. Let the direction of the flow be in the positive x direction and the velocity gradient of the shear flow be in the y direction parallel to the axis of the disturbance. The vorticity vectors then lie in the z direction perpendicular to the axis of the disturbance. Since $\overline{V}$ is directed in the x direction and varies only with y far from the disturbance, we can write

$$\overline{V} \Big|_{x = -\infty} = U(y)\hat{\imath} \qquad (3\text{-}6)$$

Now if the disturbance is small, we can write

$$\overline{V}(x, y, z) = U(y)\ \hat{\imath} + \overline{v}(x, y, z) \qquad (3\text{-}7)$$

where

$$\overline{v}(x, y, z) = u(x, y, z)\ \hat{\imath} + v(x, y, z)\ \hat{\jmath} + w(x, y, z)\ \hat{k} \qquad (3\text{-}8)$$

It is seen that $\overline{v}$ is considered to be a small perturbation on the undisturbed primary flow $U(y)\ \hat{\imath}$. (Refer to sketch of flow system and disturbance on the following page.)

If we compare equations (3-1) and (3-7) we see that

$$u' = U(y) + u, \quad v' = v, \quad w' = w \qquad (3\text{-}9)$$

Substituting (3-9) into (3-2), (3-3), (3-4), and (3-5) and noting

$$U\ O\ (1) \qquad u, v, w\ O\ (\delta)$$

we can neglect terms of the form

$$u_i \frac{\partial u_j}{\partial x_i} \quad O\ (\delta^2)$$

for $i = j = 1, 2, 3$ with the following result

$$U \frac{\partial u}{\partial x} + vU' = -\frac{1}{\rho} \frac{\partial P}{\partial x} \qquad (3\text{-}10)$$

$$U \frac{\partial v}{\partial x} = -\frac{1}{\rho} \frac{\partial P}{\partial y} \qquad (3\text{-}11)$$

$$U \frac{\partial w}{\partial x} = -\frac{1}{\rho} \frac{\partial P}{\partial z} \qquad (3\text{-}12)$$

$$\nabla \circ \overline{v} = \frac{\partial u}{\partial x} + \frac{\partial v}{\partial y} + \frac{\partial w}{\partial z} = 0 \qquad (3\text{-}13)$$

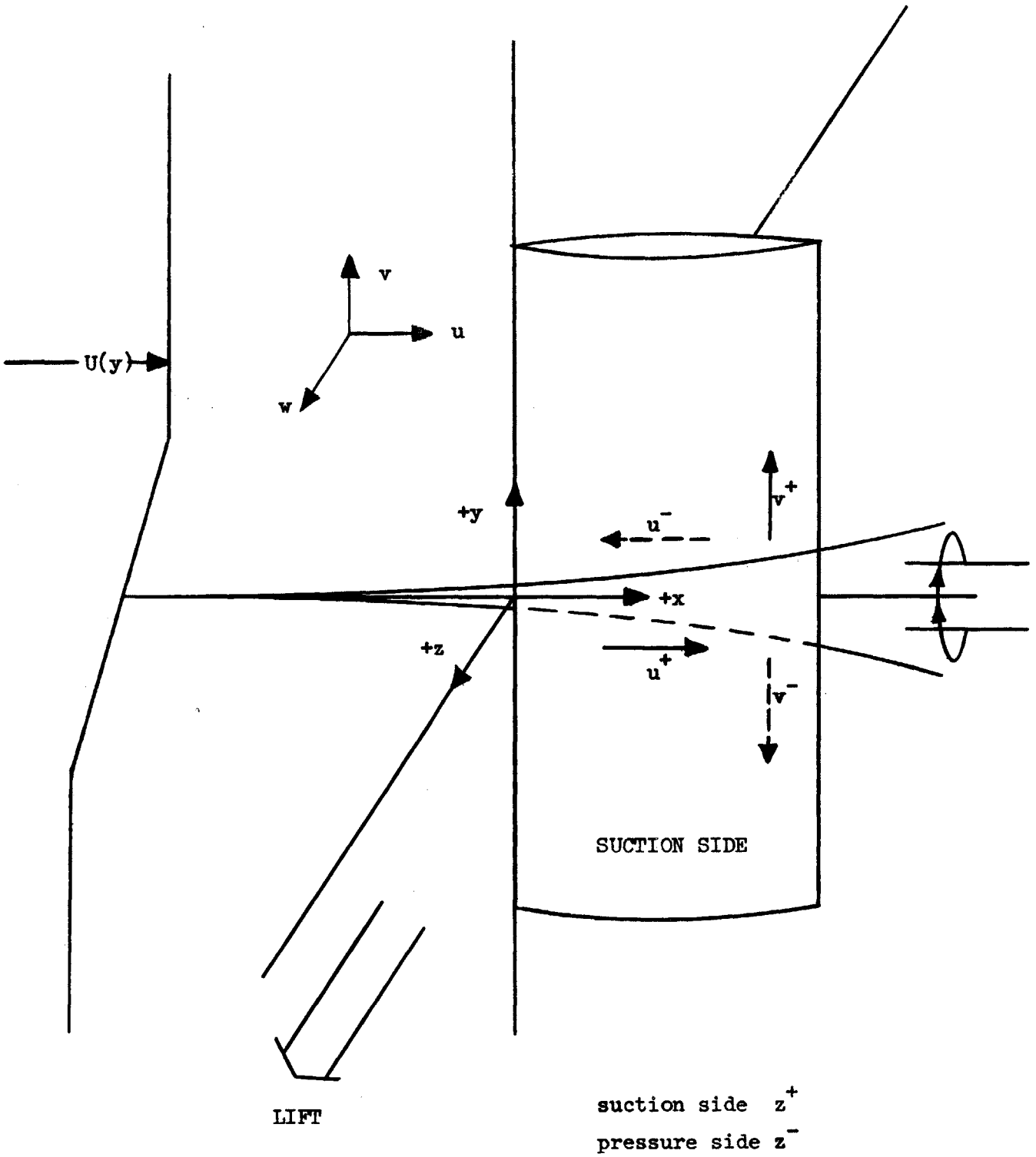

FIGURE 3 SKETCH OF FLOW SYSTEM AND DISTURBANCE

where U' denotes d/dy U(y). We note that the above forms are linear in the perturbation velocity $\bar{v}$. Following Hawthorne's procedure, we eliminate P between (3-11) and (3-12) with the result

$$\frac{\partial}{\partial x}\left[\frac{\partial}{\partial y}(U\,w) - \frac{\partial}{\partial z}(U\,v)\right] = 0$$

and since $v = w = 0$ at $x = -\infty$

$$\frac{\partial}{\partial y}(U\,w) - \frac{\partial}{\partial z}(U\,v) = 0 \tag{3-14}$$

In a similar manner, from equations (3-10) and (3-11)

$$\frac{\partial}{\partial x}\left[\frac{\partial}{\partial x}(U\,v) - \frac{\partial}{\partial y}(U\,u)\right] = \frac{\partial}{\partial y}(U'\,v) \tag{3-15}$$

and from equations (3-10) and (3-12)

$$\frac{\partial}{\partial x}\left[\frac{\partial}{\partial z}(U\,u) - \frac{\partial}{\partial x}(U\,w)\right] = -\frac{\partial}{\partial z}(U'\,v) \tag{3-16}$$

Hawthorne notes that if a vector $U\,\bar{v}$ is defined, then the above equations become the following (in order)

$$(\nabla \times (U\,\bar{v})) \circ \hat{i} = 0 \tag{3-17}$$

$$\frac{\partial}{\partial x}\left[(\nabla \times (U\,\bar{v})) \circ \hat{k}\right] = \frac{\partial}{\partial y}(U'\,v) \tag{3-18}$$

$$-\frac{\partial}{\partial x}\left[(\nabla \times (U\,\bar{v})) \circ \hat{j}\right] = \frac{\partial}{\partial z}(U'\,v) \tag{3-19}$$

and if $U\,\bar{v}$ is of the form

$$U\,\bar{v} = \nabla(U\,\phi) + \hat{i}\,U\,A(x, y, z) \tag{3-20}$$

then (3-17) is satisfied identically. The corresponding forms of (3-18) and (3-19) are

$$\frac{\partial}{\partial x}\left[-\frac{\partial}{\partial y}(U\,A)\right] = \frac{\partial}{\partial y}(U\,v) \tag{3-21a}$$

and

$$\frac{\partial}{\partial x}\left[\frac{\partial}{\partial z}(U\,A)\right] = -\frac{\partial}{\partial z}(U'\,v) \tag{3-21b}$$

An integration of equations (3-21) shows that

$$\frac{\partial A}{\partial x} = -\frac{U'}{U}\,v + \frac{f(x)}{U} \tag{3-22}$$

From equation (3-20) the velocity components can be written as

$$u = \frac{\partial \phi}{\partial x} + A \tag{3-23}$$

$$v = \frac{\partial \phi}{\partial y} + \frac{U'}{U}\phi = \frac{1}{U}\frac{\partial}{\partial y}(U\phi) \tag{3-24}$$

$$w = \frac{\partial \phi}{\partial z} \tag{3-25}$$

The corresponding vorticity components are

$$\xi = -\frac{U'}{U}\frac{\partial \phi}{\partial z} \tag{3-26}$$

$$\eta = \frac{\partial A}{\partial z} \tag{3-27}$$

$$\zeta = \frac{U'}{U}\frac{\partial \phi}{\partial x} - \frac{\partial A}{\partial y} - U' \tag{3-28}$$

where $\overline{\Omega} = \xi\, i + \eta\, j + \zeta\, k$.

If we now substitute the velocity components given by equations (3-23),(3-24), and (3-25) into the continuity equation (3-13) and use the result (3-22) with $f(x) = 0$, we obtain

$$\nabla \circ \overline{v} = \nabla^2 \phi + \left[\frac{U''}{U} - 2\left|\frac{U'}{U}\right|^2\right]\phi = 0 \tag{3-29}$$

We note that the above equations are dependent on the condition that $|u_i| << |U|$; therefore, the value of U cannot approach zero, no can there be any stagnation points in the flow about the disturbance. It is convenient at this point to deduce the linearized form of the pressure equation. The linearized equations in this form were used by von Kármán and Tsien[1] and Honda[2]. If we differentiate equations (3-10), (3-11), and (3-12) with respect to x, y, and z respectively and add the results, we obtain

$$-\frac{1}{\rho}\nabla^2 P = 2U'\frac{\partial v}{\partial x} + U\frac{\partial}{\partial x}\left[\frac{\partial u}{\partial x} + \frac{\partial v}{\partial y} + \frac{\partial w}{\partial z}\right]$$

The last term is zero from continuity. Substituting $\frac{\partial v}{\partial x}$ from (3-11) we obtain

$$\nabla^2 P = 2\frac{U'}{U}\frac{\partial P}{\partial y} \tag{3-30}$$

3.2 Von Kármán and Tsien's Lifting Line Theory

Von Kármán and Tsien[1] worked with the equation for pressure (eq. 3-30) and noted that the fundamental solutions of that equation may be written

$$P_{KT}(y, z; k)\cos kx, \quad P_{KT}(y, z; k)\sin kx$$

For the boundary conditions at $x = \pm \infty$, $P = 0$, an even function of x is required. $P(x, y, z)$ may then be written as the Fourier cosine integral

$$P(x, y, z) = \frac{1}{\pi} \int_0^\infty P_{KT}(y, z; k) \cos kx \, dk \tag{3-31}$$

Substituting equation (3-31) into equations (3-11) and (3-12) and integrating with respect to x the following expressions for the velocity components v and w are obtained:

$$v(x, y, z) = v(0, y, z) - \frac{1}{\pi\rho U} \int_0^\infty \frac{\partial}{\partial y} P_{KT}(y, z; k) \frac{\sin kx}{k} \, dk \tag{3-32}$$

$$w(x, y, z) = w(0, y, z) - \frac{1}{\pi\rho U} \int_0^\infty \frac{\partial}{\partial z} P_{KT}(y, z; k) \frac{\sin kx}{k} \, dk \tag{3-33}$$

Von Kármán and Tsien note that because the above integrals are odd functions of x and at $x = -\infty$ the perturbation velocities v and w are zero, the following relations hold:

$$v(0, y, z) = \frac{1}{2} v(\infty, y, z) = \frac{1}{2} v_T(y, z) \tag{3-34}$$

$$w(0, y, z) = \frac{1}{2} w(\infty, y, z) = \frac{1}{2} w_T(y, z) \tag{3-35}$$

The above equations define the relationships between the v and w velocities at the plane of the lifting line ($x = 0$) and the 'Trefftz' plane ($x = +\infty$).

Expanding $P_{KT}(y, z; k)$ in a Taylor series in k

$$P_{KT}(y, z; k) = P_{KT}(y, z; 0) + k \left[\frac{\partial P_{KT}}{\partial k}\right]_{k=0} + \frac{1}{2} k^2 \left[\frac{\partial^2 P_{KT}}{\partial k^2}\right]_{k=0^+} - - - \tag{3-36}$$

Substituting equations (3-34), (3-35), and (3-36) into equations (3-32) and (3-33) and taking the limit as $x \to +\infty$ the following relations are obtained:

$$v_T = \frac{-1}{\rho U} \frac{\partial}{\partial y} P_{KT}(y, z; 0), \quad w_T = \frac{-1}{\rho U} \frac{\partial}{\partial z} P_{KT}(y, z; 0)$$

For convenience, a potential function is defined

$$\Lambda_{KT}(y, z) = - P_{KT}(y, z; 0) \tag{3-37}$$

and the velocities in the Trefftz plane become the following:

$$v_T = \frac{1}{\rho U} \frac{\partial \Lambda_{KT}}{\partial y}, \quad w_T = \frac{1}{\rho U} \frac{\partial \Lambda_{KT}}{\partial z} \tag{3-38}$$

The differential equation to be satisfied by Λ_{KT} is obtained by substituting $-\Lambda_{KT}(y, z)$ for $P(x, y, z)$ in equation (3-30) since this is the form of the fundamental solution for $k = 0$.

$$\nabla^2_{y,z} \Lambda_{KT} = 2 \frac{U'}{U} \frac{\partial}{\partial y} \Lambda_{KT} \tag{3-39}$$

3.3 Solutions of the Perturbation Potential Equation

It is convenient at this point to consider an alternative higher order form of equation (3-29)

$$\frac{\partial}{\partial y} \left[U \nabla^2 \phi + U \phi \left[\frac{U''}{U} - 2 \left| \frac{U'}{U} \right|^2 \right] \right] = 0 \tag{3-40a}$$

which is, in terms of the usual form of the continuity equation (3-13)

$$\frac{\partial}{\partial y} \left[U (\nabla \circ \bar{v}) \right] = 0 \tag{3-40b}$$

An equivalent form of equations (3-40a) and (3-40b) is

$$U \nabla^2 v = U'' v \tag{3-40c}$$

which is that used by Lighthill[25]. The fundamental solutions to equations (3-40) include those of equation (3-29) plus a third solution introduced by the additional differentiation.

We now apply the familiar procedure of separation of variables to equations (3-40). Let

$$\phi(x, y, x) = F(y)\, G(x, z) \tag{3-41}$$

and

$$\nabla^2_{x,z} G(x, z) = \lambda^2 G(x, z) \tag{3-42}$$

We then have the third order equations for F(y)

$$\frac{d}{dy} \left[U \left[F'' + F \left[\lambda^2 + \frac{U''}{U} - 2 \frac{U'^2}{U^2} \right] \right] \right] = 0 \tag{3-43a}$$

which may be written in the equivalent form

$$\frac{d}{dy} \left[Y'' - 2 \frac{U'}{U} Y' + \lambda^2 Y \right] = 0 \tag{3-43b}$$

where

$$Y(y) = F(y)\, U(y) \tag{3-44}$$

The corresponding forms of (3-43a) and (3-43b) representing the separation of the lower order equation (3-29) are

$$F'' + F \left[\lambda^2 + \frac{U''}{U} - 2 \frac{U'^2}{U^2} \right] = 0 \tag{3-45a}$$

and

$$Y'' - 2 \frac{U'}{U} Y' + \lambda^2 Y = 0 \tag{3-45b}$$

Equation (3-45b) is that used by Honda[2] who assumed the solution of equation (3-30) to be of the form $P(x, y, z) = \rho\, Y(y)\, P_H(x, z)$. The fundamental solu-

tions to equations (3-40) are most easily obtained by expressing the separated form of equation (3-40c) as a second order equation in the variable

$$\psi = Y' = (FU)' \tag{3-46}$$

We have from equations (3-24), (3-41), and (3-46)

$$v = G(x, z)\,\frac{\psi}{U}$$

Substituting this for v in equation (3-40c) and using (3-42) we have the result:

$$\frac{d^2}{dy^2}\left(\frac{\psi}{U}\right) + \frac{\psi}{U}\left[\lambda^2 - \frac{U''}{U}\right] = 0 \tag{3-47}$$

The form of the fundamental solutions of equation (3-47) for velocity profiles in which $\frac{U''}{U} = \beta^2$ is

$$\frac{\psi}{U} = C_1 \sin\sqrt{\lambda^2 - \beta^2}\, y + C_2 \cos\sqrt{\lambda^2 - \beta^2}\, y \tag{3-48a}$$

The corresponding form of the solution for Y is then

$$Y = C_1 \int U \sin\sqrt{\lambda^2 - \beta^2}\, y\, dy + C_2 \int U \cos\sqrt{\lambda^2 - \beta^2}\, y\, dy + C_3 \tag{3-48b}$$

and the desired fundamental solutions for F are

$$F(y) = \frac{C_1 \int U \sin\sqrt{\lambda^2 - \beta^2}\, y\, dy}{U} + \frac{C_2 \int U \cos\sqrt{\lambda^2 - \beta^2}\, y\, dy}{U} + \frac{C_3}{U} \tag{3-48c}$$

The constant C_3 is taken to be zero to satisfy the lower order continuity equation (3-29) or equations (3-45). We now consider possible solutions of the following cases:

1) $U'' = \beta = 0$ $\qquad U(y) = U_R + U'y$

2) $U''/U = \beta^2$ $\qquad U(y) = U_R(e^{\beta(y-h)}; \sinh, \cosh \beta(y-h))$

3) $U''/U = -\beta^2$ $\qquad U(y) = U_R(\sin, \cos \beta(y-h))$

Case 1) $U(y) = U_R + U'y$

$$F(y) = \frac{C_1 \int U \sin \lambda y\, dy}{U} + \frac{C_2 \int U \cos \lambda y\, dy}{U}$$

Because of the linear form of U(y) in this case, carrying out the indicated integrations we have

$$F(y) = C_1\left[\cos \lambda y - \frac{U' \sin \lambda y}{\lambda U(y)}\right] + C_2\left[\sin \lambda y + \frac{U' \cos \lambda y}{\lambda U(y)}\right] \tag{3-49}$$

The first fundamental solution in equation (3-49) is that used by Honda[2]

who considered a linear model of a boundary shear layer at the edges of a uniform layer (U(y) = constant) confined by two parallel walls.

Case 2) $U(y) = U_R \exp(\beta(y-h))$

$$F(y) = \frac{C_1 \int \exp(\beta(y-h)) \sin \sqrt{\lambda^2 - \beta^2}\, y\, dy}{\exp(\beta(y-h))} + \frac{C_2 \int \exp(\beta(y-h)) \cos \sqrt{\lambda^2 - \beta^2}\, y\, dy}{\exp(\beta(y-h))}$$

performing the indicated integrations:

$$F(y) = C_1 \sin \sqrt{\lambda^2 - \beta^2}\, y + C_2 \cos \sqrt{\lambda^2 - \beta^2}\, y \qquad (3\text{-}50)$$

Case 3) $U(y) = U_R \cos \beta(y-h)$

$$F(y) = \frac{C_1 \int \cos \beta(y-h) \sin \sqrt{\lambda^2 + \beta^2}\, y\, dy}{\cos \beta(y-h)} + \frac{C_2 \int \cos \beta(y-h) \cos \sqrt{\lambda^2 + \beta^2}\, y\, dy}{\cos \beta(y-h)}$$

performing the indicated integrations:

$$F(y) = C_1 \left[\cos \sqrt{\lambda^2 + \beta^2}\, y + \frac{\beta \sin \sqrt{\lambda^2 + \beta^2}\, y \tan \beta(y-h)}{\sqrt{\lambda^2 + \beta^2}} \right] + C_2 \left[\sin \sqrt{\lambda^2 + \beta^2}\, y - \frac{\beta \cos \sqrt{\lambda^2 + \beta^2}\, y \tan \beta(y-h)}{\sqrt{\lambda^2 + \beta^2}} \right] \qquad (3\text{-}51)$$

In addition to the above fundamental solutions, we have for U constant the solutions

$$F(y) = C_1 \sin \lambda\, y + C_2 \cos \lambda\, y \qquad (3\text{-}52)$$

which is obtained by setting $\beta = 0$ in equations (3-50) or (3-51). Through the use of the above fundamental solutions for various velocity distributions U(y) a wide variety of flow situations may be investigated.

In a lifting line approach to this rotational flow problem, as in the usual application, the desired quantity is the w component of velocity at the lifting line. We are then able to consider solutions of equations (3-29) or (3-40) at the Trefftz plane ($x = +\infty$) where there is no x dependence through the use of the relations between v_T, w_T and v_{OL}, w_{OL} given by equations (3-34) and (3-35). We then desire solutions of equation (3-42) in the Trefftz plane

$$\frac{d^2}{dz^2} G_T(z) = \lambda^2 G_T(z) \qquad (3\text{-}53)$$

The general solutions of (3-53) are the following:

$$G_T(z) = C_1 \cosh \lambda z + C_2 \sinh \lambda z \tag{3-54}$$

The fundamental solutions obtained for F(y) are valid for all x and are not restricted to use in the Trefftz plane.

It is instructive to note the relationship between the form of the perturbation potential in the Trefftz plane and the potential function used by von Kármán and Tsien, $\Lambda_{KT}(y, z)$.

$$\Lambda_{KT}(y, z) = \rho U \phi_T(y, z) = \rho FUG_T(z) \tag{3-55}$$

3.4 General Lifting Line Solution

We can now express the form of the perturbation potential in the Trefftz plane from equation (3-41)

$$\phi_T(y, z) = \sum_{n=1}^{\infty} Q(\lambda_n) F_n(y) G_{Tn}(z) \tag{3-56}$$

The $F_n(y)$ are the eigenfunctions of equations (3-45) which are linear combinations of the fundamental solutions given by equations (3-49), (3-50), (3-51), or (3-52) or other appropriate solutions of equation (3-47) depending on the form of the shear velocity profile U(y). The eigenvalues λ_n are determined in accordance with the imposed boundary conditions on $F_n(y)$. These boundary conditions shall be that v = 0 at the walls ($y = \pm \ell/2$) and that v and P be continuous in y throughout the flow. These conditions are equivalent to the requirements

$$\frac{d}{dy}(FU) = 0 \qquad y = \pm \ell/2 \tag{3-57a}$$

$$\frac{d}{dy}(FU) \text{ and } (FU) \text{ are continuous} \tag{3-57b}$$

These relations follow from the equations

$$v(x, y, z) = G(x, z) \frac{(FU)'}{U} \tag{3-57c}$$

and

$$P(x, y, z) = -\rho \frac{\partial}{\partial x} G(x, z) (FU) \tag{3-57d}$$

which are consistent with equation (3-11). Equation (3-57d) indicates the relationship between Honda's[2] expression for the pressure and the perturbation potential

$$P(x, y, z) = -\rho \frac{\partial}{\partial x} G(x, z)(FU) = + \rho P_H(x, z)(FU)$$

therefore

$$P_H(x, z) = - \frac{\partial}{\partial x} G(x, z) \tag{3-58}$$

Also, from equation(3-57d) we have the useful result

$$\phi(x, y, z) = - \frac{1}{\rho U} \int_{-\infty}^{x} P(x, y, z)\, dx \tag{3-59}$$

Therefore

$$\phi_T(y, z) = - \frac{1}{\rho U} \lim_{x \to \infty} \int_{-\infty}^{x} P(x, y, z)\, dx \tag{3-60}$$

From equation (3-59) and the results of von Kármán and Tsien[1] we note that $\phi(x, y, z)$ is an odd function of x and also that $\phi(0, y, z) = \frac{1}{2} \phi_T(\infty, y, z)$ which is consistent with equations (3-34) and (3-35).

The functions $G_{Tn}(z)$ in equation (3-56) are of the form given in equation (3-54) with the boundary condition that the w component of velocity be zero at the side walls of the channel:

$$\frac{d}{dz} G_T(z) = 0 \quad z = \pm d/2 \tag{3-61}$$

To determine the unique solution for $\phi_T(y, z)$ we require a relationship between the lift on the lifting line and the induced velocities in the Trefftz plane far downstream of the lifting line. In accordance with von Kármán and Tsien the assumption of equal and opposite pressure forces on the lifting line at $Z = 0^{\pm}$ and the requirement that $\phi(x, y, z)$ be an odd function of x from equation (3-59) we have the following relation for $\phi_T(y, z)$

$$\phi_T(y, 0^+) = - \phi_T(y, 0^-) \tag{3-62a}$$

Therefore, from equation (3-24)

$$v_T(y, 0^+) = - v_T(y, 0^-) \tag{3-62b}$$

We then relate the trailing circulation in the "wake" of the airfoil or lifting line to the spanwise or v velocity components in the Trefftz plane using the chosen sign convention.

$$\frac{1}{\rho U} \frac{dL(y)}{dy} = v_T(y, 0^+) - v_T(y, 0^-) \tag{3-63a}$$

Then using equation (3-62b) we have the following:

$$v_T(y, 0^{\pm}) = \pm \frac{1}{2} \frac{1}{\rho U} \frac{dL(y)}{dy} \tag{3-63b}$$

We then write L(y) in terms of the usual thin airfoil notation

$$L(y) = \frac{1}{2} \rho U^2 c \, C_L = \pi \rho c U^2 (\alpha_o + w_{LL}/U) \tag{3-64a}$$

where c is the chord of the airfoil and α_o is the geometrical angle of attack. Differentiating equation (3-64a) we have

$$\frac{d}{dy} L(y) = 2\pi\rho \, c \, \alpha_o \, UU' + \pi\rho \, c \, \frac{d}{dy} (Uw_{LL}) \tag{3-64b}$$

We can now write from equations (3-14) and (3-34)

$$\frac{d}{dy} (Uw_{LL}) = \frac{\partial}{\partial z} (Uv_{LL}) = \frac{1}{2} \frac{\partial}{\partial z} \left[U \, v_T(y, 0^{\pm}) \right] \tag{3-65}$$

We then have from (3-63b), (3-64b), and (3-65)

$$v_T(y, 0^{\pm}) = \pm \pi c \alpha_o U' \pm \frac{\pi c}{4} \frac{\partial}{\partial z} \left[v_T(y, 0^{\pm}) \right] \tag{3-66a}$$

and, from equation (3-24)

$$v_T(y, 0^{\pm}) = \frac{1}{U} \frac{\partial}{\partial y} \left[U\phi_T(y, 0^{\pm}) \right] \tag{3-66b}$$

Substituting (3-66b) into (3-66a) we have

$$\frac{\partial}{\partial y} \left[U\phi_T(y, 0^{\pm}) \right] \mp \frac{\pi c}{4} \frac{\partial^2}{\partial y \partial z} \left[U\phi_T(y, 0^{\pm}) \right] = \pm \pi c \alpha_o UU' \tag{3-67}$$

We can now write from equation (3-56)

$$\phi_T(y, 0^{\pm}) = \sum_{n=1}^{\infty} Q^{\pm}(\lambda_n) \, F_n(y) \, G_{Tn}(0^{\pm}) \tag{3-68}$$

Substituting this expression for $\phi_T(y, 0^{\pm})$ in equation (3-67) yields the following

$$\sum_{n=1}^{\infty} Q^{\pm}(\lambda_n) \frac{d}{dy} (UF_n(y)) \left[G_{Tn}(0^{\pm}) \mp \frac{\pi c}{4} \frac{\partial}{\partial z} G_{Tn}(0^{\pm}) \right] = \pm \pi c \alpha_o UU' \tag{3-69}$$

Equation (3-69) is the desired relation for the determination of the constant $Q^{\pm}(\lambda_n)$.

We can define, for convenience, a change in the two dimensional lift coefficient as ΔC_{Lo}, and from equations (3-64a),(3-35), and (3-25) we have the result

$$L(y) = \frac{1}{2} \rho U^2 c \, (C_{Lo} + \Delta C_{Lo}) = \pi \rho c U^2 (\alpha_o + \frac{w_{LL}}{U})$$

Therefore

$$\frac{\Delta C_{Lo}}{C_{Lo}} = \frac{w_{LL}}{U\alpha_o} = \frac{w_T(y, 0)}{2U\alpha_o} = \frac{1}{2U\alpha_o} \frac{\partial}{\partial z} \phi_T(y, 0^{\pm}) \tag{3-70}$$

3.5 Orthogonality of Eigenfunctions (FU) and Their Derivatives (FU)'

To solve equation (3-69) we must establish the orthogonality of the function $\frac{d}{dy}(FU)$ in the interval $(\frac{-\ell}{2}, +\frac{\ell}{2})$. It is convenient to demonstrate the orthogonality of these functions for the most general case in which the shear velocity profile U(y) is continuous but U'(y) and higher derivatives are not continuous. This permits the shear velocity profile to consist of matched individual profiles for which the fundamental solutions of equation (3-47) are known.

We will now consider the general case of a shear flow consisting of three matched continuous profiles $U_0(y)$, $U_1(y)$ and $U_2(y)$ as shown in the following sketch:

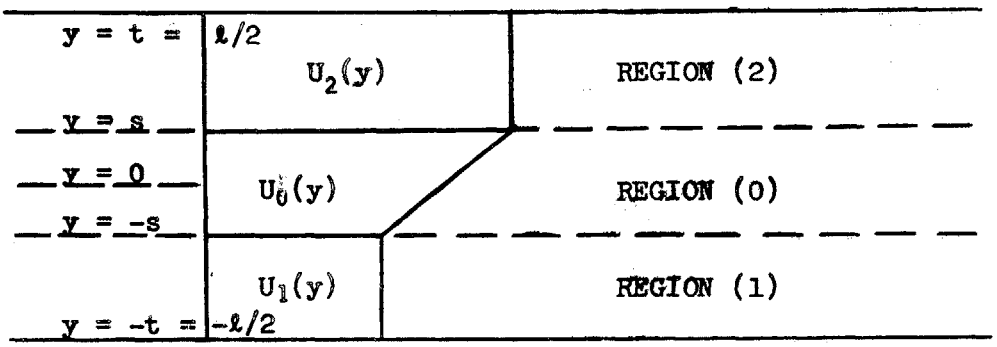

Corresponding to the velocity profiles in region (0), (1), and (2) we have the respective solutions F_0, F_1, F_2; Y_0, Y_1, Y_2; and ψ_0, ψ_1, ψ_2 of equations (3-45a), (3-45b), and (3-47). The boundary conditions from equations (3-57a) and (3-57b) are

$$
\begin{aligned}
&1)\ y = t = \ell/2 && (F_2U_2)' = Y'_2 = \psi_2 = 0 \\
&2)\ y = s && (F_2U_2)' = (F_0U_0)';\ \ Y'_2 = Y'_0;\ \ \psi_2 = \psi_0 \\
&3)\ y = s && F_2 = F_0;\ \ Y_2 = Y_0 \\
&4)\ y = -s && F_0 = F_1;\ \ Y_0 = Y_1 \\
&5)\ y = -s && (F_0U_0)' = (F_1U_1)';\ \ Y'_0 = Y'_1;\ \psi_0 = \psi_1 \\
&6)\ y = -t = -\ell/2 && (F_1U_1)' = Y'_1 = \psi_1 = 0
\end{aligned}
\qquad (3\text{-}71)
$$

We can now consider a general Sturm-Liouville problem of the form:

$$p\frac{d^2\psi}{dy^2} + \frac{dp}{dy}\frac{d\psi}{dy} + q\psi + \lambda^2 r\psi = 0 \qquad (3\text{-}72)$$

Let ψ_m and ψ_n be two eigenfunctions of this equation for corresponding eigenvalues λ_m and λ_n. The requirement that

$$(\lambda_m^2 - \lambda_n^2)\int_{-t}^{+t} r\,\psi_m\,\psi_n\,dy = (\lambda_m^2 - \lambda_n^2)\int_{-t}^{-s} r_1\,\psi_{1m}\,\psi_{1n}\,dy$$

$$+ (\lambda_m^2 - \lambda_n^2)\int_{-s}^{+s} r_0\,\psi_{0m}\,\psi_{0n}\,dy + (\lambda_m^2 - \lambda_n^2)\int_{+s}^{+t} r_2\,\psi_{2m}\,\psi_{2n}\,dy = 0$$

is the following

$$\begin{aligned} &p_2(\psi_{2m}\,\psi'_{2n} - \psi_{2n}\,\psi'_{2m})\Big|_{\ell/2} - p_1(\psi_{1m}\,\psi'_{1n} - \psi_{1n}\,\psi'_{1m})\Big|_{-\ell/2} \\ &+ \Big[p_0(\psi_{0m}\,\psi'_{0n} - \psi_{0n}\,\psi'_{0m}) - p_2(\psi_{2m}\,\psi'_{2n} - \psi_{2n}\,\psi'_{2m})\Big]_s \\ &+ \Big[p_1(\psi_{1m}\,\psi'_{1n} - \psi_{1n}\,\psi'_{1m}) - p_0(\psi_{0m}\,\psi'_{0n} - \psi_{0n}\,\psi'_{0m})\Big]_{-s} = 0 \end{aligned} \qquad (3\text{-}73)$$

We now consider the two differential equations

$$Y'' - \frac{2U'}{U}Y' + \lambda^2 Y = 0 \qquad (3\text{-}45b)$$

and

$$\left(\frac{\psi}{U}\right)'' + \frac{\psi}{U}\left[\lambda^2 - \frac{U''}{U}\right] = 0 \qquad (3\text{-}47)$$

for equation (3-45b): $p = r = \frac{1}{U^2}$, $q = 0$

for equation (3-47): $p = r = \frac{1}{U^2}$, $q = \frac{2U'^2}{U^4} - \frac{2U''}{U^3}$

It can be easily shown that equation (3-73) with ψ replaced by Y is satisfied exactly through the use of the boundary conditions in terms of Y in equation (3-71) and the fact that at $y = s$, $U_0 = U_2$ and at $y = -s$, $U_0 = U_1$. This confirms the result that

$$(\lambda_m^2 - \lambda_n^2)\int_{-\ell/2}^{\ell/2} \frac{1}{U^2}\,Y_m\,Y_n\,dy = 0 \qquad (3\text{-}74)$$

which was used by Honda[2].

We now consider equation (3-73) in ψ with the boundary conditions of equation (3-71) in terms of ψ. Using these boundary conditions and the fact that at $y = s$, $U_0 = U_2$ and at $y = -s$, $U_0 = U_1$, equation (3-73) becomes

$$\begin{aligned} &\frac{1}{U_0^2}\Big[\psi_{0m}(\psi'_{0n} - \psi'_{2n}) - \psi_{0n}(\psi'_{0m} - \psi'_{2m})\Big]_s \\ &+ \frac{1}{U_0^2}\Big[\psi_{0m}(\psi'_{1n} - \psi'_{0n}) - \psi_{0n}(\psi'_{1m} - \psi'_{0m})\Big]_{-s} = 0 \end{aligned} \qquad (3\text{-}75a)$$

We now write equation (3-45b) in the equivalent form

$$\psi' = \frac{2U'}{U}\psi - \lambda^2 Y \tag{3-75b}$$

Therefore, at $y = s$

$$\psi'_{0n} = \frac{2U'_0}{U_0}\psi_{0n} - \lambda^2_n Y_{0n}$$

$$\psi'_{2n} = \frac{2U'_2}{U_2}\psi_{2n} - \lambda^2_n Y_{2n}$$

and $\psi'_{0n} - \psi'_{2n} = \frac{2U'_0}{U_0}\psi_{0n} - \frac{2U'_2\psi_{0n}}{U_2} = 2\psi_{0_n}\left(\frac{U'_0}{U_0} - \frac{U'_2}{U_2}\right)$ (3-75c)

since $Y_{0n} = Y_{2n}$ and $\psi_{0_n} = \psi_{2n}$

In the same manner, at $y = s$

$$\psi'_{0m} - \psi'_{2m} = \frac{2U'_0}{U_0}\psi_{0m} - \frac{2U'_2}{U_2}\psi_{0m} = 2\psi_{0m}\left(\frac{U'_0}{U_0} - \frac{U'_2}{U_2}\right) \tag{3-75d}$$

Using equations (3-75c) and (3-75d) we note that the first term of equation (3-75a) is identically zero. In the same manner, the second term of equation (3-75a) can be shown to be zero. We have now established that

$$(\lambda^2_m - \lambda^2_n)\int_{-\ell/2}^{\ell/2} \frac{d/dy\,(F_m U)\; d/dy\,(F_n U)}{U^2}\,dy = 0 \tag{3-76}$$

provided that the boundary conditions specified by equations (3-57a) and (3-57b) are satisfied and U(y) is continuous.

Using (3-76) we can now solve equation (3-69) for the constant $Q^{\pm}(\lambda_n)$. Multiplying equation (3-69) through by $\frac{1}{U^2}\frac{d}{dy}(F_n(y)U)$ and integrating the result from $(-\ell/2)$ to $(\ell/2)$ we have the result

$$Q^{\pm}(\lambda_n) = \frac{\pm\pi c\alpha_0 \int_{-\ell/2}^{\ell/2} U'/U\; d/dy(F_n U)\,dy}{\left[G_{Tn}(0^{\pm}) \mp \pi c/4\; \partial/\partial z G_{Tn}(0^{\pm})\right]\int_{-\ell/2}^{\ell/2}\left[d/dy(F_n U)\right]^2 U^{-2}\,dy} \tag{3-77}$$

It is interesting to note that the functions $\psi' = (FU)''$ are continuous at the match points ($y = \pm s$) if, in addition to U(y) being continuous, U'(y) is continuous at $y = \pm s$. This can be seen from equations (3-75c) and (3-75d).

3.6 General Solution for Arbitrary U(y)

It is convenient to determine the required solutions of equation (3-54) with the boundary condition given by equation (3-61) at this point since these

solutions are independent of the choice of U(y).

$$G_T(z) = C_1 \cosh \lambda z + C_2 \sinh \lambda z \tag{3-54}$$

$$\frac{d}{dz} G_T(\pm D) = 0 \tag{3-61}$$

The required solutions are

$$G_T(z^+) = (\cosh \lambda z - \tanh \lambda D \sinh \lambda z)$$

$$G_T(z-) = (\cosh \lambda z + \tanh \lambda D \sinh \lambda z) \tag{3-78a}$$

Using equation (3-78a) we have the result

$$\left[G_{Tn}(0\pm) \mp \frac{\pi c}{4} \frac{\partial}{\partial z} G_{Tn}(0\pm)\right] = 1 + \frac{\pi c \lambda_n \tanh \lambda_n D}{4} \tag{3-78b}$$

Substituting equation (3-78b) into equation (3-77) for $Q^{\pm}(\lambda_n)$

$$Q^{\pm}(\lambda_n) = \frac{\pm \pi c \alpha_0 \int_{-\ell/2}^{\ell/2} \frac{U'}{U} \frac{d}{dy} (F_n U)\, dy}{\left[1 + \frac{\pi c \lambda_n}{4} \tanh \lambda_n D\right] \int_{-\ell/2}^{\ell/2} \left[\frac{d}{dy} (F_n U)\right]^2 \frac{1}{U^2}\, dy} \tag{3-79}$$

The corresponding form of $Q^{\pm}(\lambda_n)$ for the case of a flow unbounded in the z direction is obtained by setting $\tanh \lambda_n D = 1$.

We can now write the final form of the desired solution for $\Delta C_{Lo}/C_{Lo}$ using equations (3-68), (3-70), and (3-78).

$$\frac{\Delta C_{Lo}}{C_{Lo}} = \frac{\mp 1}{2U\alpha_o} \sum_{n=1}^{\infty} Q^{\pm}(\lambda_n) F_n(y) \lambda_n \tanh \lambda_n D \tag{3-80}$$

Equations (3-79) and (3-80) constitute the general solution of the lifting line problem for any properly chosen shear velocity distribution U(y). It is probable that most realistic shear velocity profiles can be fabricated from matched U(y) for which the solutions of equation (3-47) are so-called elementary solutions of the forms in equation (3-49) through (3-52). We will investigate particular solutions for selected U(y) in the following section.

Combining equations (3-79) and (3-80) we have

$$\frac{\Delta C_{Lo}}{C_{Lo}} = -2 \sum_{n=1}^{\infty} \frac{\int_{-\ell/2}^{\ell/2} \frac{U'}{U} \frac{d}{dy} (F_n U)\, dy \left[\frac{F_n(y)}{U(y)}\right]}{\int_{-\ell/2}^{\ell/2} \left[\frac{d}{dy} (F_n U)\right]^2 \frac{1}{U^2}\, dy \left[1 + \frac{1}{\frac{\pi}{4} \lambda_n c \tanh \lambda_n D}\right]} \tag{3-81}$$

It is worthwhile to note that the integrals in the numerator and the denominator of equation (3-81) are of the forms (using $\psi = (FU)'$)

$$\int U'\left(\frac{\psi}{U}\right) dy \qquad \text{and} \qquad \int \left(\frac{\psi}{U}\right)^2 dy$$

which from equation (3-48a) are the following

$$\int U'(\sin,\ \cos \sqrt{\lambda^2 - \beta^2}\, y)dy \quad \text{and} \quad \int (\sin,\ \cos \sqrt{\lambda^2 - \beta^2}\, y)^2\, dy$$

These integrals are evaluated easily.

We have, therefore, reduced the solution of a rather complicated bounded shear flow problem to one of the determination of eigenfunctions and the evaluations of integrals, all of elementary forms. The most difficult part of the solution is the determination of the eigenvalues λ_n for matched velocity profiles where the derivatives of U(y) are continuous only in two or more finite regions.

It is instructive to express the general solution for $\Delta C_{Lo}/C_{Lo}$ (equation 3-81) in non-dimensional form. If we non-dimensionalize according to the following scheme:

$$\text{length}^* = \frac{\text{length}}{c} \qquad \text{velocity}^* = \frac{\text{velocity}}{U_R}$$

$$\phi^* = \frac{\phi}{U_R c} = \left(\frac{Q}{U_R c}\right) FG \qquad L^* = \frac{L}{\rho U_R^2 c} = \frac{1}{2} U^{*2} C_L$$

we have the result

$$\frac{\Delta C_{Lo}}{C_{Lo}} = -2 \sum_{n=1}^{\infty} \frac{\int^{AR} \frac{1}{U^*} \frac{d}{dy^*}(U^*) \frac{d}{dy^*}(F_n U^*)\, dy^*\, F_n / U^*}{\int^{AR} \left[\frac{d}{dy^*}(F_n U^*)\right]^2 \frac{dy^*}{U^{*2}} \left[1 + \frac{1}{\frac{\pi}{4} \lambda_n^* \tanh \lambda_n^* D^*}\right]}$$

where F is dimensionless and $\lambda_n^* \propto \frac{1}{AR} = \frac{c}{\ell} = \frac{1}{\ell^*}$

3.7 Particular Solution for Continuous Profile with $U'' = 0$

We first consider velocity profiles of the form $U(y) = U_R + U'y$ for which the eigenfunctions $F_n(y)$ will be of the form (3-49). The simplest and yet still interesting example of this is the continuous - constant vorticity profile described in the following sketch:

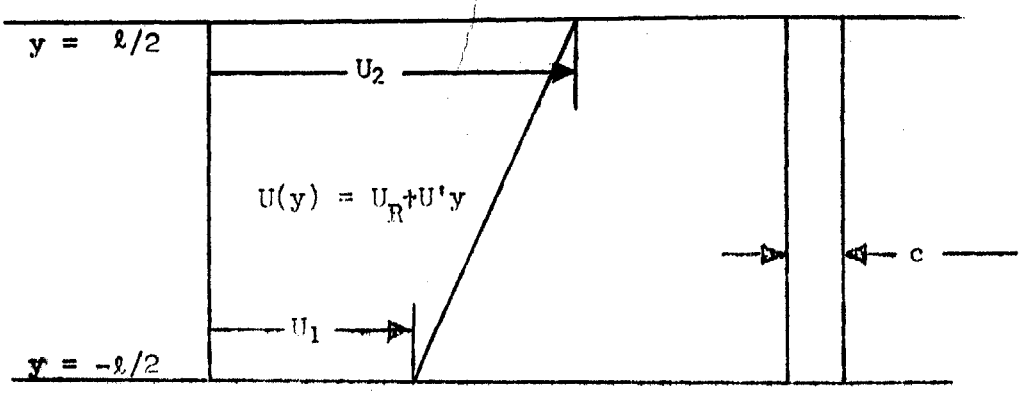

For this flow geometry, only one continuous eigenfunction $F_n(y)$ is required.

$$F_n(y) = \sin \lambda_n y + \frac{U' \cos \lambda_n y}{\lambda_n U(y)} \tag{3-82a}$$

and

$$\frac{d}{dy}(F_n U) = \lambda_n U \cos \lambda_n y \tag{3-82b}$$

The boundary condition (3-57a) determines the eigenvalues in this case:

$$\lambda_n = n\pi/\ell \qquad \text{for n odd} \tag{3-82c}$$

The requirement of continuity of pressure and velocity as given by equation (3-57b) is satisfied since (UF_n) and $\frac{d}{dy}(UF_n)$ are continuous in this case.

Substituting equations (3-82) into equation (3-81) and simplifying, we have the result:

$$\frac{\Delta C_{Lo}}{C_{Lo}} = \frac{-8}{\pi^2} \sum_{n=1}^{\infty} \frac{(-1)^{n-1/2} \left[\frac{(U_2-U_1)}{U(y)} \sin \frac{n\pi y}{\ell} + \frac{(U_2-U_1)^2}{U^2 \pi n} \cos \frac{n\pi y}{\ell} \right]}{n^2 \left[1 + \frac{1}{\frac{n\pi^2}{4} \left(\frac{c}{\ell}\right) \tanh \left(\frac{n\pi D}{\ell}\right)} \right]} \tag{3-83}$$

3.8 Particular Solution for Matched Profile with U'' = 0

The second problem to be solved is that of a shear flow consisting of a velocity profile with a constant vorticity layer in the center region which is bounded by two regions of uniform flow between confining walls. The geometry of this flow is shown in the sketch following. The boundary conditions for the solution of this problem are those given in equation (3-71). The eigenfunctions given in equation (3-84) are denoted by F_0, F_1, and F_2 corresponding to regions (0), (1), and (2) and are forms of equations (3-49) or (3-52).

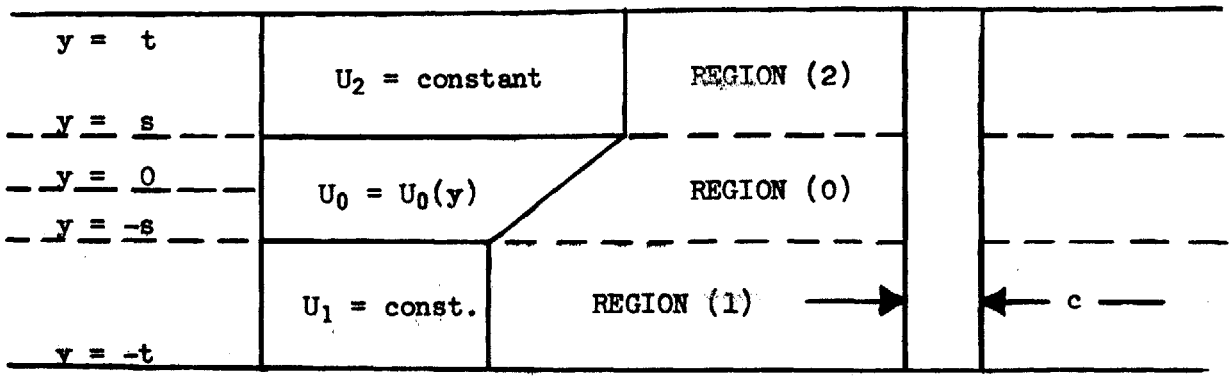

$$F_0(y) = \left[\sin \lambda(s-t) \cos \lambda(s-t) + \frac{\lambda U_2}{U'_0} + \frac{U'_0}{\lambda U_0(y)} \sin^2 \lambda(s-t) \right] \cos \lambda(y-t)$$
$$+ \left[\sin^2 \lambda(s-t) - \frac{U'_0}{\lambda U_0(y)} \left[\frac{\lambda U_2}{U'_0} + \sin \lambda(s-t) \cos \lambda(s-t) \right] \right] \sin \lambda(y-t) \qquad (3\text{-}84a)$$

$$F_1(y) = \left[\sin 2\lambda s + \frac{\lambda U_2}{U'_0} \frac{\sin \lambda(s+t)}{\sin \lambda(s-t)} \right] \cos \lambda(y+t) \qquad (3\text{-}84b)$$

$$F_2(y) = \frac{\lambda U_2}{U'_0} \cos \lambda(y-t) \qquad (3\text{-}84c)$$

The characteristic equation to be satisfied for the determination of the characteristic values λ_n is the following:

$$\theta_n^2 \sin \left(\frac{2\theta_n}{\mu} \right) = \frac{(U_2 - U_1)^2}{4U_2 U_1} \left[\theta_n \left(\cos \left(\frac{2\theta_n}{\mu} \right) - \cos 2\theta_n \right) + \sin 2\theta_n \sin^2 \left(\frac{1}{\mu} - 1 \right) \theta_n \right] \qquad (3\text{-}85a)$$

where $\theta_n = \lambda_n s$ and $\mu = \frac{s}{t} = \frac{b}{\ell}$

It can be shown that the characteristic equation (3-85a) has an infinite number of special eigenvalues which are integer multiples of $\frac{\pi}{\ell}$. We shall call these 'degenerate eigenvalues' and denote them by the subscript $(\frac{m}{\mu})$. The degenerate eigenvalues are given as follows:

$$\lambda_{(\frac{m}{\mu})} = \frac{m}{\mu} \frac{\pi}{\ell} \qquad (3\text{-}85b)$$

where (m) and $(\frac{m}{\mu})$ are *both even* or *both odd* integers. The eigenfunctions (3-84) corresponding to the degenerate eigenvalues require special consideration in that they assume a different form for these particular eigenvalues. As a result of this, it can be shown that the solution (equation 3-81) corresponding to *even* degenerate eigenvalues is trivial; i.e. $\Delta C_{Lo}/C_{Lo}(y; \lambda_{(\frac{m}{\mu})}) = 0, (\frac{m}{\mu})$ even. For *odd* values of $(\frac{m}{\mu})$, the corresponding degenerate solutions

must be considered in the total solution.

If the implications of this degeneracy are taken into account, equation (3-85a) is valid for $0 < \mu \leq 1$. For the limiting case of $\mu = 1$, i.e. when the shear profile is continuous across the duct, $\lambda_n = n\pi/\ell$; the even values of n are excluded since they are trivial. This is then the same result as obtained in equation (3-82c). The final solution for the limiting case is simply equation (3-83).

For the non-degenerate case, equations (3-84), (3-85a) and (3-81) constitute the solution. The integrals of the functions $\frac{d}{dy}(F_n U)$ in equation (3-81) although simple in form, are algebraically complex, and an efficient evaluation of the solution requires the use of a digital computer.

Refer to Appendix II for further discussion of this problem and the listing of a digital computer program which has been used successfully to obtain final solutions for the non-degenerate case.

3.9 Particular Solution for Continuous Cosine Velocity Profile

In this problem we choose the case in which the velocity profile is of the form $U(y) = U_R \cos \beta y$. This is a symmetrical profile about the axis $y = 0$ which is bounded in the y direction at $y = \pm\frac{\ell}{2}$. The geometry of the flow is shown in the following sketch:

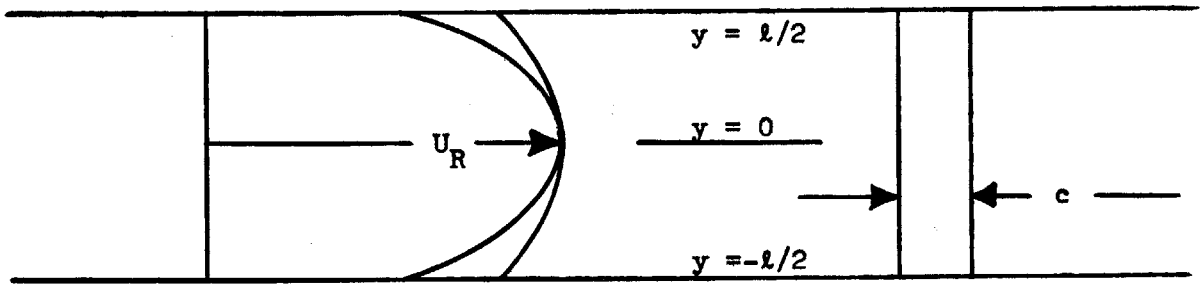

It is apparent that $\beta < \frac{\pi}{\ell}$ to exclude zero and negative U(y). We note that through the consideration of velocity profiles of this form, we are approaching the familiar developed profiles found in internal flow situations.

The eigenfunctions of this problem are forms of the first fundamental solution given in equation (3-51) which can be written in the equivalent form

$$F(y) = \frac{\sqrt{\lambda^2+\beta^2}}{2\cos \beta y}\left[\frac{\cos\,(\beta-\sqrt{\lambda^2+\beta^2})y}{(\beta-\sqrt{\lambda^2+\beta^2})} - \frac{\cos\,(\beta+\sqrt{\lambda^2+\beta^2})y}{(\beta+\sqrt{\lambda^2+\beta^2})}\right] \tag{3-86a}$$

from which

$$\frac{d}{dy}(FU) = \sqrt{\lambda^2+\beta^2}\, U_R \cos \beta y \sin \sqrt{\lambda^2+\beta^2}\, y \tag{3-86b}$$

The eigenvalues λ_n are determined by the boundary condition at the walls

$$\sqrt{\lambda_n^2+\beta^2} = \frac{2n\pi}{\ell} \quad \text{or} \quad \lambda_n = \sqrt{\frac{4n^2\pi^2}{\ell^2} - \beta^2} \tag{3-86c}$$

Substituting equations (3-86) into equation (3-81) we have the following solution:

$$\frac{\Delta C_{Lo}}{C_{Lo}} = \frac{2\beta\ell}{\cos^2 \beta y} \sum_{n=1}^{\infty}\left[\frac{\cos(\beta+2n\pi/\ell)y}{(\beta\ell+2n\pi)} - \frac{\cos(\beta-2n\pi/\ell)y}{(\beta\ell-2n\pi)}\right] x$$

$$\frac{\left[\frac{\sin(\beta\ell/2+n\pi)}{(\beta\ell+2n\pi)} - \frac{\sin(\beta\ell/2-n\pi)}{(\beta\ell-2n\pi)}\right]}{\left[1 + \frac{1}{\frac{\pi}{4}\left(\frac{c}{\ell}\right)\sqrt{4n^2\pi^2-\beta^2\ell^2}\tanh\left[\sqrt{4n^2\pi^2-\beta^2\ell^2}\,\frac{D}{\ell}\right]}\right]} \tag{3-87}$$

We note that β can be chosen arbitrarily provided that the condition $\beta < \frac{\pi}{\ell}$ is satisfied.

3.10 Particular Solution for Matched Cosine-Uniform Profile

For this last problem, we consider velocity profiles characteristic of those of boundary (shear) layers at the edge of a layer of uniform flow. The geometry of the flow is described in the following sketch:

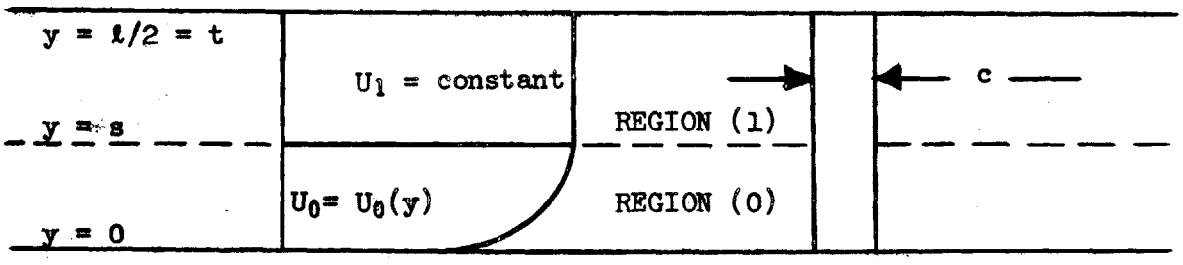

where $U_0(y) = U_1 \cos \beta(y - s)$ for $\beta < \pi/2s$.

The eigenfunctions for this problem are forms of equations (3-51) and (3-52).

$$F_0(y) = \cos \sqrt{\lambda^2+\beta^2}\, y + \frac{\beta}{\sqrt{\lambda^2+\beta^2}} \sin \sqrt{\lambda^2+\beta^2} y \tan \beta(y-s) \tag{3-88a}$$

$$F_1(y) = \frac{\lambda \sin \sqrt{\lambda^2+\beta^2}\, s \cos \lambda(y-t)}{\sqrt{\lambda^2+\beta^2} \sin \lambda(s-t)} \tag{3-88b}$$

The characteristic equation to be satisfied for the determination of the characteristic values λ_n is the following:

$$\frac{\tan \sqrt{\lambda^2 + \beta^2}s}{\sqrt{\lambda^2 + \beta^2}} = \frac{\tan \lambda(s-t)}{\lambda} \qquad (3\text{-}89)$$

Equations (3-88), (3-89), and (3-81) constitute the solution for this problem provided that the limits of integration of the integrals in (3-81) are taken to be 0 to $\ell/2$.

Particular examples of solutions for $\Delta C_{Lo}/C_{Lo}$, using the equations developed in Sections 3.7 through 3.10, are presented in Appendices I and III.

4. FIRST THEORETICAL APPROXIMATION

The following development provides a relatively simple method for the calculation of lift on a thin untwisted airfoil of infinite span in a somewhat idealized shear flow. The main purpose of developing such a solution is to determine the general behavior and the order of magnitude of the effects on lift caused by the induced secondary flows, and to investigate the usefulness of a linearized inviscid approach to the solution of the general problem. The analysis is approximate in that first order effects dependent on the secondary flows themselves are neglected.

The geometry of the flow is described in the following sketch:

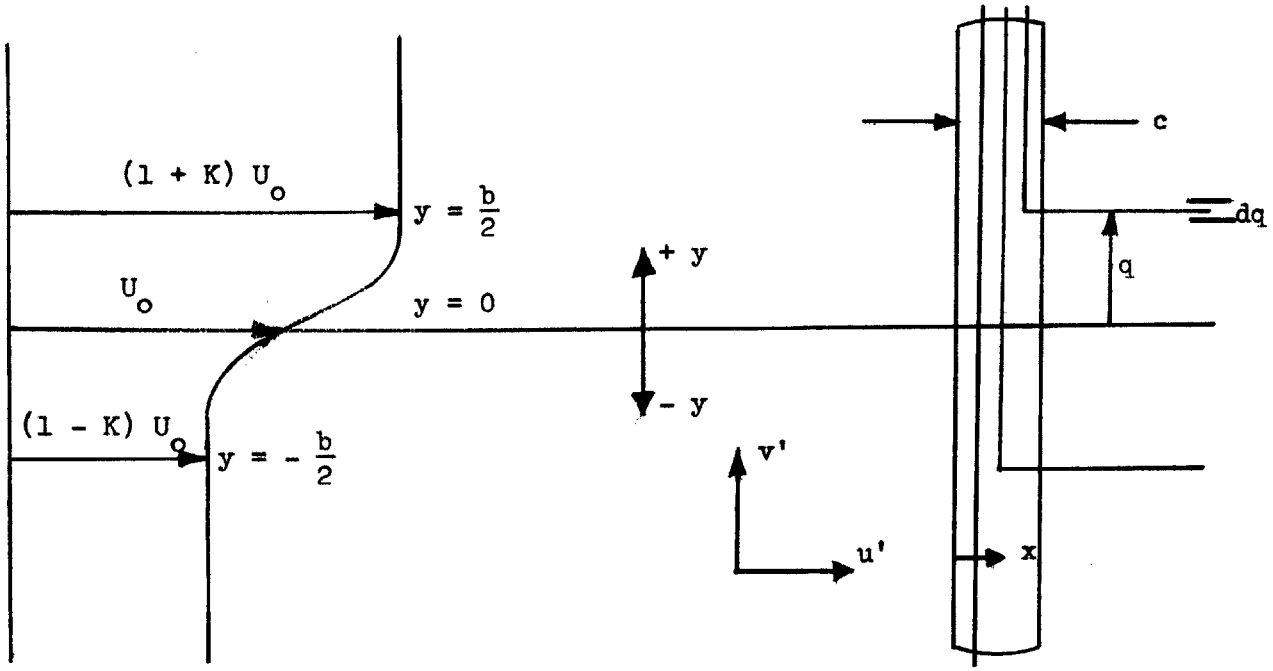

The velocity profile representing the primary flow approaching the airfoil upstream from infinity is given by:

$$U(y) = (1+K)\,U_o \qquad b/2 \le y < \infty \qquad (4\text{-}1a)$$

$$U(y) = U_o + \Omega_o y + Ay^3 + By^5 + \cdots \qquad -b/2 \le y \le b/2 \qquad (4\text{-}1b)$$

$$U(y) = (1-K)\,U_o \qquad -\infty < y \le -b/2 \qquad (4\text{-}1c)$$

4.1 Theoretical Development

We begin the analysis with the following result from Prandtl's lifting line theory:

$$dw_{LL}(y) = \frac{d\Gamma_{TR}(q)}{4\pi(y-q)}$$

where $w_{LL}(y)$ is the velocity normal to the plane of the airfoil at the lifting line induced by the circulation $d\Gamma_{TR}(q)$ trailing behind the airfoil. We then take

$$d\Gamma_{TR}(q) = \left[v_{TEP}(q) - v_{TES}(q) \right] dq$$

where v_{TEP} is the spanwise velocity along the trailing edge of the airfoil on the pressure side, and v_{TES} is the spanwise velocity along the trailing edge of the airfoil on the suction side.

Then

$$w_{LL}(y) = \frac{1}{4\pi} \int_{-\infty}^{+\infty} \frac{\left[v_{TEP}(q) - v_{TES}(q) \right] dq}{(y - q)}$$

The Euler equation of motion for the 'y' velocity component in frictionless and incompressible flow is the following:

$$u' \frac{\partial v'}{\partial x} + v' \frac{\partial v'}{\partial y} + w' \frac{\partial v'}{\partial z} = - \frac{1}{\rho} \frac{\partial P}{\partial y} \qquad (3\text{-}3)$$

taking $u' = U(y) + u \qquad v' = v \qquad w' = w$ (3-9)

where u, v, w are assumed small compared to U(y), the following linearized equation is obtained

$$U(y) \frac{\partial v}{\partial x} = - \frac{1}{\rho} \frac{\partial P}{\partial y} \qquad (3\text{-}11)$$

or $$v(x) = - \frac{1}{\rho U(y)} \int_0^x \frac{\partial P}{\partial y} dx + v(x = 0)$$

where x = 0 is taken as the leading edge of the airfoil. For thin airfoils with sharp leading edges $v(x = 0) \approx 0$

and $$v(x) = - \frac{1}{\rho U(y)} \int_0^x \frac{\partial P}{\partial y} dx$$

As a first approximation to the actual pressure distribution, we assume that the static pressure distribution about the airfoil can be written in terms of the familiar pressure coefficient as determined from two-dimensional airfoil section data, i.e.

$$P(x, y) = P_\infty + \frac{1}{2} \rho \, C_p(x) \, U^2(y)$$

and

$$\frac{\partial P}{\partial y} = \rho\, C_p(x)\, UU'$$

we then have

$$v(x) = -\frac{1}{\rho U(y)} \int_0^x \rho\, C_p(x)\, UU'\, dx = -U' \int_0^x C_p(x)\, dx$$

$$v_{TEP} = -U' \int_0^c C_{pp}(x)\, dx \; ; \quad v_{TES} = -U' \int_0^c C_{ps}(x)\, dx$$

where C_{pp} is the pressure side C_p and C_{ps} is the suction side C_p then

$$w_{LL}(y) = -\frac{\int_0^c \left[C_{pp}(x) - C_{ps}(x) \right] dx}{4\pi} \int_{-\infty}^{+\infty} \frac{U'(q)dq}{(y-q)}$$

but $$\int_0^c \left[C_{pp}(x) - C_{ps}(x) \right] dx = c\, C_{Lo} = 2\pi\, \alpha_o c$$

therefore

$$w_{LL}(y) = -\frac{c\alpha_o}{2} \int_{-\infty}^{+\infty} \frac{U'(q)dq}{(y-q)}$$

where C_{Lo} is the two-dimensional lift coefficient and α_o is the geometrical angle of attack. In accordance with the usual lifting line approximation based on the induced angle of attack

$$\frac{\Delta C_{Lo}}{C_{Lo}} = \frac{w_{LL}}{\alpha_o U} \tag{3-70}$$

where ΔC_{Lo} is defined as the change in the two-dimensional lift coefficient as before. We then have the result

$$\frac{\Delta C_{Lo}}{C_{Lo}} = \frac{-c}{2U(y)} \int_{-\infty}^{+\infty} \frac{U'(q)dq}{(y-q)} = \frac{-c}{2U(y)}\, I(y) \tag{4-2}$$

where $$I(y) = \int_{-\infty}^{+\infty} \frac{U'(q)dq}{(y-q)} \tag{4-3}$$

4.2 Solution of the Integral I(y)

The solution of the integral I(y) is determined in two regions - the inner solution within the shear layer $-\frac{b}{2} \le y \le \frac{b}{2}$ and the outer solution outside the shear layer. We first require that $U'(q) = 0$ at the edges of the shear layer and that $U'(q)$ is finite and continuous within the shear layer. Since $U'(q) = 0$ outside the shear layer, the integral becomes

$$I(y) = \int_{-b/2}^{b/2} \frac{U'(q)dq}{(y-q)} \qquad (4\text{-}4)$$

Inner Solution

In this region, the principal value of the integral is required. This can be readily evaluated if the following changes in variables are made:

$$y = -\frac{b}{2}\cos\theta \qquad 0 \le \theta \le \pi \qquad (4\text{-}5a)$$

$$q = -\frac{b}{2}\cos\phi \qquad 0 \le \phi \le \pi \qquad (4\text{-}5b)$$

and if $U'(q)$ is expressed as a series in $\sin n\phi$, i.e.

$$U'(q) = \Omega_o + 3Aq^2 + 5Bq^4 + 7Cq^6 + - - = \sum_n k_n \sin n\phi \qquad (4\text{-}6)$$

the integral then becomes

$$I = \int_0^{\pi} \frac{\left[\sum_n k_n \sin n\phi\right] \sin\phi \, d\phi}{\cos\phi - \cos\theta}$$

It can then be shown that

$$I = -\pi \sum_n k_n \cos n\theta \qquad (4\text{-}7)$$

The solution will now be carried through for a general 7th. degree polynomial in y

$$U(y) = U_o + \Omega_o y + Ay^3 + By^5 + Cy^7 \qquad (4\text{-}8)$$

Changing variables (substituting equation (4-5b)) in equation (4-6)

$$U'(\phi) = \Omega_o + A'\cos^2\phi + B'\cos^4\phi + C'\cos^6\phi = \sum_n k_n \sin n\phi$$

where

$$A' = \frac{3Ab^2}{4} \qquad B' = \frac{5Bb^4}{16} \qquad C' = \frac{7Cb^6}{64} \qquad (4\text{-}9)$$

Solving for k_n

$$k_n = \frac{2}{\pi}\int_0^{\pi} \left[\Omega_o + A'\cos^2\phi + B'\cos^4\phi + C'\cos^6\phi\right] \sin n\phi \, d\phi$$

or

$$k_n = \frac{2}{\pi}\left(\Omega_o I_{(o)} + A'I_{(2)} + B'I_{(4)} + C'I_{(6)}\right) \qquad (4\text{-}10)$$

where

$$I_{(p)} = \int_0^{\pi} \cos^p\phi \sin n\phi \, d\phi \qquad (p \text{ even}) \qquad (4\text{-}11)$$

The integral $I_{(p)}$ exists only for n odd and is given by the following expression

$$I_{(p)} = (-1)^{n+1/2} \left[\frac{\cos^{p+1}\phi}{p+1} + \sum_{k=1}^{n-1/2} (-1)^k \frac{[n^2-1]\,[n^2-9]\,-\,-\,-\,[n^2-(2k-1)^2]\,\cos^{2k+p+1}\phi}{(2k)!\;(2k+p+1)} \right]_0^{\pi} \tag{4-12}$$

Outer Solution

The outer solution may be evaluated easily by the substitution

$$\frac{1}{y-q} = \frac{1}{y} + \frac{q}{y^2} + \frac{q^2}{y^3} + \frac{q^3}{y^4} + \frac{q^4}{y^5} + - - -$$

since in this region

$$|q| < |y|$$

For a 7th. degree polynomial in y (equation (4-8)) equation (4-4) becomes

$$I = \int_{-b/2}^{b/2} \left[\Omega_o + 3Aq^2 + 5Bq^4 + 7Cq^6\right] \left[\frac{1}{y} + \frac{q}{y^2} + \frac{q^2}{y^3} + - - -\right] dq$$

This, after integration, becomes

$$\begin{aligned} I(y) = {} & 2\Omega_o \left[1/y^* + 1/3y^{*3} + 1/5y^{*5} + - - -\right] \\ & + 6A \left(\frac{b}{2}\right)^2 \left[1/3y^* + 1/5y^{*3} + 1/7y^{*5} + - - -\right] \\ & + 10B \left(\frac{b}{2}\right)^4 \left[1/5y^* + 1/7y^{*3} + 1/9y^{*5} + - - -\right] \\ & + 14C \left(\frac{b}{2}\right)^6 \left[1/7y^* + 1/9y^{*3} + 1/11y^{*5} + - - -\right] \end{aligned} \tag{4-13}$$

where $$y^* = y/\left(\frac{b}{2}\right) \tag{4-14}$$

4.3 Solution for Two Parameter 5th. Degree Polynomial

A two parameter, 5th. degree polynomial in y satisfying the boundary conditions at $y = \pm \frac{b}{2}$ and meeting the desired velocity profile requirements from equation (4-1) is as follows:

$$U(y) = U_o + \Omega_o y + \left[\frac{5KU_o}{2} - \Omega_o b\right] \frac{y^3}{\left(\frac{b}{2}\right)^3} + \left[\frac{\Omega_o b}{2} - \frac{3KU_o}{2}\right] \frac{y^5}{\left(\frac{b}{2}\right)^5} \tag{4-15}$$

where K and Ω_o are arbitrary.

Substituting the appropriate constants from equation (4-15) as defined in equations (4-8) and (4-9) into equation (4-10)

$$k_n = \frac{2}{\pi}\left[\Omega_o\left[I_{(0)}(n) - 6I_{(2)}(n) + 5I_{(4)}(n)\right] + \frac{15KU_o}{b}\left[I_{(2)}(n) - I_{(4)}(n)\right]\right]$$

or
$$k_n = \frac{2}{\pi}\left[\Omega_o\alpha(n) + \frac{15KU_o}{b}\beta(n)\right] \tag{4-16}$$

where
$$\alpha(n) = I_{(0)}(n) - 6I_{(2)}(n) + 5I_{(4)}(n) \tag{4-17a}$$

$$\beta(n) = I_{(2)}(n) - I_{(4)}(n) \tag{4-17b}$$

Tabulated values of $\alpha(n)$ and $\beta(n)$ for the first 10 values of n are as follows:

n	$\alpha(n)$	$\beta(n)$	n	$\alpha(n)$	$\beta(n)$
1	0	+0.26667	11	+0.01425	-0.00347
3	-1.21905	+0.19047	13	+0.00807	-0.00199
5	+0.40630	-0.08888	15	+0.00531	-0.00130
7	+0.07384	-0.01731	17	+0.00343	-0.00085
9	+0.02837	-0.00683	19	+0.00228	-0.00058

The complete inner solution is then given by

$$\frac{\Delta C_{Lo}}{C_{Lo}} = \frac{c}{U(y)}\sum_n\left[\Omega_o\alpha(n) + \frac{15KU_o}{b}\beta(n)\right]\cos n\theta$$

where
$$\theta = \cos^{-1}\left[\frac{-y}{(\frac{b}{2})}\right] \quad -\frac{b}{2} \le y \le \frac{b}{2} \tag{4-18}$$

After substitution of the required constants into equation (4-13) and simplification, the complete outer solution becomes the following:

$$\frac{\Delta C_{Lo}}{C_{Lo}} = \frac{\mp c}{2U(\pm y)}\left[2\Omega_o\left[\frac{1}{2}\ln\frac{(1+\mu)}{(1-\mu)} - \sum_{n=1}^{\infty}\frac{\mu^{n}(n+14)}{(n+2)(n+4)}\right] + \frac{60KU_o}{b}\sum_{n=1}^{\infty}\frac{\mu^n}{(n+2)(n+4)}\right] \tag{4-19}$$

for $\mu < 1$ where $\mu = |(\frac{b}{2})/y| = |1/y^*|$

Note that the sign of $\Delta C_{Lo}/C_{Lo}$ is negative for y positive. The inner and outer solutions are equivalent at $y = \pm(\frac{b}{2})$ ($y^* = \pm 1$) as can be verified by numerical substitution. The form of the outer solution at these shear layer boundary points is the following:

$$\frac{\Delta C_{Lo}}{C_{Lo}} = \frac{\mp c}{2U(\pm b/2)}\left[\frac{10KU_o}{b} - \frac{4\Omega_o}{3}\right]$$

4.4 Solution for Two Parameter, 7th. Degree Polynomial

Using equations (4-2) and (4-4), we can, after differentiating, obtain the result

$$\frac{d}{dy}\left(\frac{\Delta C_{Lo}}{C_{Lo}}\right) = \frac{cU'(y)}{2U^2(y)} \int_{-b/2}^{b/2} \frac{U'(q)dq}{(y-q)} + \frac{c}{2U(y)} \int_{-b/2}^{b/2} \frac{U'(q)dq}{(y-q)^2}$$

The last term in this equation may be integrated by parts, and, through the use of the boundary condition $U'(\pm\frac{b}{2}) = 0$, the equation becomes

$$\frac{d}{dy}\left(\frac{\Delta C_{Lo}}{C_{Lo}}\right) = -\frac{\Delta C_{Lo}}{C_{Lo}} \frac{U'(y)}{U(y)} - \frac{c}{2U(y)} \int_{-b/2}^{b/2} \frac{U''(q)dq}{(y-q)}$$

or $$\frac{d}{dy}\left(U(y)\,\frac{\Delta C_{Lo}}{C_{Lo}}\right) = \frac{-c}{2} \int_{-b/2}^{b/2} \frac{U''(q)}{(y-q)}\,dq$$

It is then possible to assure continuity of the slope of $\frac{\Delta C_{Lo}}{C_{Lo}}$ if $U''(-\frac{b}{2}, +\frac{b}{2}) = 0$.

A two parameter, 7th. degree polynomial in y satisfying the required boundary conditions at $y = \pm(\frac{b}{2})$ with the additional requirement that $U'' = 0$ at $y = \pm(\frac{b}{2})$ and meeting the desired velocity profile requirements from equation (4-1) is as follows:

$$U(y) = U_o + \Omega_o y + \left[\frac{35KU_o}{8} - \frac{3\Omega_o b}{2}\right] \frac{y^3}{(\frac{b}{2})^3} + \left[\frac{-42KU_o}{8} + \frac{3\Omega_o b}{2}\right] \frac{y^5}{(\frac{b}{2})^5} + \left[\frac{15KU_o}{8} - \frac{\Omega_o b}{2}\right] \frac{y^7}{(\frac{b}{2})^7} \qquad (4\text{-}20)$$

where K and Ω_o are arbitrary as before.

Substituting the appropriate constants from equation (4-20) as defined in equations (4-8) and (4-9) into equation (4-10)

$$k_n = \frac{2}{\pi}\left[\Omega_o\left[I_{(0)}(n) - 9I_{(2)}(n) + 15I_{(4)}(n) - 7I_{(6)}(n)\right] + \frac{105KU_o}{4b}\left[I_{(2)}(n) - 2I_{(4)}(n) + I_{(6)}(n)\right]\right]$$

or $$k_n = \frac{2}{\pi}\left[\Omega_o \gamma(n) + \frac{105KU_o}{4b}\,\delta(n)\right] \qquad (4\text{-}21)$$

where

$$\gamma(n) = I_{(0)}(n) - 9I_{(2)}(n) + 15I_{(4)}(n) - 7I_{(0)}(n) \qquad (4\text{-}22a)$$

$$\delta(n) = I_{(2)}(n) - 2I_{(4)}(n) + I_{(6)}(n) \qquad (4\text{-}22b)$$

Tabulated values of $\gamma(n)$ and $\delta(n)$ for the first 10 values of n are as follows:

n	$\gamma(n)$	$\delta(n)$	n	$\gamma(n)$	$\delta(n)$
1	0	+0.15238	11	-0.00292	+0.00047
3	-0.81259	+0.05078	13	-0.00129	+0.00020
5	+0.66482	-0.08772	15	-0.000**	+0.000**
7	-0.10236	+0.01528	17	-0.000**	+0.000**
9	-0.01288	+0.00199	19	-0.000**	+0.000**

The complete inner solution is then given by

$$\frac{\Delta C_{Lo}}{C_{Lo}} = \frac{c}{U(y)} \sum \left[\Omega_o \gamma(n) + \frac{105KU_o}{4b} \delta(n) \right] \cos n\,\theta \qquad (4\text{-}23)$$

where $\theta = \cos^{-1}\left[\frac{-y}{(b/2)}\right]$ $\qquad -\frac{b}{2} \leq y \leq \frac{b}{2}$

After substitution of the required constants into equation (4-13) and simplification, the complete outer solution becomes the following:

$$\frac{\Delta C_{Lo}}{C_{Lo}} = \frac{\mp c}{2U(\pm y)} \left[2\Omega_o \left[\frac{1}{2} \ln \frac{(1+\mu)}{(1-\mu)} - \sum_{n=1}^{\infty} \frac{\mu^n (n^2+12n+92)}{(n+2)(n+4)(n+6)} \right] + \frac{420KU_o}{b} \sum_{n=1}^{\infty} \frac{\mu^n}{(n+2)(n+4)(n+6)} \right] \qquad (4\text{-}24)$$

for $\mu < 1$ where $\mu = |(\frac{b}{2})/y| = |1/y^*|$ The sign convention is as before.

The inner and outer solutions are equivalent at the edges of the shear layer where the outer solution becomes the following:

$$\frac{\Delta C_{Lo}}{C_{Lo}} = \frac{\mp c}{2U(\pm \frac{b}{2})} \left[\frac{7KU_o}{b} - \frac{8\Omega_o}{15} \right]$$

This procedure may be extended to include velocity profiles for any degree odd polynomial in y with the appropriate boundary conditions.

The form of the outer solution for I(y) is particularly amenable to superposition for the calculation of images. In this manner, the effects of plane boundaries in the 'irrotational' region of the flow may be considered. In the physical sense these boundaries would represent wind tunnel walls or internal passage boundaries.

It is also interesting to note that the above solutions for I(y) may be superimposed to include symmetrical shear velocity profiles such as wakes or jets.

Tabulated values of $I_{(0)}(n)$, $I_{(2)}(n)$, $I_{(4)}(n)$ and $I_{(6)}(n)$ for the first 10 values of n will be found at the end of this section. The requirements that the inner and outer solutions must match at $y = \pm(\frac{b}{2})$ yields the following relations which may be used to check the accuracy and the convergence of the numerical values:

$$\sum_{n=1}^{\infty} (I_{(0)}(n) - I_{(2)}(n)) = 1 \qquad (n \text{ odd})$$

$$\sum_{n=1}^{\infty} (I_{(2)}(n) - I_{(4)}(n)) = 1/3 \qquad (n \text{ odd})$$

$$\sum_{n=1}^{\infty} (I_{(4)}(n) - I_{(6)}(n)) = 1/5 \qquad (n \text{ odd})$$

4.5 Relation to Lifting Line Theory for Wings of Finite Span

To investigate the relationship between this approximation and the classical lifting line theory for wings of finite span, we can write as a general expression for the strength of the trailing vortex sheet

$$-\frac{d\Gamma_{TR}}{dy} = \frac{1}{\rho U}\frac{dL}{dy} = \frac{1}{2U}\frac{d}{dy}\left[U^2 c\, C_{Lo}\left(1 + \frac{\Delta C_{Lo}}{C_{Lo}}\right)\right]$$

therefore,

$$w_{LL}(y) = -\frac{1}{8\pi}\int_{-\ell/2}^{\ell/2} \frac{d}{dq}\left[c\, C_{Lo} U^2\left(1 + \frac{\Delta C_{Lo}}{C_{Lo}}\right)\right]\frac{dq}{U(q)(y-q)}$$

and $$\frac{\Delta C_{Lo}}{C_{Lo}} = \frac{-1}{4C_{Lo}U(y)}\int_{-\ell/2}^{\ell/2} \frac{d}{dq}\left[c\, C_{Lo}\, U^2\left(1 + \frac{\Delta C_{Lo}}{C_{Lo}}\right)\right]\frac{dq}{U(q)(y-q)} \qquad (4\text{-}25)$$

Equation (4-25) may be thought of as a modified lifting line equation (for variable c, C_{Lo}, and U) for shear flows.

For the case in which C_{Lo} and c are constant, equation (4-25) becomes

$$\frac{\Delta C_{Lo}}{C_{Lo}} = \frac{-c}{4U(y)}\int_{-\ell/2}^{\ell/2} \frac{d}{dq}\left[U^2\left(1 + \frac{\Delta C_{Lo}}{C_{Lo}}\right)\right]\frac{dq}{U(q)(y-q)} \qquad (4\text{-}26)$$

For airfoils of infinite span, if we neglect $\frac{\Delta C_{Lo}}{C_{Lo}}$ as being small compared to 1, equation (4-26) becomes

$$\frac{\Delta C_{Lo}}{C_{Lo}} = \frac{-c}{2U(y)} \int_{-\infty}^{+\infty} \frac{U'(q)}{(y-q)}\, dq \qquad (4\text{-}2)$$

This is the original result obtained in the theoretical development of Section (4.1). We now consider in greater detail the term (from equation (4-26))

$$\frac{d}{dq}\left[U^2\left(1 + \frac{\Delta C_{Lo}}{C_{Lo}}\right)\right]$$

This can be written in the equivalent form

$$2U^2\left[\frac{U'}{U}\left(1 + \frac{\Delta C_{Lo}}{C_{Lo}}\right) + \frac{1}{2}\frac{d}{dq}\left(\frac{\Delta C_{Lo}}{C_{Lo}}\right)\right]$$

For airfoils of infinite span, the assumption that $\frac{\Delta C_{Lo}}{C_{Lo}}$ is small compared to 1 is acceptable, but neglect of the term $\frac{1}{2}\frac{d}{dq}(\Delta C_{Lo}/C_{Lo})$ compared to U'/U is questionable since, in general, these terms may be of the same order. For wings of finite span, neither of these approximations is acceptable since both $\Delta C_{Lo}/C_{Lo}$ and $d/dq(\Delta C_{Lo}/C_{Lo})$ are large, in particular at the wing tips $\Delta C_{Lo}/C_{Lo} = -1$.

It is instructive to verify that the general equation (4-25) becomes the classical lifting line integro-differential equation for the case where U = constant:

$$\frac{\Delta C_{Lo}}{C_{Lo}} = \frac{-1}{4C_{Lo}} \int_{-\ell/2}^{\ell/2} \frac{d}{dq}\left[c\, C_{Lo}\left(1 + \frac{\Delta C_{Lo}}{C_{Lo}}\right)\right] \frac{dq}{(y-q)}$$

which becomes

$$\Gamma(y) = \frac{cUC_{Lo}}{2} - \frac{c}{4} \int_{-\ell/2}^{\ell/2} \frac{d\Gamma(q)}{(y-q)} \qquad (4\text{-}27)$$

using the substitution

$$\Gamma(y) = \frac{cUC_{Lo}}{2}\left(1 + \frac{\Delta C_{Lo}}{C_{Lo}}\right)$$

It is of fundamental importance to note that in this approximate analysis no consideration is given to vorticity in the flow other than that of the usual trailing vortex sheet resulting from the variation of L(y) along the span. There is, therefore, an incompleteness in the description of the true kinematics of the flow.

Theoretical results obtained through the use of this first theoretical approximation are presented in Appendix I.

TABLE $I_{(p)}(n)$

n	$I_{(0)}(n)$	$I_{(2)}(n)$	$I_{(4)}(n)$	$I_{(6)}(n)$
1	2.00000	0.66667	0.40000	0.28571
3	0.66667	0.93333	0.74286	0.60317
5	0.40000	0.43810	0.52698	0.52814
7	0.28571	0.29842	0.31573	0.34832
9	0.22222	0.22800	0.23483	0.24365
11	0.18182	0.18492	0.18839	0.19233
13	0.15385	0.15573	0.15772	0.15991
15	0.13452	0.13452	0.13582	0.13717
17	0.11765	0.11847	0.11932	0.12024
19	0.10526	0.10588	0.10646	0.10710

$$\sum_{n=1}^{19} (I_{(0)}(n) - I_{(2)}(n)) = 1.00247$$

$$\sum_{n=1}^{19} (I_{(2)}(n) - I_{(4)}(n)) = 0.33593$$

$$\sum_{n=1}^{19} (I_{(4)}(n) - I_{(6)}(n)) = 0.20237$$

5. EXPERIMENTAL PROGRAM

The experimental phase of this investigation was initiated with experiments on shear flows about a circular cylinder. These experiments were performed in a very low speed 'smoke flow' tunnel, and, largely because of flow separation problems, the results obtained consisted of visual observations of a qualitative nature which were recorded on photographs. The main part of the experimental program consisted of measurements of local lift coefficients and spanwise distributions of lift on thin symmetrical airfoils in monotonic shear flows consisting of a layer of rotational flow bounded by two layers of relatively uniform flow. Data was obtained for three different geometries based on the ratio of the airfoil chord to the shear layer thickness (c/2s).

5.1 Smoke Flow Experiments

The smoke flow experiments were carried out in a very low speed wind tunnel (velocities of the order of 1 ft/sec) which was designed specifically for this type of work by R. G. Schwind[27]. The test section for the shear flow experiments was moved upstream of Schwind's original test section, and a canvas enclosure was placed over it to reduce extraneous light and reflection on the Plexiglas walls and roof of the 8" by 16" rectangular duct for photographic purposes. The photographs were taken with a Polaroid camera; the illumination was supplied by two stage lights which were positioned above and on the side of the test section.

The smoke was produced in a 'smoke generator' described by Schwind[27] in which vacuum pump oil is heated to approximately 250°C in an electrically heated stainless steel tube. The temperature of the smoke is essentially that of the surrounding air at the injection point, and, as reported by Schwind, the density of the smoke is within 1% of the density of the air at the same pressure and temperature. The probes used to introduce the smoke into the shear flow consisted of a horizontal rake that could be traversed

across the duct vertically, and a vertical rake that could be traversed across the duct horizontally. The disturbance of the rakes which were of small diameter tubing was negligible in comparison to the disturbance of the 2" diameter cylinder. The shear flow was produced by inserting a non-uniform thickness of honeycomb (varying in thickness from 3" to 6") upstream of the test section and downstream of the turbulence reducing screens in the tunnel. The velocity profile produced varied from approximately 1.0 ft/sec to 1.5 ft/sec over a shear layer thickness of apprxomately 3". The shear layer was bounded above and below by layers of relatively uniform flow. (Refer to sketch of velocity profile on page 39).

Velocity measurements were made with a portable hot-wire set; the velocity profile measurements indicated a decay in the ratio of maximum to minimum velocities in the shear flow of about 10% in a streamwise flow length of approximately 3'. The observed downward displacement of a streamline on the high velocity side of the shear layer in the vertical plane of symmetry of the flow was approximately 1/2 cylinder diameter, and the observed origin of the downward motion of this streamline was approximately 3 cylinder diameters upstream of the disturbance. The complex nature of shear flows about cylindrical bodies where viscous effects must be taken into consideration both in the boundary layers of the body and in the separated flow downstream of it is discussed by Toomre[28].

A photograph of the apparatus and the smoke generator is shown in Figure 41 in Appendix VI. A close-up of the aluminum honeycomb and the test cylinder is shown in the second photograph of Figure 41. The two photographs in Figure 42 show the horizontal and the vertical smoke rakes in place in the test section. The warping of the Bernoulli surfaces can be seen clearly in the first photograph.

The photographs in Figure 43 indicate the displacement effect in the plane of symmetry of the cylinder and the extent of the separation of the

flow downstream of the cylinder. The upwards flow of fluid in the separated region is due in part to the pressure gradient caused by the disturbance of the cylinder and wake in the shear flow, but there is some contribution from buoyancy effects resulting from a change in density of the fluid in the wake. The change in density arises from the heating of the cylinder and the relatively stagnant fluid in the separated region by the lights used to illuminate the test section. This 'thermal convection effect' was predominant in convecting boundary layer fluid upwards in smoke flow experiments about thin airfoils at zero angle of attack when no separation was present. The second photograph in Figure 43 indicates that the displacement effect is propagated into the layer of low velocity uniform flow from the shear layer above.

The streamline patterns in the surfaces of constant stagnation pressure (disregarding the unsteadiness near the separated regions) are shown in the two photographs in Figure 44. The smoke filaments in the first photograph originate in the high velocity uniform layer above the shear layer. The smoke filaments in the second photograph originate within, but on the low velocity side of the shear layer.

5.2 Low Speed Wind Tunnel Experiments

The low speed wind tunnel used for the thin airfoil experiments was designed by S. R. Montgomery[29]. The wind tunnel is fitted with a special test section designed originally for cascade work although this equipment was not used in the shear flow experiments. A rectangular fibreboard channel was inserted into the test section, and a flow by-pass (a feature of the original test section design) was sealed off with a hinged flap. The side walls of the channel were fitted with circular inserts which supported the airfoils and enabled the angle of attack to be varied. Felt bearings between the airfoil surface and the fibreboard inserts enabled the airfoils to be traversed across the test section in a spanwise direction. An overall

view of the experimental apparatus with the large chord airfoil in position in the test section is shown in Figure 45 in Appendix VI.

The honeycomb structure used to produce the sheared velocity profile was inserted upstream of the test section and was supported from the downstream side by the rectangular channel. The problems encountered in the design and the mechanical shaping of the honeycomb and a suggested design procedure are discussed in detail in Appendix IV. The frontal area of the honeycombs used was 20" by 30" (the inside dimensions of the test section), and the streamwise thickness varied from approximately 4" to 16". During the course of this investigation, two honeycombs were used - the first to produce a shear layer approximately 10" thick which will be referred to as the 'large shear layer', and the second to produce a shear layer approximately 4" thick referred to as the 'small shear layer'. The two honeycombs are shown in the photographs in Figure 46. No appreciable decay of the shear profiles was noted in the flow length of the test section which is consistent with the observations of Owen and Zienkiewicz[30].

The airfoils used were NACA 0012 symmetrical profiles with chords of 3" and 6" and spans in excess of 5' which enabled the 30" test section to be traversed with one chordwise distribution of static pressure taps. The pressure taps were located on both surfaces of the airfoils, the 3" chord airfoil having a total of 29 taps and the 6" chord airfoil having a total of 26 taps. The geometry of the airfoils affected the positioning of the pressure taps; the first tap was located at about 4% chord on the 3" chord airfoil and at about 2% chord on the 6" chord airfoil. The pressure taps were staggered on opposite sides of the trailing edges because of the thinness of the section in this region. The pressure taps were drilled from the finished surfaces of the airfoils into tubes that had been inserted into milled spanwsie slots.

The 3" chord airfoil was fabricated by butt soldering four brass sec-

tions end to end after the individual sections had been machined on a blade profiler. The 6" chord airfoil was assembled from 4 leading edge and 4 trailing edge aluminum sections which were attached to a steel center support. These sections were staggered along the span of the airfoil. In both cases, the pressure tube slots were milled after the airfoils were assembled to eliminate alignment problems. The coordinates of the blade profile are tabulated in Reference 31. A full size sketch of the 6" chord profile is shown below.

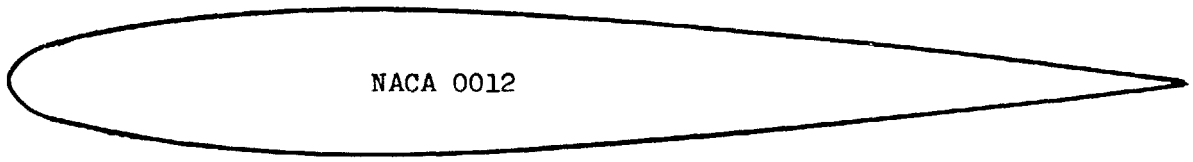

The two airfoils are shown in the first photograph in Figure 47.

The second photograph in Figure 47 shown the probes that were used in the experimental work (in addition to the airfoils). A triple pronged total pressure probe with a direction sensitive yaw probe in the center was used to measure the total pressure distribution in the undisturbed flow. The three total pressure readings gave an indication of the local departure from the desired two-dimensional flow. This non-uniformity of total pressure in planes normal to the span of the airfoil was negligibly small in the small shear layer experiments, but of a greater magnitude in the large shear layer experiment. The largest value measured being approximately 10% of the local average total pressure. The local non-uniformities of total pressure in this case were attributed to the particular type of honeycomb used (refer to Appendix IV).

A single yaw probe was positioned downstream of the airfoil and was used to measure local total pressures in planes normal to the span of the

airfoil when the airfoil was in position at zero angle of attack (excluding the region of the thin wake behind the airfoil). These measurements of total pressure were used in the calculation of the local pressure coefficient and agreed well with the measurements of total pressure in the undisturbed flow. The angular position of the airfoil with respect to the tunnel axis was measured through the use of a protractor (see Figure 47) which was fitted over the chord of the airfoil and layed flat along the tunnel wall. This device had a least count of $1/4^{\circ}$ and readings could be taken to within one half of this magnitude.

The large shear layer experiment was complicated somewhat by axial swirl in the flow, but the amount of swirl was reduced by about a factor of four in the small shear layer experiments. The airfoil itself was used to measure the swirl in terms of the location of the local spanwise zero lift angle with respect to a selected reference position. The results of these measurements for both the large and small shear layers are presented in Figure 4 on the following page.

Because of the local non-uniformities in total pressure and the axial swirl, and, in addition, to reduce the magnitude of the effects of extraneous error, all pressure distributions were measured in both clockwise and counter-clockwise directions from the local zero lift position. The agreement between the clockwise and counter-clockwise lift coefficient data will be shown in the figures following.

Before beginning the shear flow experiments, measurements of the characteristics of the airfoils in a uniform flow downstream of a uniform piece of 4" thick honeycomb were made. It was found that to achieve a linear relation between C_{Lo} and α_o, the airfoils required trip wires which were instaled at the 10% chord position on both surfaces. The uniform flow experiments were performed for two Reynolds numbers for the 3" chord airfoil since in a shear flow of the type considered here there is a change in local Reynolds

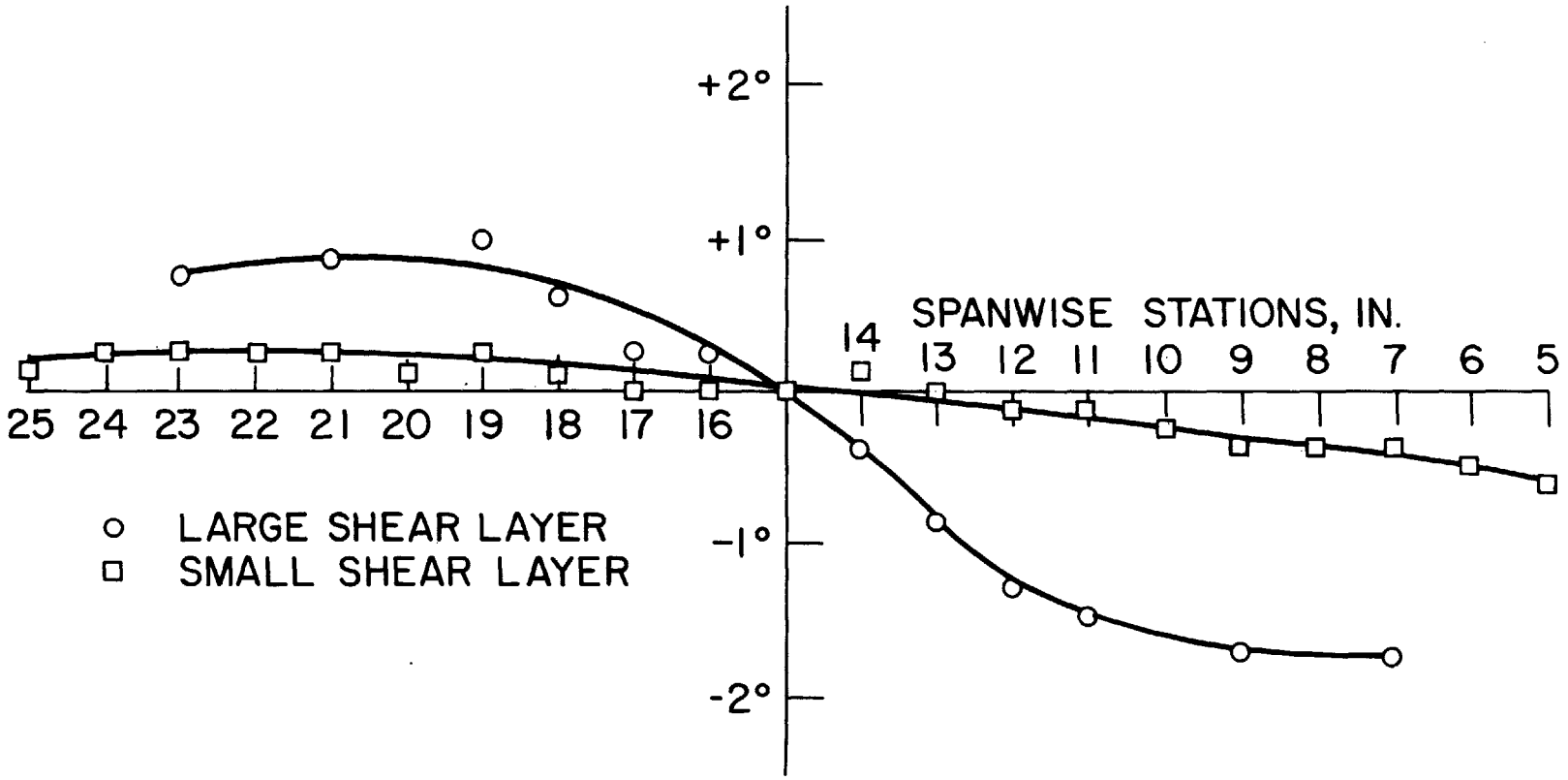

FIGURE 4 VARIATION OF LOCAL SPANWISE ZERO LIFT ANGLE RELATIVE TO 15 IN. POSITION.

number of a factor of approximately 1.5 along the span of the airfoil. The results of the uniform flow experiments are presented in Figure 5. Because Reynolds number effects were found to be small as a result of the use of the trip wires, the average curves (shown as the dotted lines in Figure 5) were used as the reference curves for the shear flow experiments. The average curves are represented approximately by the relation

$$C_{Lo} = (0.91)\, 2\pi\, \alpha_o$$

The data shown in Figure 5 includes the stall region (beyond the relatively linear portion of the C_{Lo}, α_o curve), and, although this region was investigated in some of the shear flow experiments, for the most part, data was taken in the range of from 2° to 8° angle of attack inclusively.

5.3 Large Shear Layer - Small Chord Experiment

The experimental velocity profile for the large shear layer experiment is shown in Figure 6. The velocity variation is from approximately 57 ft/sec to 95 ft/sec over a shear layer thickness of about 10". Various analytical approximations were used to describe the velocity profile, and these are indicated also in Figure 6. The linear fits for two values of the shear layer thickness (2s) were approximations for use with the lifting line theory, and the polynomial fit was used in conjunction with the first theoretical approximation. The magnitudes of the local non-uniformities are clearly indicated in Figure 6, and it is apparent that some uncertainly is involved in establishing definite regions of shear and uniform flow.

Measurements of local lift coefficients were made at various spanwise stations excluding the regions of flow near the tunnel walls. The averaged results from the clockwise and counter-clockwise measurements are presented in Figure 7 and Figure 8. The measurements were made with respect to the local spanwise zero lift angle. The experimental results indicate a maximum local lift coefficient at the low velocity edge of the shear layer (9" station) and a minimum local lift coefficient at the high velocity edge of the shear layer (19" station). The local lift coefficient decreased monotonic-

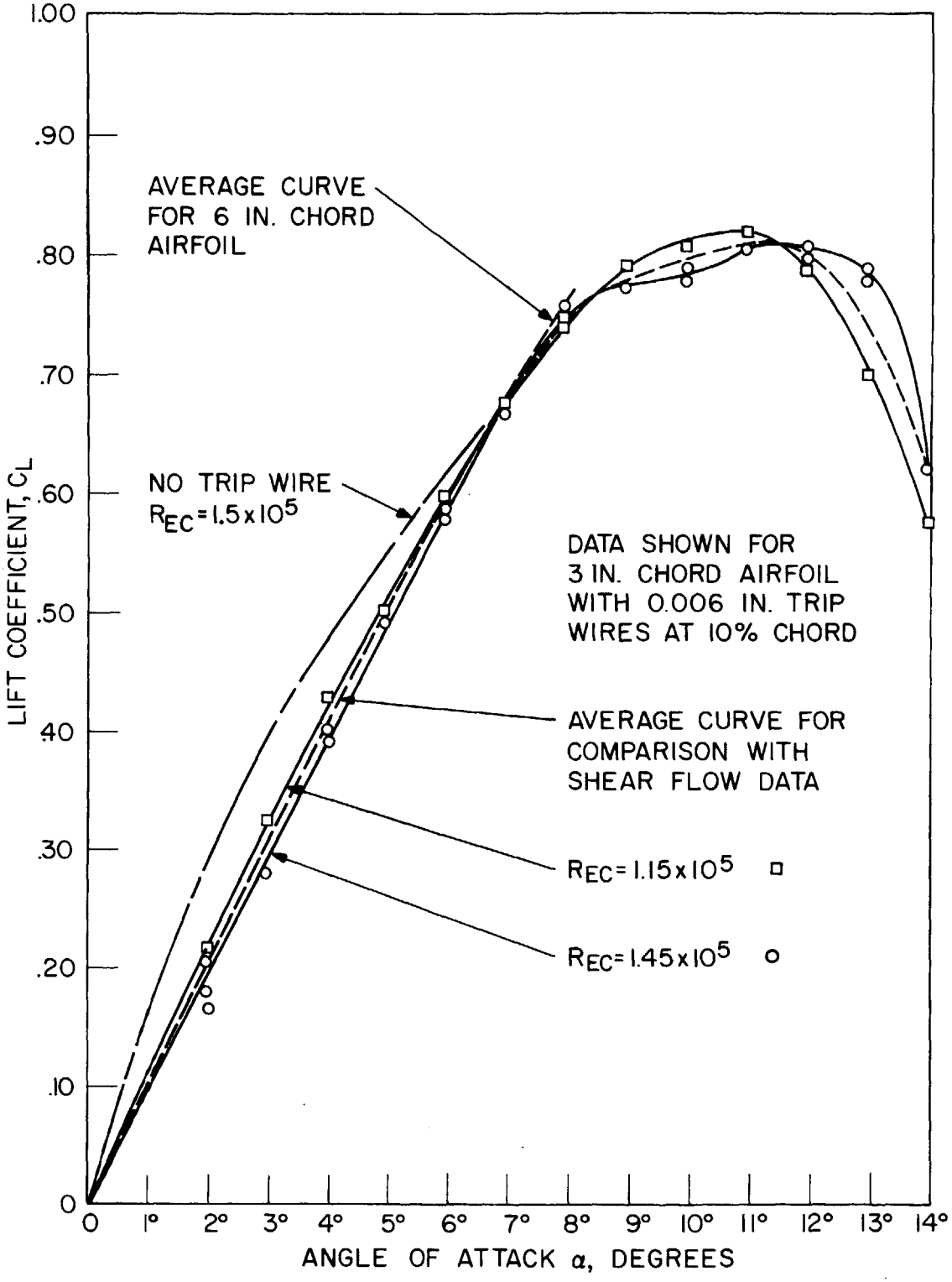

FIGURE 5 PERFORMANCE OF NACA 0012 AIRFOIL IN UNIFORM FLOW-EFFECT OF REYNOLDS NUMBER.

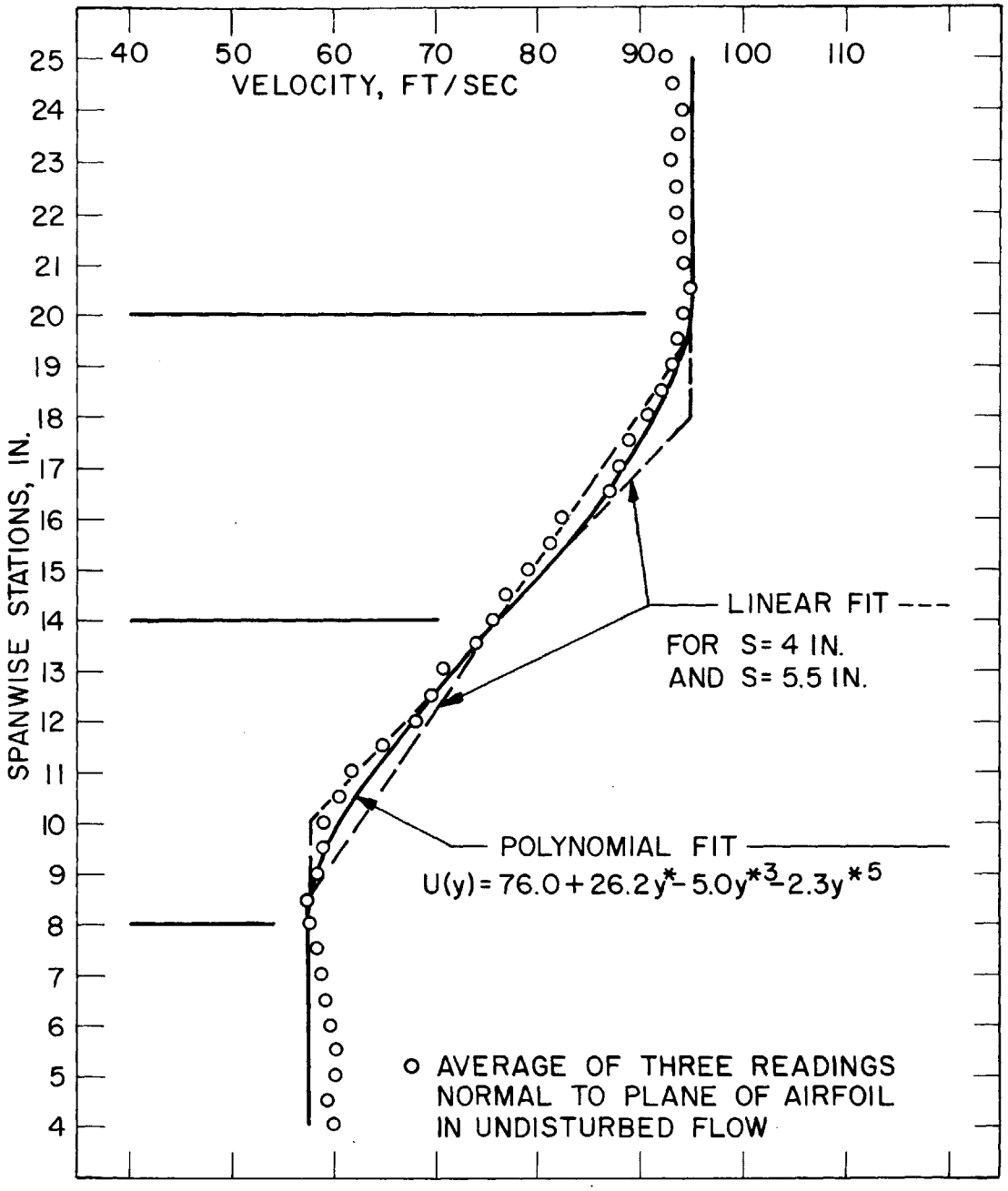

FIGURE 6 EXPERIMENTAL SHEAR FLOW VELOCITY PROFILE LARGE SHEAR LAYER.

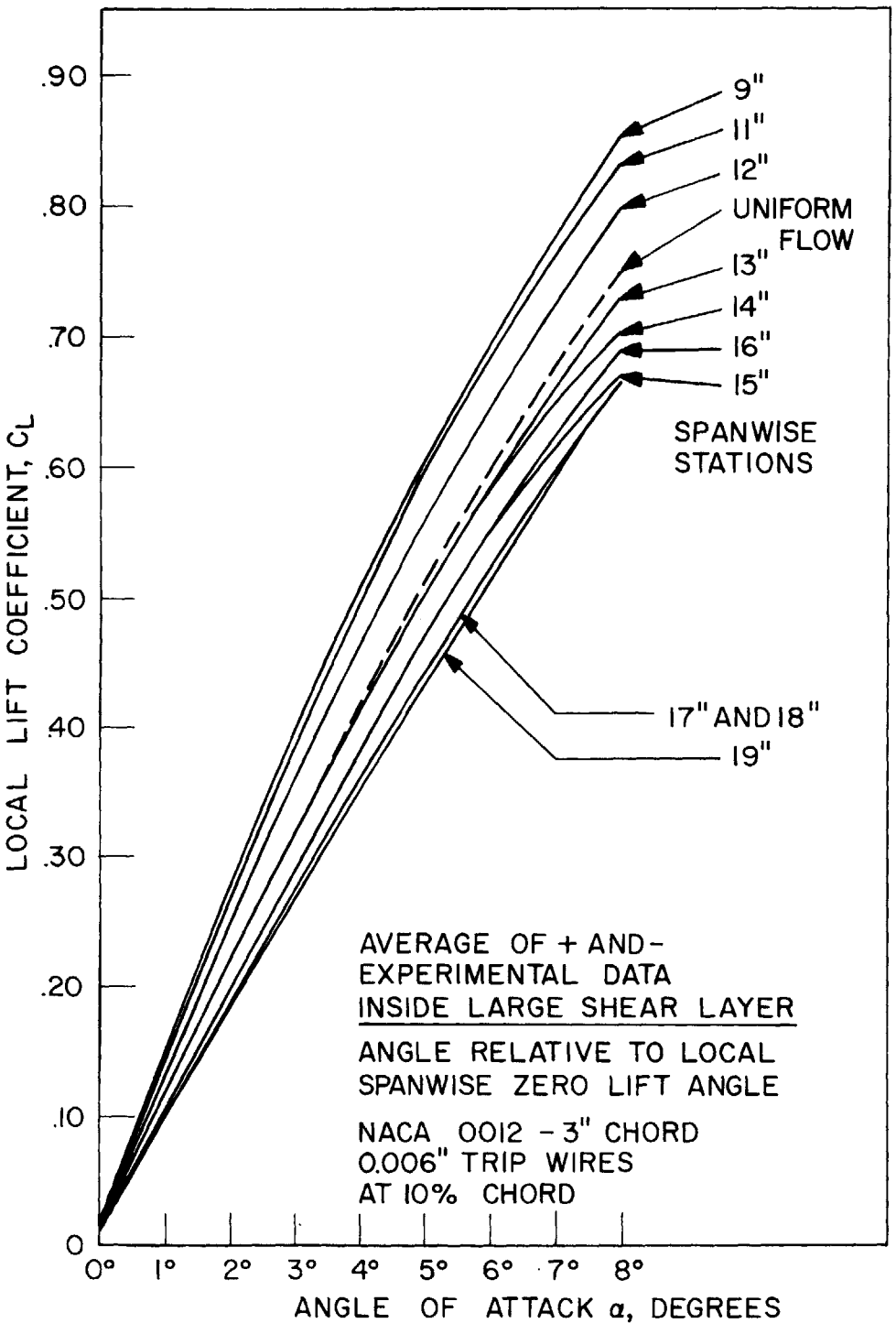

FIGURE 7 AIRFOIL IN SHEAR FLOW.

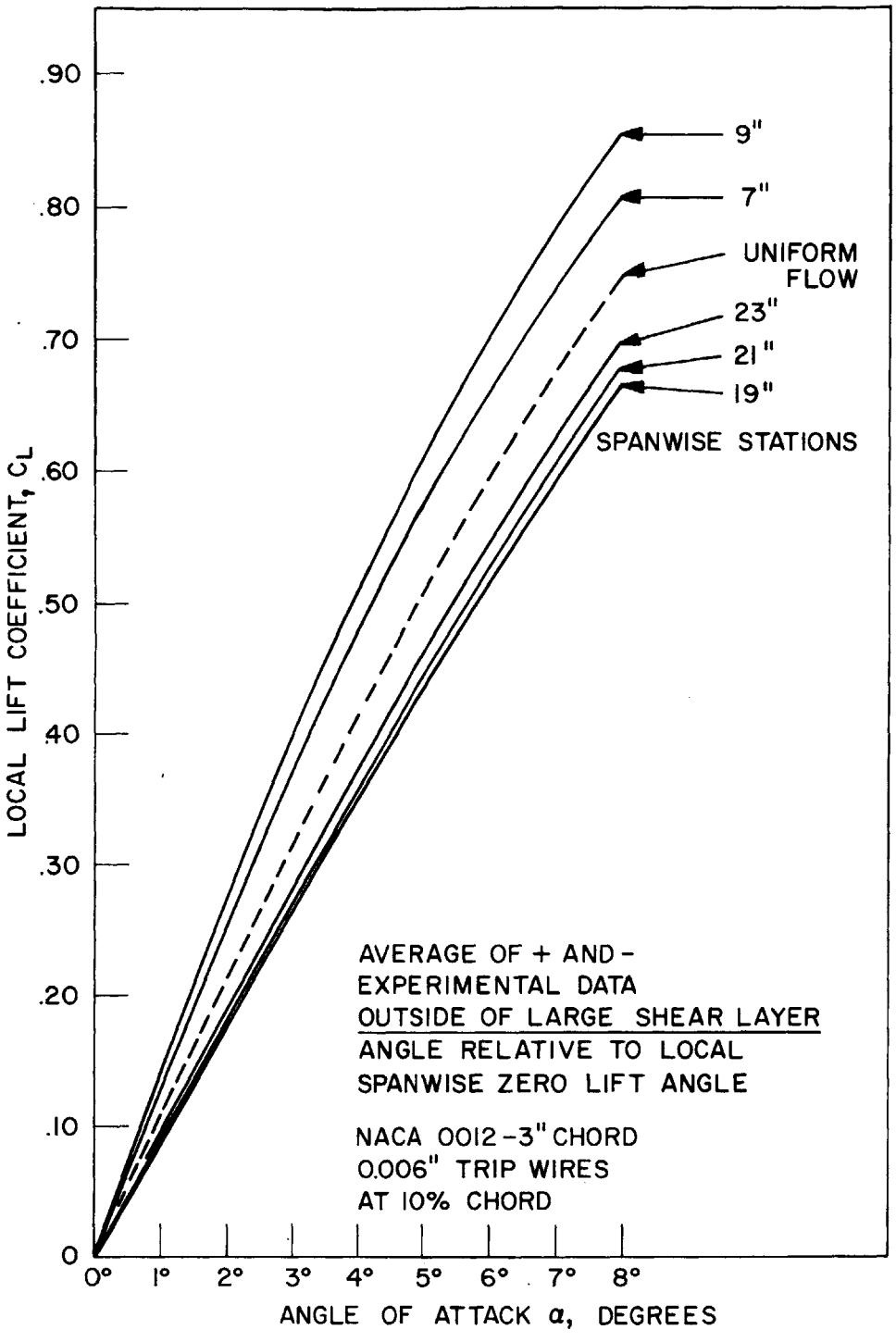

FIGURE 8 AIRFOIL IN SHEAR FLOW.

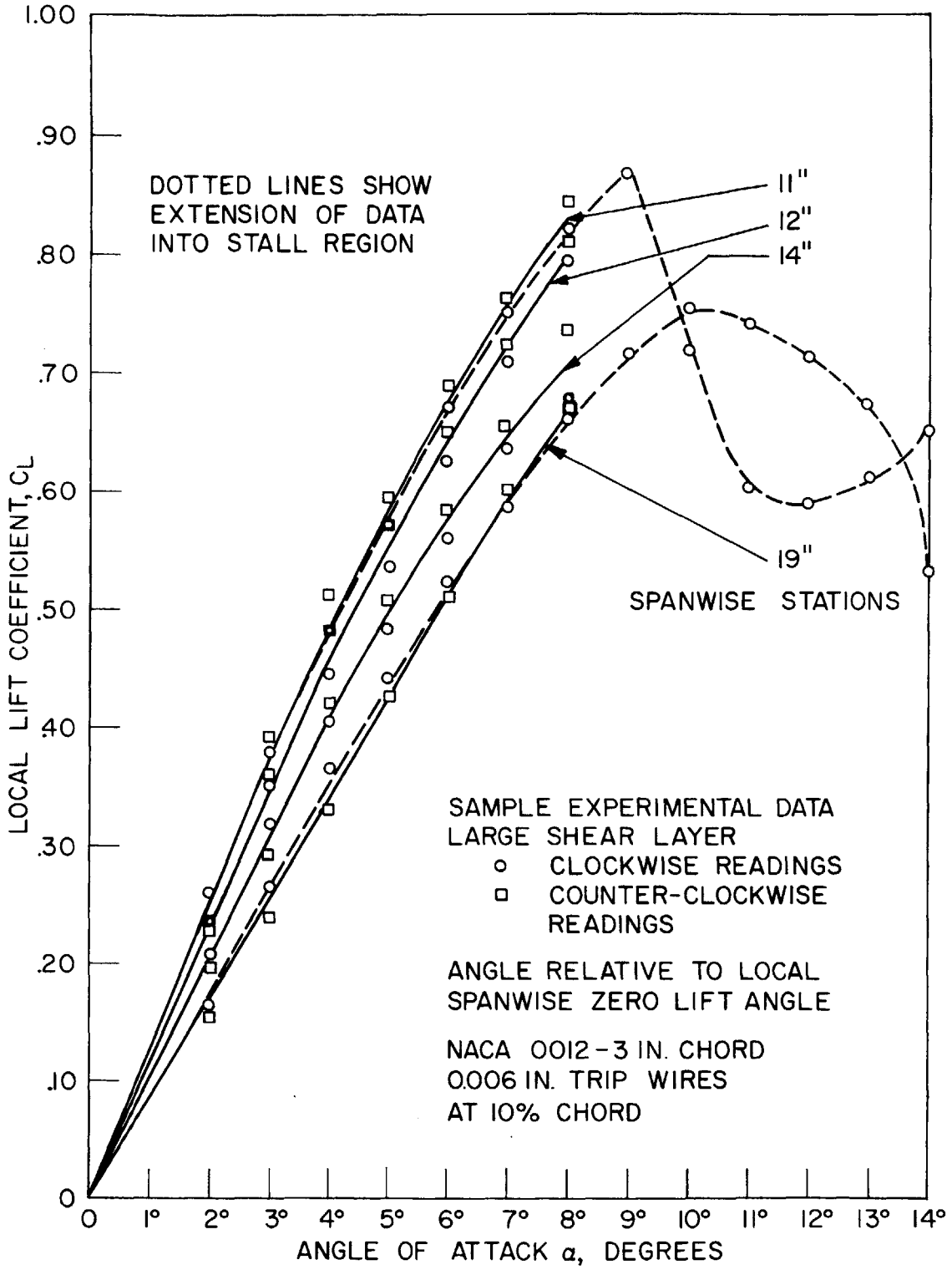

FIGURE 9 AIRFOIL IN SHEAR FLOW.

ally across the shear layer from the 9" station to the 19" station except for some irregularity at high angles of attack as shown in Figure 7. The uniform flow characteristics were not observed at the center of the shear layer, but are found on the low velocity side of it indicating that the induced angle of attack is not zero at the center of the shear layer. This effect is confirmed by the results of the lifting line theory. The data in Figure 8 indicates a consistent variation in local lift coefficient towards the uniform flow value with increasing distance from the shear layer in the regions of relatively uniform flow.

As an indication of the appearance of the clockwise and counter-clockwise data before averaging, four sets of original data are shown in Figure 9. The solid curves indicate the averaged results for each spanwise station. The data is representative of the entire set of measurements for this experiment. It is worthwhile to note that although the gradient of the local lift coefficient changes sign between the regions of sheared and uniform flow, the lift itself varies monotonically from a maximum in the high velocity uniform region to a minimum in the low velocity uniform region. This is, of course, excluding the regions of flow adjacent to the tunnel walls where the wall boundary layer effects are dominant.

5.4 Small Shear Layer - Small Chord Experiment

The velocity profile for the small shear layer - small chord experiment is shown in Figure 10. A comparison of Figure 10 with Figure 6 shows a reduction of local non-uniformities in this shear profile. The velocity profile was approximated well by the linear fit used in conjunction with the lifting line theory. The velocity variation is from approximately 69 ft/sec to 109 ft/sec over a shear layer thickness of about 4". This results in an approximate increase of 250% in U' at the center of the shear layer as compared with the large shear layer velocity profile.

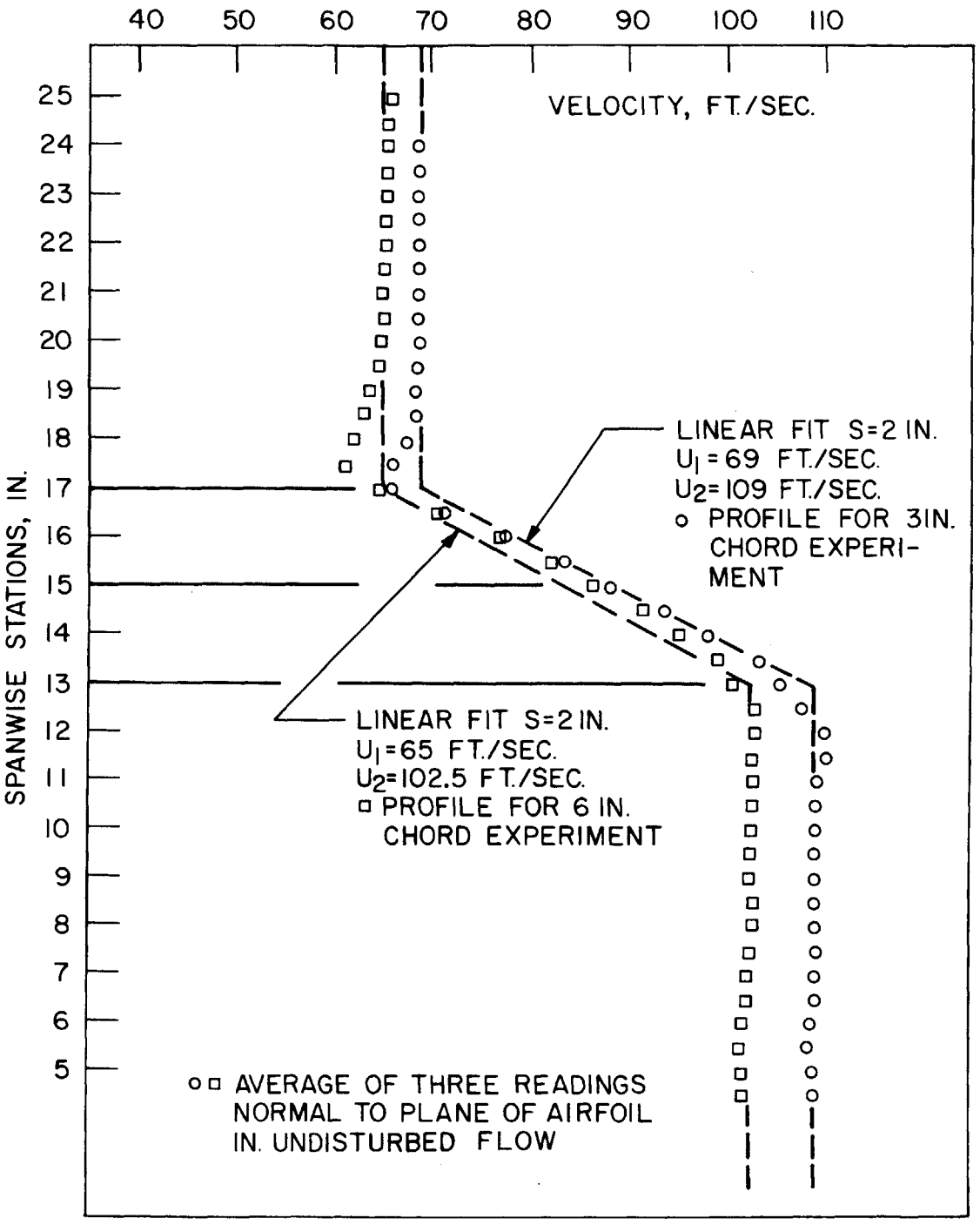

FIGURE 10 EXPERIMENTAL SHEAR FLOW VELOCITY PROFILES - SMALL SHEAR LAYER.

The results of the measurements of local lift coefficients are presented in Figure 11 and Figure 12 for the regions inside the shear layer and outside the shear layer respectively. The variation of C_L with spanwise position is more consistent here than in the previous set of data for the large shear layer; this is attributed to the reduction of axial swirl in the flow and the production of a more homogeneous shear profile in this case. The data in Figure 11 indicates again that the uniform flow characteristics were approached on the low velocity side of the center of the shear layer. The uniform flow result was closely approached in the uniform flow regions at the 5" and 25" spanwise stations as shown in Figure 12.

A set of sample data for four spanwise stations showing both clockwise and counter-clockwise readings is presented in Figure 13.

5.5 Small Shear Layer - Large Chord Experiment

The experimental velocity profile for this experiment is shown in Figure 10. It is essentially of the same form as that of the small chord experiment. The results of the measurements of local lift coefficients are shown in Figure 14 and Figure 15 for the regions inside the shear layer and outside of the shear layer respectively. The magnitudes of the changes in local lift coefficient as a function of spanwise position are greater in this case than for the small chord experiment. A set of sample data indicating the clockwise and counter-clockwise readings for four spanwise stations is presented in Figure 16.

The experimental results presented here and in Sections 5.3 and 5.4 are compared with theoretical results in Section 6.1.

5.6 Pressure Coefficient Distributions

A fundamental assumption of the lifting line theory is that the local lift coefficient is dependent only on the local angle of attack and the two-dimensional characteristic of the airfoil section, i.e.

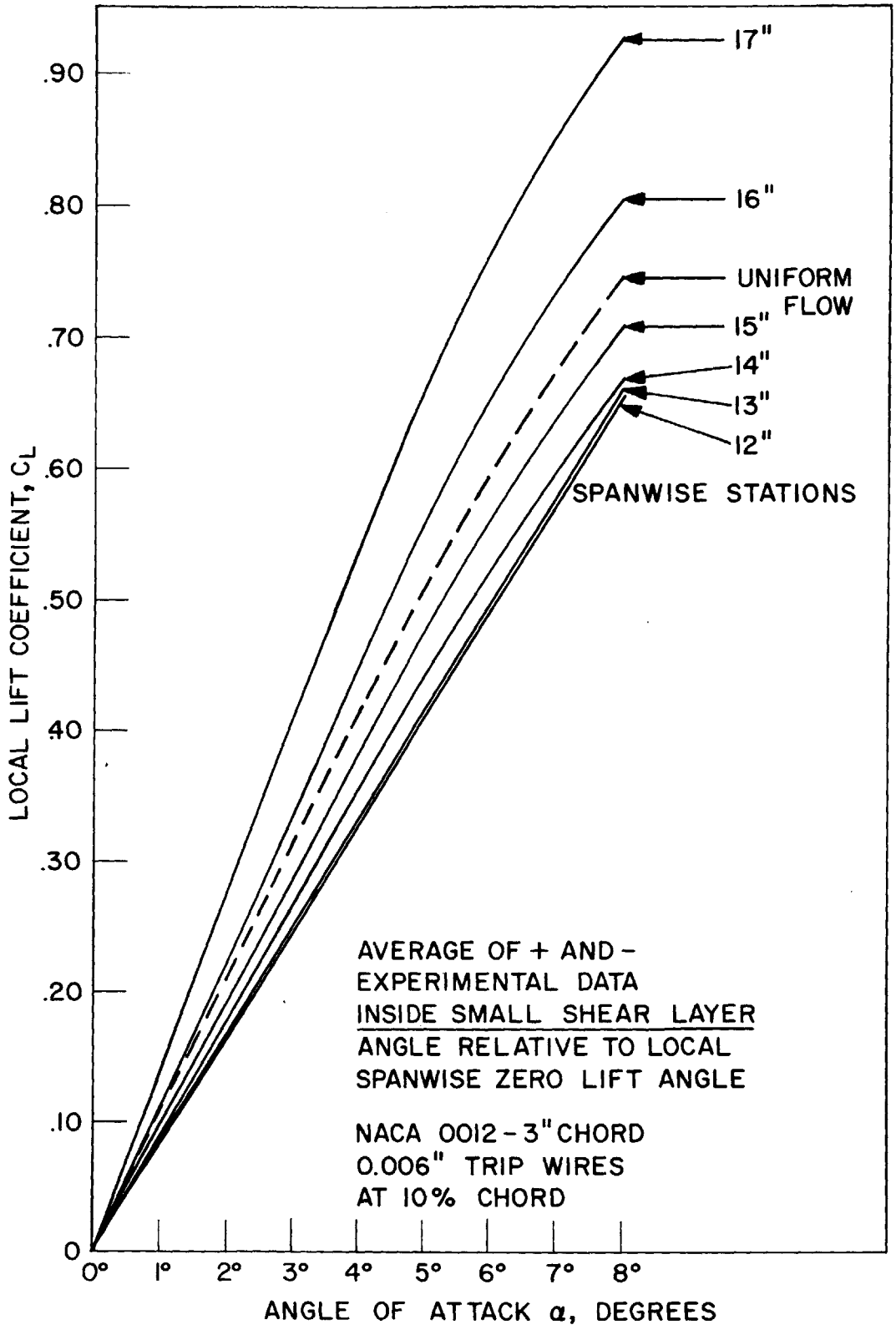

FIGURE 11 AIRFOIL IN SHEAR FLOW.

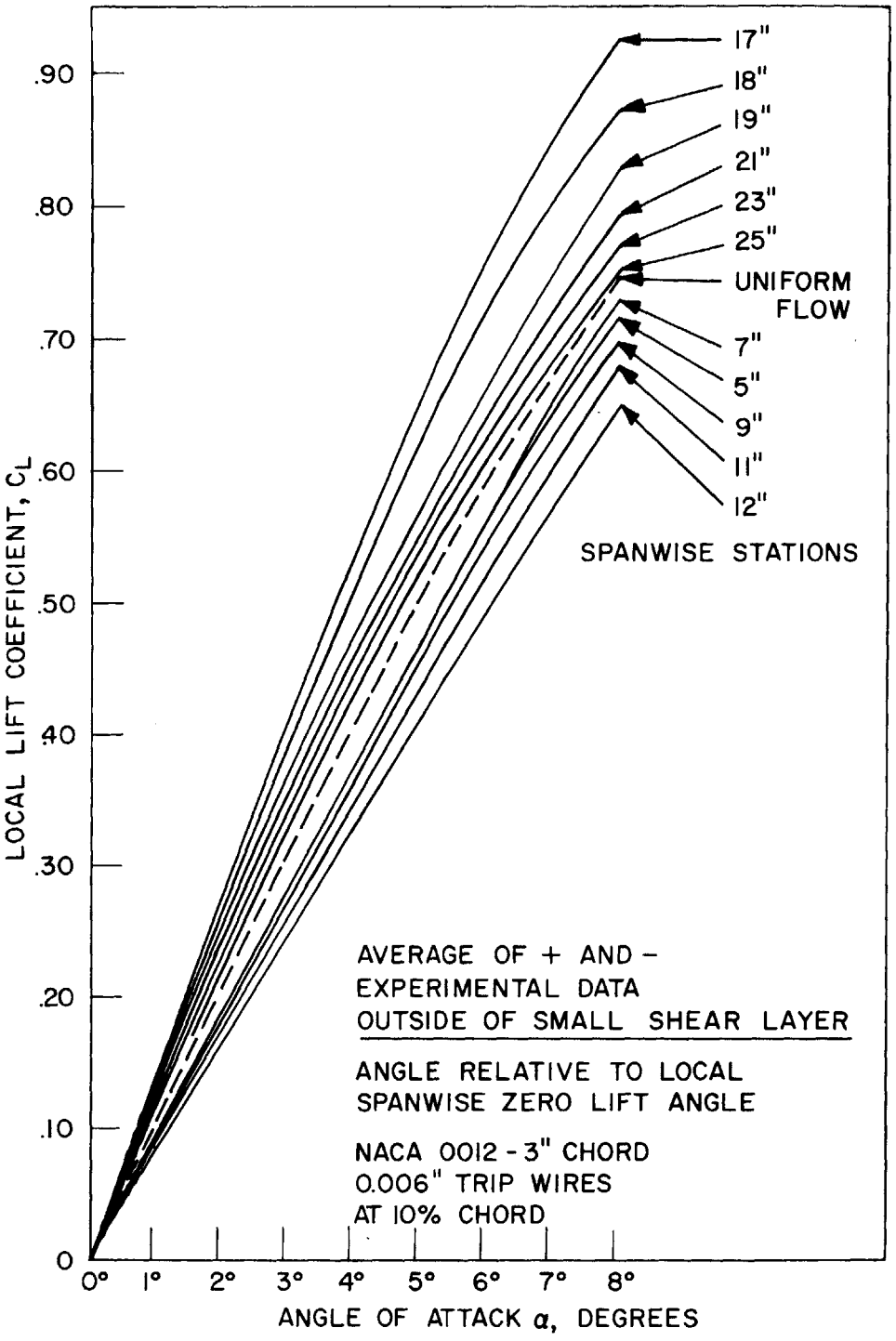

FIGURE 12 AIRFOIL IN SHEAR FLOW.

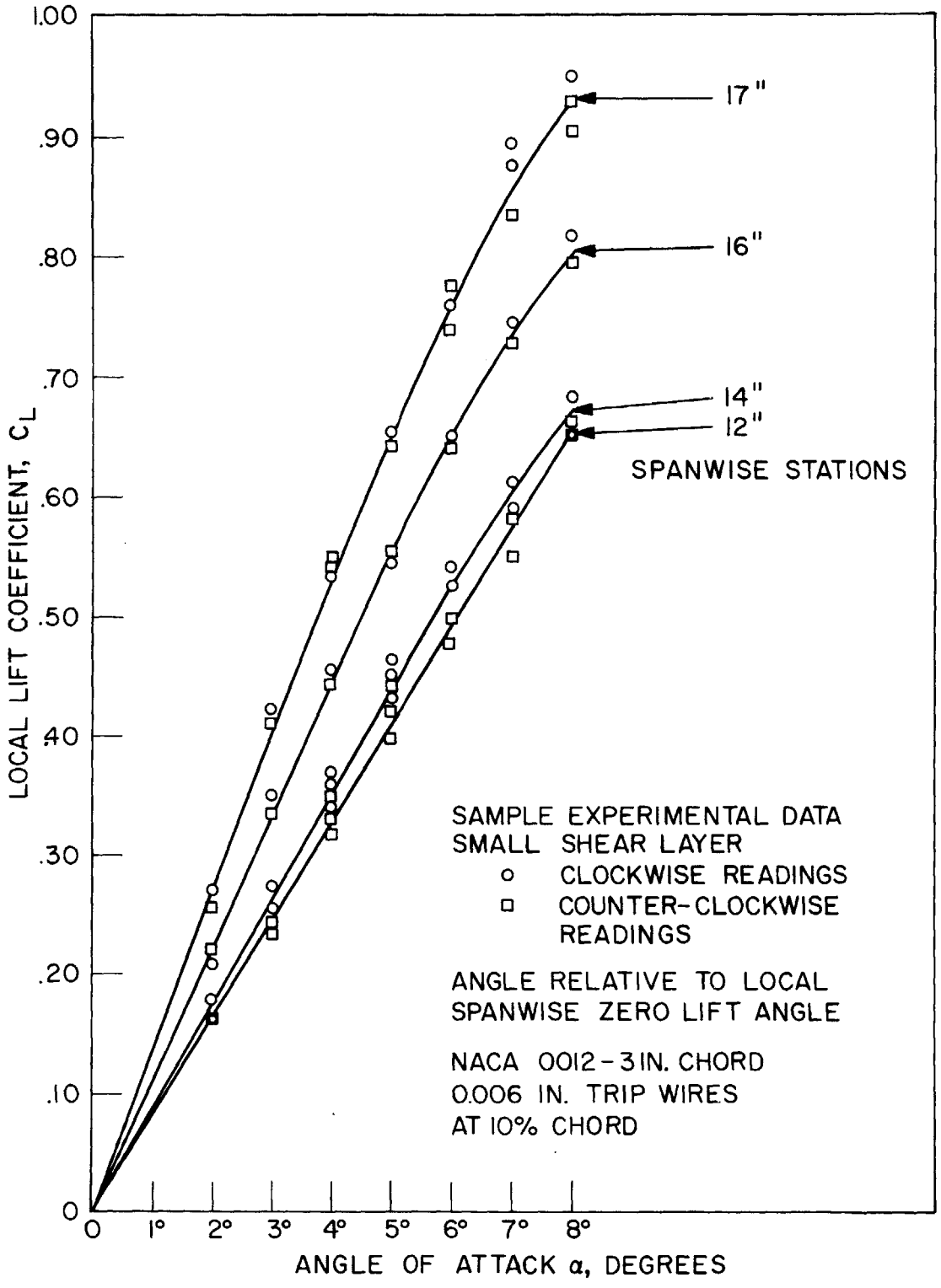

FIGURE 13 AIRFOIL IN SHEAR FLOW.

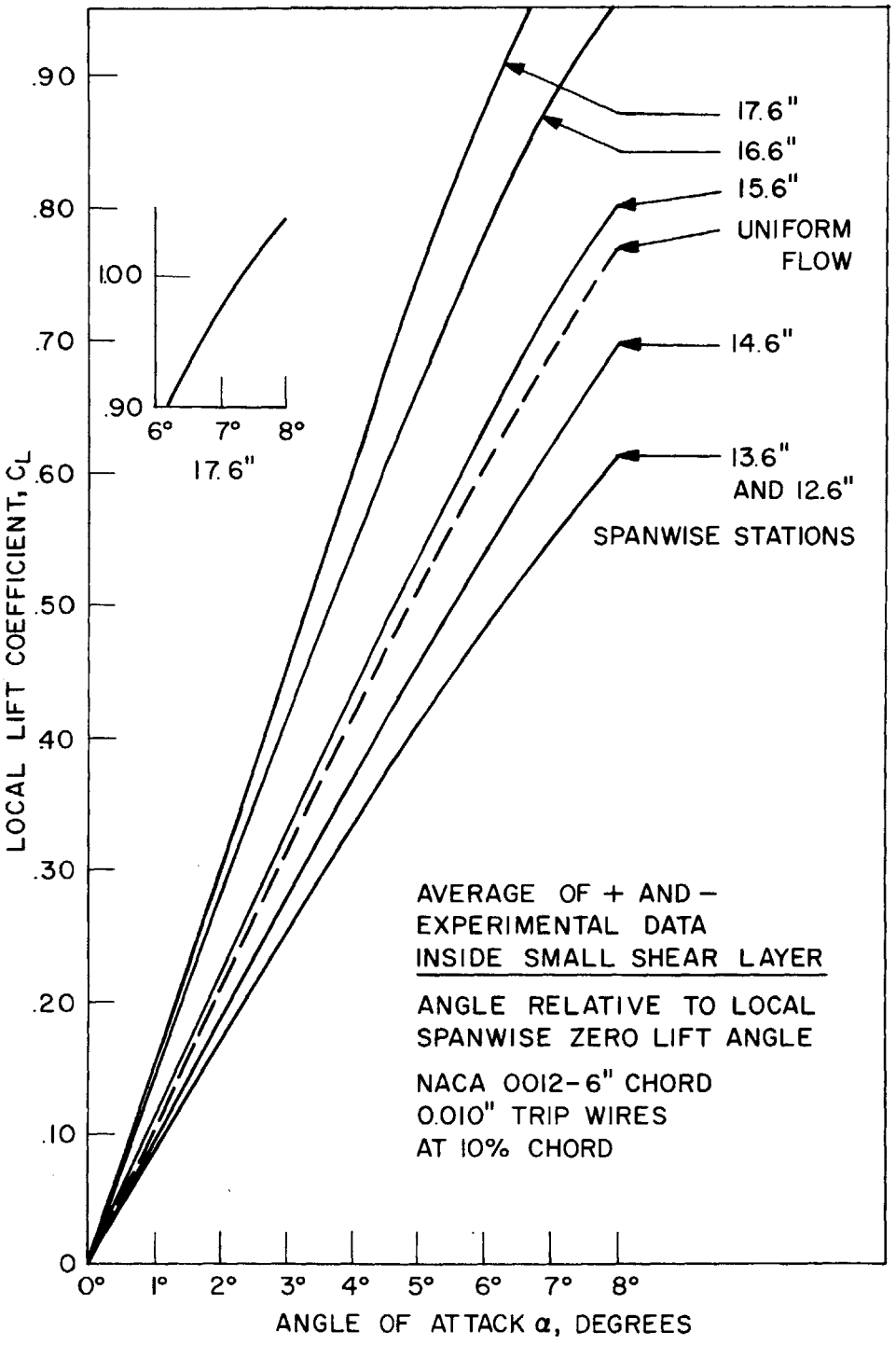

FIGURE 14 AIRFOIL IN SHEAR FLOW.

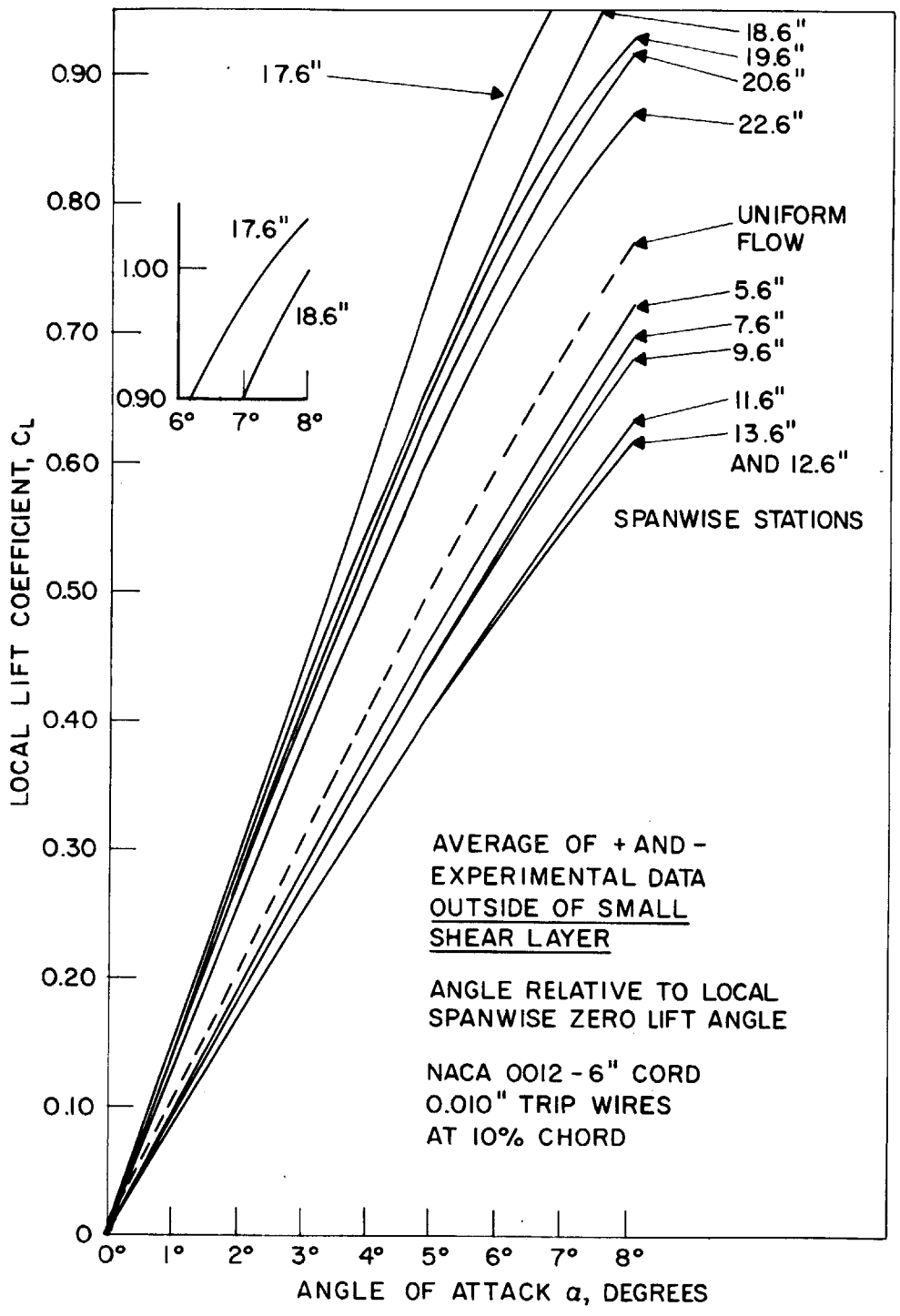

FIGURE 15 AIRFOIL IN SHEAR FLOW

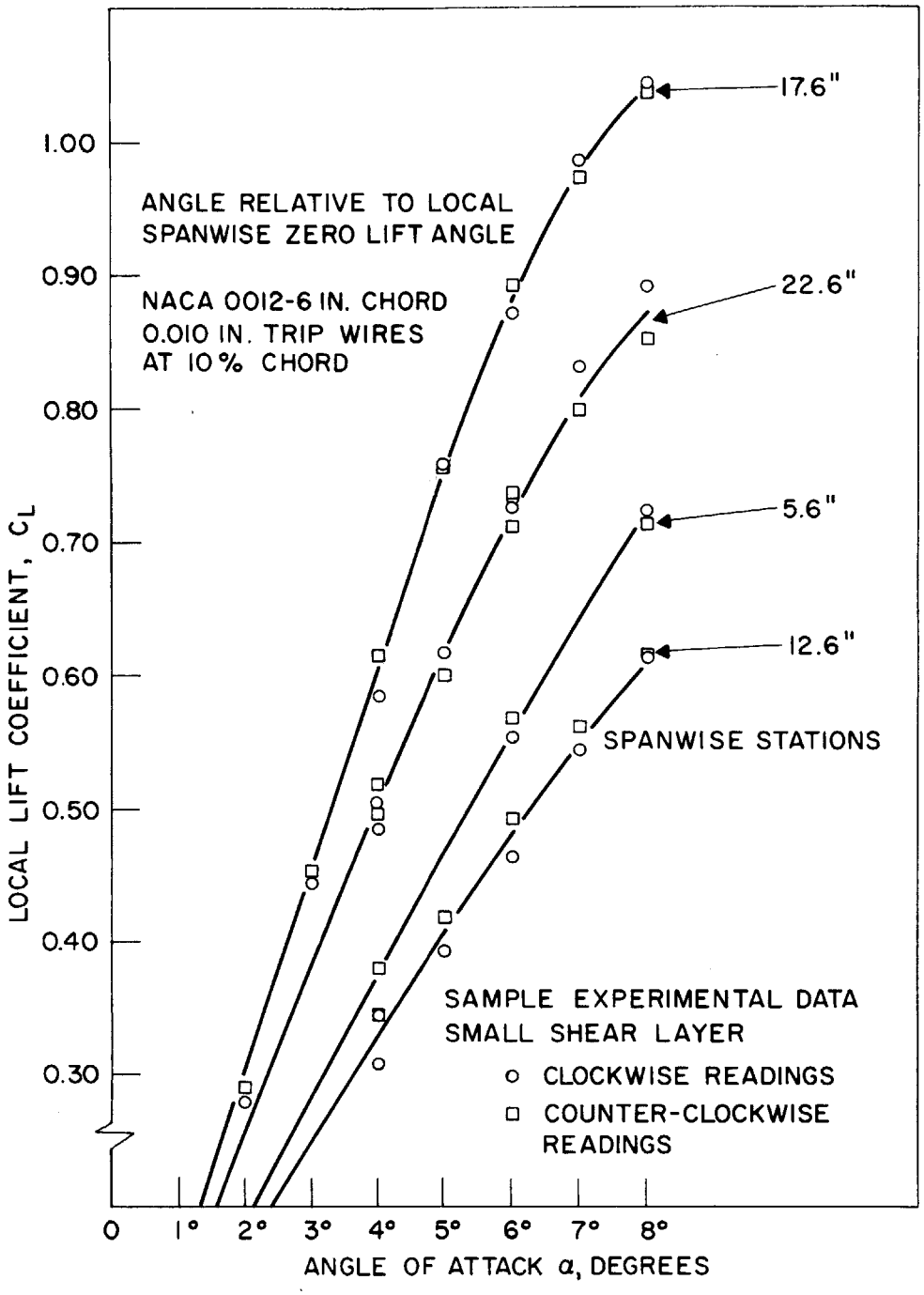

FIGURE 16 AIRFOIL IN SHEAR FLOW

$$C_L = C_{Lo}\left(1 + \frac{w_{LL}}{U\alpha_o}\right)$$

If the above assumption is valid, pressure coefficient distributions are a function of the local value of C_L. Therefore, ideally, pressure coefficient distributions at any position in the shear flow having the same value of local lift coefficient should be comparable with each other and these, in turn, should be comparable with the pressure coefficient distribution at the same C_L in a uniform flow.

The above supposition is not expected to be valid in all cases since we cannot postulate that the stall characteristics are related in such an elementary manner to the local value of C_L, i.e. the onset of stall in a shear flow does not necessarily occur when the local value of C_L reaches the value of C_{Lo} at the onset of stall in a uniform flow. In addition to stall phenomena, local Reynolds number effects might affect the comparison of pressure coefficient distributions in some cases. A departure from a 'two-dimensional' pressure coefficient distribution as a result of the distortion of Bernoulli surfaces in a shear flow might affect the comparison - especially the comparison with uniform flow data, but this effect may not be apparant for small distortion effects since the areas under the pressure coefficient curves are necessarily the same for equivalent C_L. However, distortion effects might be detected by local anomalies in the C_p distribution, but the detection of such effects would be dependent on the accuracy and definition of the experimental measurements.

The data presented in Figure 17 shows the pressure coefficient distributions for two angles of attack on the 3" chord airfoil in uniform flow. These two curves constitute the data necessary for two corresponding points on the uniform flow curve shown in Figure 5 for a Reynolds number of 1.45×10^5. The lift coefficients are obtained by integration of the area under the C_p curves. The local low pressure readings due to the trip wire separ-

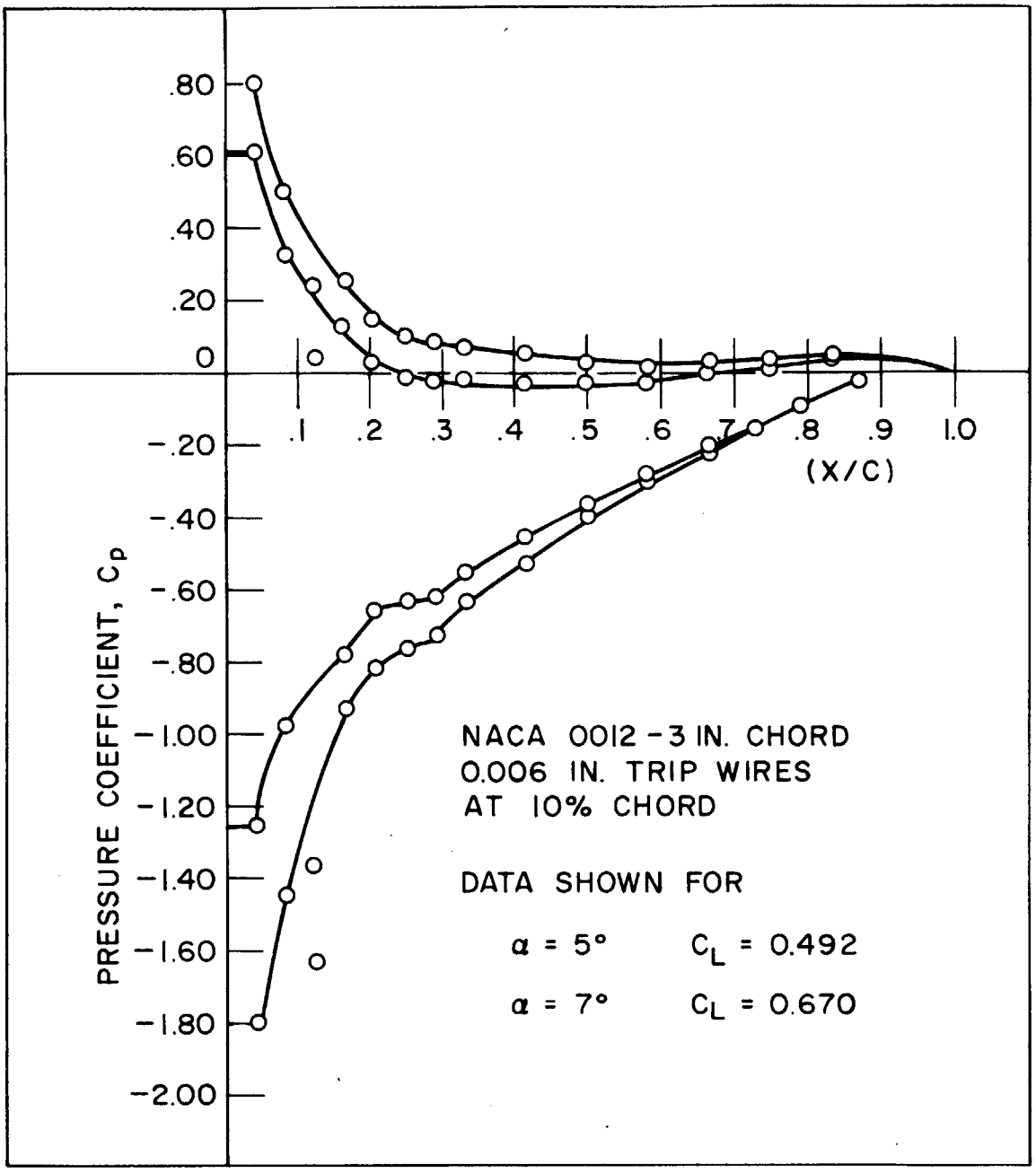

FIGURE 17 PRESSURE COEFFICIENT DISTRIBUTIONS FOR AIRFOIL IN UNIFORM FLOW.

ation bubbles may be seen in Figure 17 just beyond the 10% chord position.

Figures 18 and 19 show the comparison of C_p distributions for the same C_L at different spanwise stations in the large shear layer for two different cases. Figure 20 shows a similar comparison for data taken in the small shear layer with the 3" chord airfoil. The discrepancies between the two C_p distributions shown in each of these three figures are seen to be small. To extend the C_p comparison to the uniform flow case, the C_p distribution corresponding to a C_L of 0.492 in Figure 17 may be compared with the shear flow data of Figure 18, and the uniform flow data corresponding to a C_L of 0.670 may be compared to the shear flow data of Figure 20.

The above pressure coefficient comparisons are indications of the validity of the lifting line assumption concerning the relation between the local lift coefficient and the local angle of attack.

5.7 Separation and Stall Phenomena

Although no direct attempt was made to investigate separation and stall effects in this investigation, comments on a few general observations are in order.

The first is in relation to the onset of stall in the shear flows considered. Figure 5, page 62, indicates that the 3" chord airfoil stalls in a uniform flow at a lift coefficient of about 0.80 which corresponds to an angle of attack in the range of from 8 to 9 degrees. The term 'stall' is here taken to signify a considerable departure from the linear C_L, α curve. The data presented in Figure 7, page 64, and Figure 12, page 71, indicates that local lift coefficients in excess of 0.80 were achieved without any obvious indication of stall. This phenomena is attributed to the thinning of the boundary layer on the suction side of the airfoil by spanwise flows in the boundary layer. As evidence of this effect, Figure 48, Appendix VI, shows photographs of oil traces taken at different spanwise stations on the 3" chord airfoil in the small shear layer at a geometrical angle of attack

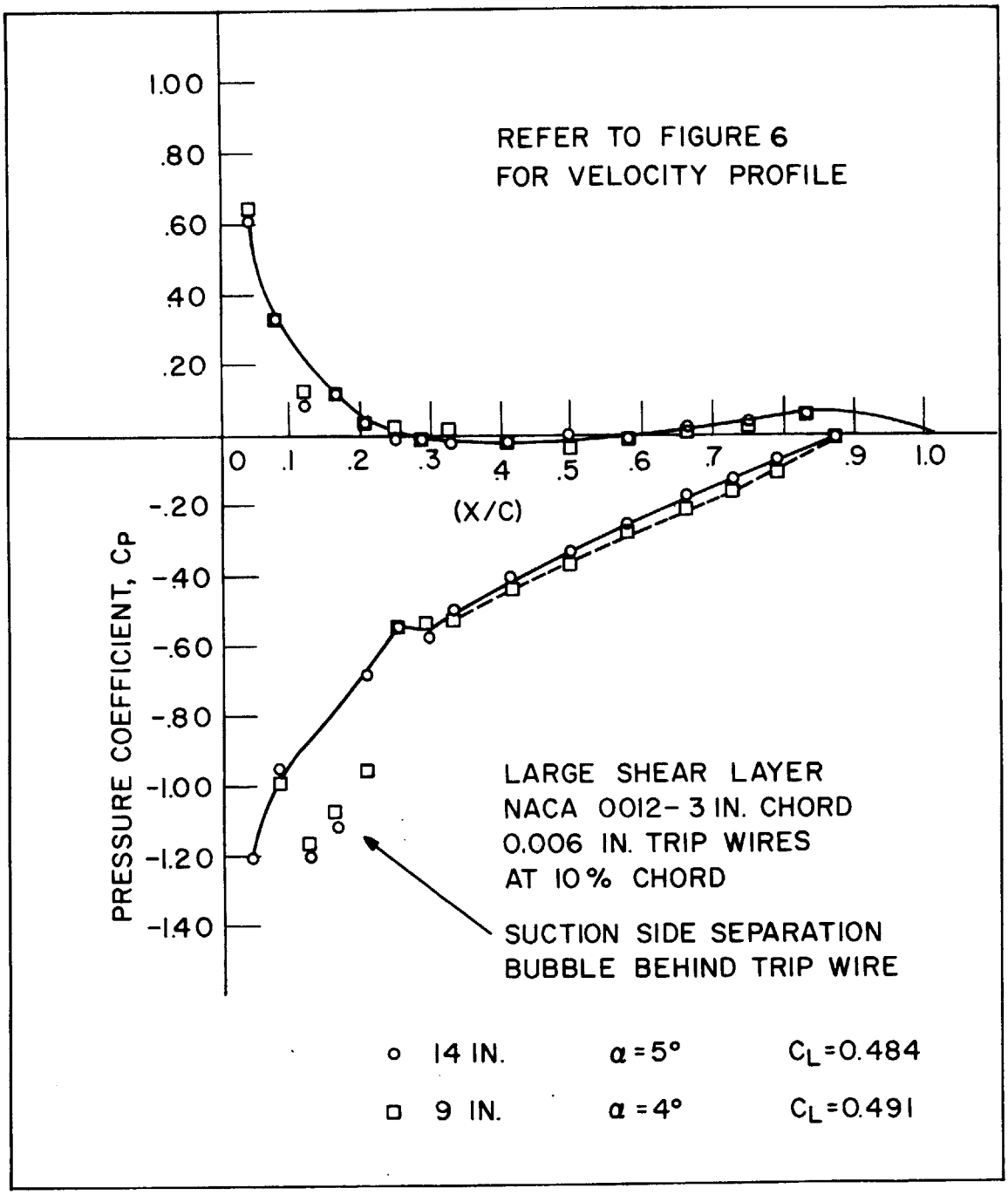

FIGURE 18 COMPARISON OF PRESURE COEFFICIENTS FOR SAME LIFT COEFFICIENT AT DIFFERENT SPANWISE STATIONS.

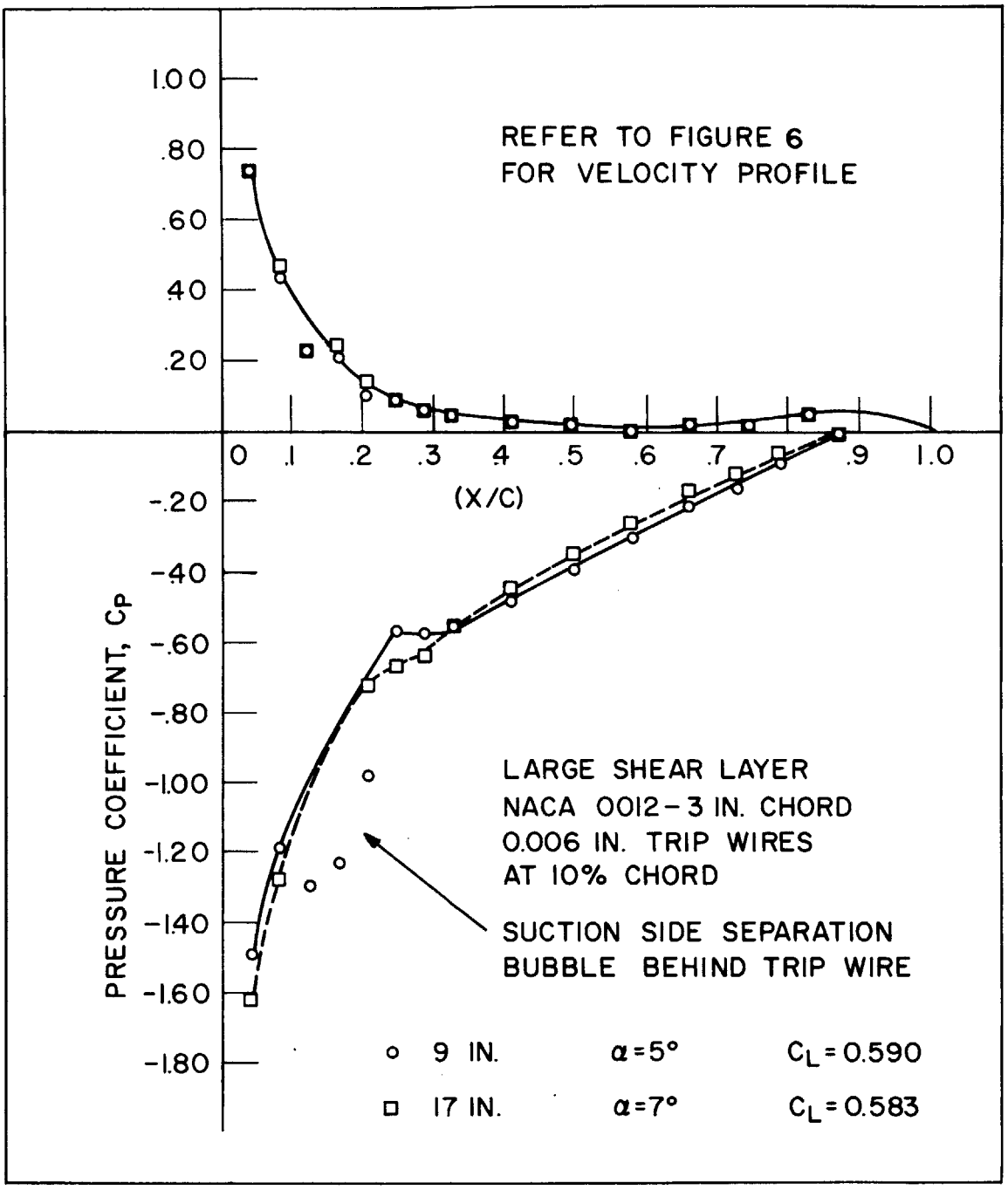

FIGURE 19 COMPARISON OF PRESSURE COEFFICIENTS FOR SAME LIFT COEFFICIENT AT DIFFERENT SPANWISE STATIONS.

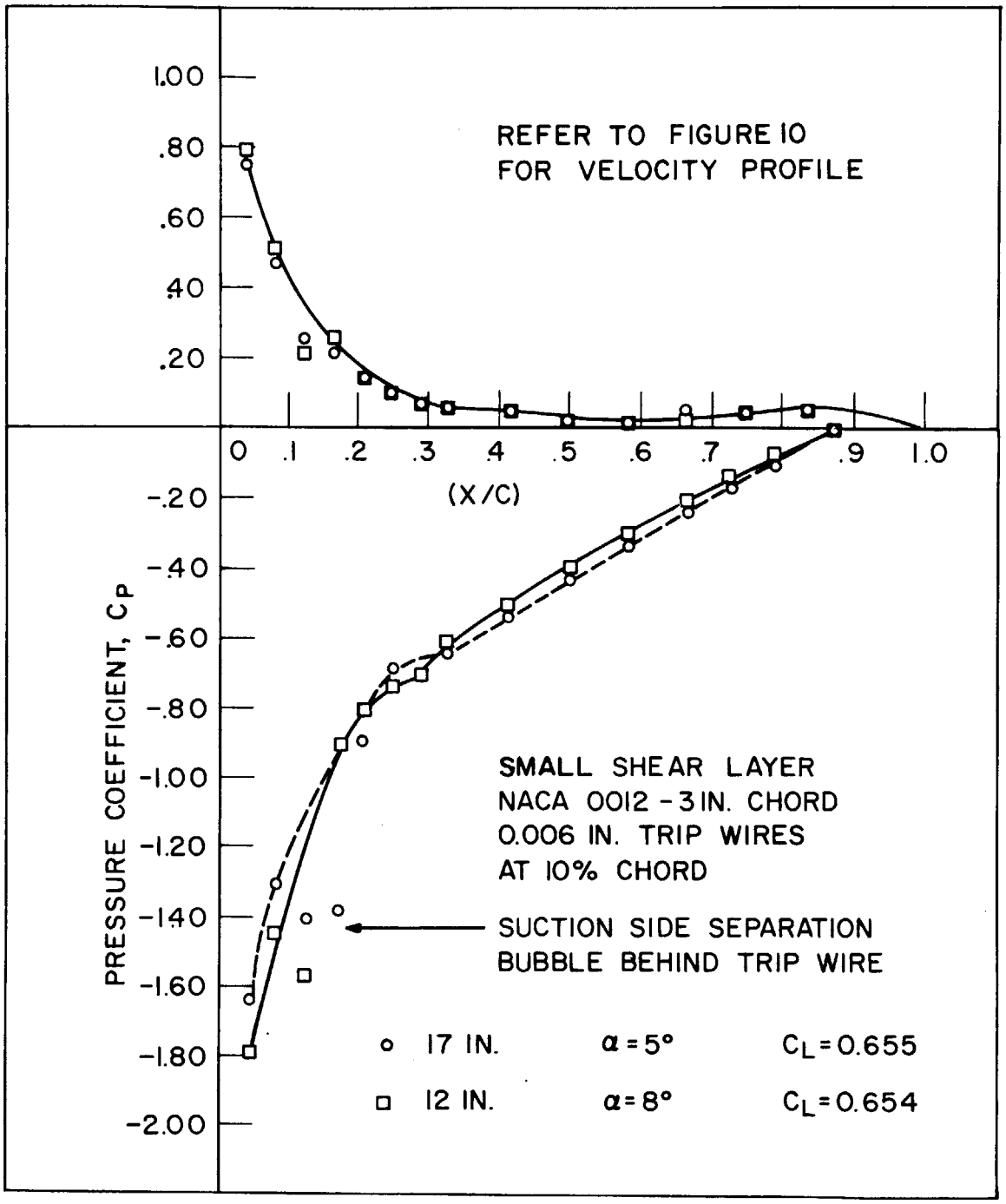

FIGURE 20 COMPARISON OF PRESSURE COEFFICIENTS FOR SAME LIFT COEFFICIENT AT DIFFERENT SPANWISE STATIONS.

of 8°. (The airfoil is shown with the leading edge up in the photographs.) The photographs, with reference to the velocity profile in Figure 10, page 68, indicate the spanwise flow of boundary layer fluid along the suction surface of the airfoil in the direction of increasing velocity U(y). This effect is clearly visible at the 17" and 15" spanwise stations, but it is small if not negligible at the 19" and 13" stations. The divergence between the oil traces at the 19" and 17" positions illustrates the thinning effect.

The last photograph in Figure 48 indicates the existence of a region of backflow (the oil was deposited at the trailing edge on the left side of the photograph) at the 17" position at a geometrical angle of attack of 10°. The oil droplet moved in a backward direction along the chord to a position near the leading edge (approximately 15% chord) and then reversed direction to flow forward and upward to the trailing edge.

6. CLOSURE

6.1 Comparison of Theory with Experiment

The experimental data presented in Sections 5.3, 5.4, and 5.5 may be categorized in a general way by the ratio of airfoil chord to shear layer thickness in each experiment, i.e. c/2s = c/b = 3/10, 3/4, and 3/2 approximately. The theoretical results of the lifting line theory are compared with the experimental data by two methods. The first is a comparison of the change in the local lift coefficient which is represented by the local value of $\Delta C_{Lo}/C_{Lo}$, and the second is a comparison of the spanwise distribution of $U^2C_L = U^2C_{Lo}\ (1 + \Delta C_{Lo}/C_{Lo})$ which is, of course, proportional to the local lift for an airfoil of fixed chord. The comparison of $\Delta C_{Lo}/C_{Lo}$ between theory and experiment is very sensitive to local non-uniformities in the shear flow, and, in a sense, is a comparison based largely on the secondary flows themselves. The comparison of U^2C_L distributions, however, is more directly dependent on the entire flow, and the perturbations may be thought of as a form of correction to a primary U^2C_{Lo} distribution. The result of this is that the effects of local non-uniformities in the flow are much more apparent in the comparisons of $\Delta C_{Lo}/C_{Lo}$ than in comparisons of U^2C_L.

The comparison of theory with experiment for the large shear layer (c/2s = 3/10) is shown in Figure 21 and Figure 22 of Appendix I. The two theoretical curves in Figure 21 correspond to the two linear velocity profile models of the experimental shear layer shown in Figure 6, page 63. The comparison of U^2C_L distributions for three geometrical angles of attack in Figure 22 are based on theoretical results for the 8" thick shear layer model.

A similar set of results for the small shear layer - small chord experiment (c/2s = 3/4) is shown in Figures 23 and 24. Here the theoretical results are based on the theoretical model of the velocity profile shown in Figure 10, page 68. The overall agreement between theory and experiment in this case

indicates an improvement over the comparison of results for the large shear layer; this is attributed to an improved shear flow (refer to Sections 5.3 and 5.4) and better agreement between the theoretical model and the experimental velocity profile. In view of the neglect of viscous effects and the linearization of the equations of motion as fundamental approximations in the lifting line theory, the agreement between the experimental data and the theoretical results in both of the above cases is good.

The comparison of theory with experiment for the small shear layer - large chord experiment (c/2s = 3/2) is shown in Figures 25 and 26. The results in Figure 25 indicate that the theory is consistently on the low side in the prediction of local lift coefficients. This same trend is evident in the results shown in Figure 26 especially within the region of the shear layer (from the 13" to the 17" spanwise stations). Some of this discrepancy can be attributed to local non-uniformities in the experimental shear flow, in particular, the local depression in stagnation pressure in the region of the 17" to 18" spanwise stations (refer to Figure 10) causes a local increase in $\Delta C_{Lo}/C_{Lo}$ and a local decrease in U^2C_L in this region. These local effects are apparent in Figures 25 and 26, but, of course, cannot account for the consistent underestimation of lift by the theory.

We shall now attempt to show that the underestimation of lift as shown in Figure 26 is due to the distortion of the Bernoulli surfaces in the flow about the airfoil. Through a consideration of the linearized equations of motion and an integration of the pressure forces over the chord of the airfoil, we can arrive at the following result (refer to Appendix I, page I-11):

$$L(y) = L_{LL}(y) + \rho U' \int_0^c \left[\int_{-\infty}^{x} (v^+ - v^-)dx \right]_{z=0} dx \qquad (6\text{-}1)$$

where L(y) is the 'true' lift, $L_{LL}(y)$ is the contribution of the lifting line theory, and the last term is the correction due to the distortion of the

Bernoulli surfaces. The integrals in equation (6-1) may be evaluated in an approximate manner (see Appendix I) to yield the result

$$\frac{L(y)}{L_{LL}(y)} \simeq 1 + \frac{c^2}{6} \frac{U'}{U} \frac{d}{dy} \left[\ln L_{LL}(y) \right] \qquad (6\text{-}2)$$

Equation (6-2) constitutes an approximate correction to the results of the lifting line theory. The lift correction in the region of the shear layer is shown by the dotted lines in Figure 26 and amounts to about 7% to 8% of the lift as calculated from the lifting line theory. The same correction, if applied to the theoretical results for the 3" chord experiments would result in an increase of lift of approximately 1% to 2% which can be considered negligible. In effect then, the results shown in Figure 25 are of academic interest only since the local lift coefficient has no significance in a shear flow where distortion effects are considerable.

The comparison of the lifting line theory with the experimental data of Mendelsohn and Polhamus[26] is shown in Figure 27. In this case, the theoretical model is based on the matched cosine - uniform velocity profile (refer to Section 3.10 and Appendix III). The 'wall boundary layer' in this case was modeled by two theoretical velocity profiles indicated in Figure 27. The agreement between theory and experiment is good considering the large chord to boundary layer thickness ratio in the experiment. The Bernoulli surface distortion effects that would certainly become significant in a 'free' shear layer with this chord to shear layer thickness ratio are substantially reduced by the presence of the wall, i.e. at the wall, the lift correction is necessarily zero (equation (6-1)) even though U' is large and U is small (assuming a slip velocity). The experimental results of Mendelsohn and Polhamus indicate a reduction of lift at the wall of about 11% based on the 'free stream' lift; the results of the lifting line theory predict reductions of approximately 10% for the boundary layer model with

U_1/U_{WALL} = 2.0 and 7% for the model with U_1/U_{WALL} = 1.54. It should be noted that the experimental data in this case is obtained from measurements on a NACA 65_1-012 airfoil at an angle of attack of 3.1^o and a Reynolds number of 3.66×10^6. Other theoretical works that have been used to approximate the experimental results of Mendelsohn and Polhamus are those of Preston[32] and Wilson[33].

The comparisons of theoretical results based on the first theoretical approximation (Section 4) with experimental data for the 3" chord airfoil in both the large and the small shear layers are shown in Figures 28 and 29 respectively.

6.2 Conclusions

The results of the experimental program have shown that significant corrections to the 'two dimensional' lift are induced by the flow of a rotational fluid about thin airfoils. In general, a smoothing of the lift distribution is obtained in which the local lift is increased in areas of low stagnation pressure and decreased in areas of relatively high stagnation pressure. The induced effects on local lift are characterized by changes in the local angle of attack, and the assumption that $L(y) = 1/2\ \rho U^2 c C_{Lo}\ (1 + w_{LL}/U\alpha_o)$ is valid in shear flows where Bernoulli surface distortion effects are negligible.

For large values of (cU'/U) in shear flows where spanwise flows are not prevented by geometry (the presence of boundary walls or symmetry), Bernoulli surface distortion effects may be considerable. The possibility of stall in areas of the flow where the induced angle of attack is large is diminished by thinning of the boundary layer on the suction side of the airfoil by spanwise flows, if, again, these spanwise flows are geometrically possible.

The theoretical results indicate good agreement between the lifting line theory and the experimental results where Bernoulli surface distortion

effects are negligible. The application of the theory is straightforward in that for the shear velocity profiles considered, the solutions are obtained in the form of elementary functions. It is here proposed that most practical shear velocity profiles can be modeled by matching the fundamental solutions presented in Section 3. The effect of Bernoulli surface distortion may be estimated by the approximate correction, and the results of the lifting line theory may be adjusted if necessary.

6.3 Recommendations for Further Study

Theoretical Work

1) Extension of the lifting line theory for a single lifting airfoil to that of a cascade of airfoils.

2) Modification of the lifting line theory to include the effects of variable chord and variable geometrical angle of attack.

3) Further theoretical work on the Bernoulli surface distortion effect.

4) The extension of the lifting line solution to the case of unbounded shear flows (uniform flow at infinity).

5) The development and programming of a general numerical solution based on the lifting line theory for bounded shear flows of any arbitrary velocity profile.

Experimental Work

1) Further investigation of the Bernoulli surface distortion effect and its interaction with boundary walls.

2) Investigation of the shear flow stall phenomena in free shear layers and in regions near boundary walls (a complicated three-dimensional boundary layer problem).

3) Extension of the experimental work in this investigation to developed shear flows (cosine profile) and boundary shear layers (cosine - uniform profile) for which theoretical results are readily available.

REFERENCES

1 von Kármán, T. and Tsien, H. S. "Lifting Line Theory for a Wing in Non-Uniform Flow" Quarterly of Appl. Math., Vol. 3, p. 1, 1945.

2 Honda, M. "Theory of a Thin Wing in a Shear Flow" Proceedings of the Royal Society, Vol. A-254, p. 372, 1960.

3 Hawthorne, W. R. "On the Theory of Shear Flow" Gas Turbine Laboratory Report, to be published, Mass. Inst. of Tech., 1965.

4 Squire, H. B. and Winter, K. G. "The Secondary Flow in a Cascade of Airfoils in a Non-Uniform Stream" Jour. of Aero. Sciences, Vol. 18, p. 271, April 1951.

5 Hawthorne, W. R. "Secondary Circulation in Fluid Flow" Proceedings of the Royal Society, Vol. A-206, p. 374, 1951.

6 Eichenberger, H. P. "Shear Flow in Bends" Mech. Eng. Thesis, Dept. of Mech. Eng., Mass. Inst. of Tech., 1951.

7 Hawthorne, W. R. "Rotational Flow Through Cascades - Part I - The Components of Vorticity" Quarterly Jour. of Mech. and Appl. Math., Vol. 8, p. 266, 1955.

8 Hawthorne, W. R. and Armstrong, W. D. "Rotational Flow Through Cascades - Part II - The Circulation About the Cascade" Quarterly Jour. of Mech. and Appl. Math., Vol. 8, p. 280, 1955.

9 Hawthorne, W. R. "The Secondary Flow about Struts and Airfoils" Jour. of Aero. Sciences, Vol. 21, p. 588, 1954.

10 Ling, A. T. "Study of Secondary Flow Effect on Single Symmetrical Aerofoils" M.S. Thesis, Dept. of Mech. Eng., Mass. Inst. of Tech., 1952.

11 Tsien, H. S. "Symmetrical Joukowski Airfoils in Shear Flow" Quarterly of Appl. Math., Vol. 1, July 1943.

12 James, D. J. "Two Dimensional Airfoils in Shear Flow - Part I" Quarterly Jour. of Mech. and Appl. Math., Vol. 4, p. 407, 1951.

13 Jones, E. E. "The Elliptic Cylinder in a Shear Flow with Hyperbolic Velocity Profile" Quarterly Jour. of Mech. and Appl. Math., Vol. 12, p. 191, 1959.

14 Murray, J. D. and Mitchell, A. R. "Flow with Variable Shear Past Circular Cylinders" Quarterly Jour. of Mech. and Appl. Math., Vol. 10, p. 13, 1957.

15 Hawthorne, W. R. "The Growth of Secondary Circulation in Frictionless Flow" Proceedings of the Cambridge Philosophical Society, Vol. 51, p. 737, 1955.

16 Smith, A. G. "On the Generation of the Streamwise Component of Vorticity for Flows in Rotating Passages" Aero. Quarterly, p. 369, November 1957.

17 Smith, L. H. "Secondary Flow in Axial Flow Turbomachinery" Trans. of ASME, Vol. 77, p. 1065, 1955.

18 Dean, R. C. "Secondary Flow in Axial Compressors" Gas Turbine Laboratory Report, Mass. Inst. of Tech., May 1954.

19 Van Le, N. "Three Dimensional Flow in a Cascade - Effect of the Boundary Layer" Gas Turbine Laboratory Report No. 22, Mass. Inst. of Tech., 1952.

20 Soderberg, O. E. "Secondary Flow and Losses in a Compressor Cascade" Gas Turbine Laboratory Report No. 46, Mass. Inst. of Tech., 1958.

21 Lighthill, M. J. "Drift" Jour. of Fluid Mech., Vol. 1, p. 31, 1956.

22 Darwin, Sir Charles "Note on Hydrodynamics" Proceedings of the Cambridge Philosophical Society, Vol. 49, p. 342, 1953.

23 Hall, I. M. "The Displacement Effect of a Sphere in a Two Dimensional Shear Flow" Jour. of Fluid Mech., Vol. 1, p. 142, 1956.

24 Lighthill, M. J. "Contributions to the Theory of the Pitot Tube Displacement Effect" Jour. of Fluid Mech., Vol. 2, p. 493, 1957.

25 Lighthill, M. J. "The Fundamental Solution for Small Three Dimensional Disturbances to a Two-Dimensional Parallel Shear Flow" Jour. of Fluid Mech., Vol. 3, p. 113, 1957.

26 Mendelsohn, R. A. and Polhamus, J. F. "Effect of the Tunnel-Wall Boundary Layer on Test Results of a Wing Protruding from a Tunnel Wall" NACA Tech. Note No. 1244, April 1947.

27 Schwind, R. G. "The Three Dimensional Boundary Layer Near a Strut" Gas Turbine Laboratory Report No. 67, Mass. Inst. of Tech., May 1962.

28 Toomre, A. "The Viscous Secondary Flow Ahead of an Infinite Cylinder in a Uniform Parallel Shear Flow" Jour. of Fluid Mech., Vol. 7, p. 145, 1959.

29 Montgomery, S. R. "The Design of a Low Speed Cascade Tunnel" Gas Turbine Laboratory Report No. 43, Mass. Inst. of Tech., January 1958.

30 Owen, P. R. and Zienkiewicz, H. K. "The Production of Uniform Shear Flow in a Wind Tunnel" Jour. of Fluid Mech., Vol. 2, p. 521, 1957.

31 Abbott, I. H., von Doenhoff, A. E. and Stivers, L. S. "Summary of Airfoil Data" NACA Report No. 824, 1945.

32 Preston, J. H. "The Interference on a Wing Spanning a Closed Tunnel, Arising from the Boundary Layers on the Side Walls, with Special Reference to the Design of Two-Dimensional Tunnels" Aeronautical Research Committee Reports and Memoranda No. 1924, Great Britain, March 1944.

33 Wilson, W. H. "Shear Flow in Boundary Layers" Aero. Eng. Thesis, Dept. of Aeronautical Engineering, Mass. Inst. of Tech., 1951.

34 Bonneville, J. and Harper, D. "An Analysis and Investigation of Two-Dimensional Flow Through Wire Screens" M.S. Thesis, Dept. of Mech. Eng., Mass. Inst. of Tech., 1951.

35 Asanuma, T. and Namba, M. "Experimental Study of Parallel Shear Flow Through a Cascade in Transonic Region" Institute of Space and Aeronautical Science, The University of Tokyo, 1963.

36 Mair, W. A. "The Distribution of Pressure on an Aerofoil, in a Stream with a Spanwise Velocity Gradient" Aero. Quarterly, Vol. 6, p. 1, 1955.

37 Rohsenow, W. M. and Choi, H. Heat, Mass, and Momentum Transfer, Prentice-Hall, Englewood Cliffs, New Jersey, 1961.

General References

Durand, W. F. (Editor) Aerodynamic Theory, Julius Springer, Berlin, 1935.

Milne-Thomson, L. M. Theoretical Aerodynamics, Second Edition, Macmillan and Co., London, 1952.

Ryshik, I. M. and Gradstein, I. S. Tables of Series, Products, and Integrals, Second Edition, Veb Deutscher Verlag Der Wissenschaften, Berlin, 1963.

Thwaites, B. (Editor) Incompressible Aerodynamics, Oxford University Press, Great Britain, 1960.

APPENDIX I

Comparison of Theory with Experiment

For a discussion of the theoretical and experimental results presented in the following figures, refer to Section 6. The theoretical results were obtained from computations based on the analyses presented in Section 3 and Section 4. The experimental data presented, except for the data of Mendelsohn and Polhamus in Figure 27, was obtained during the course of this investigation.

Figures 21 through 29

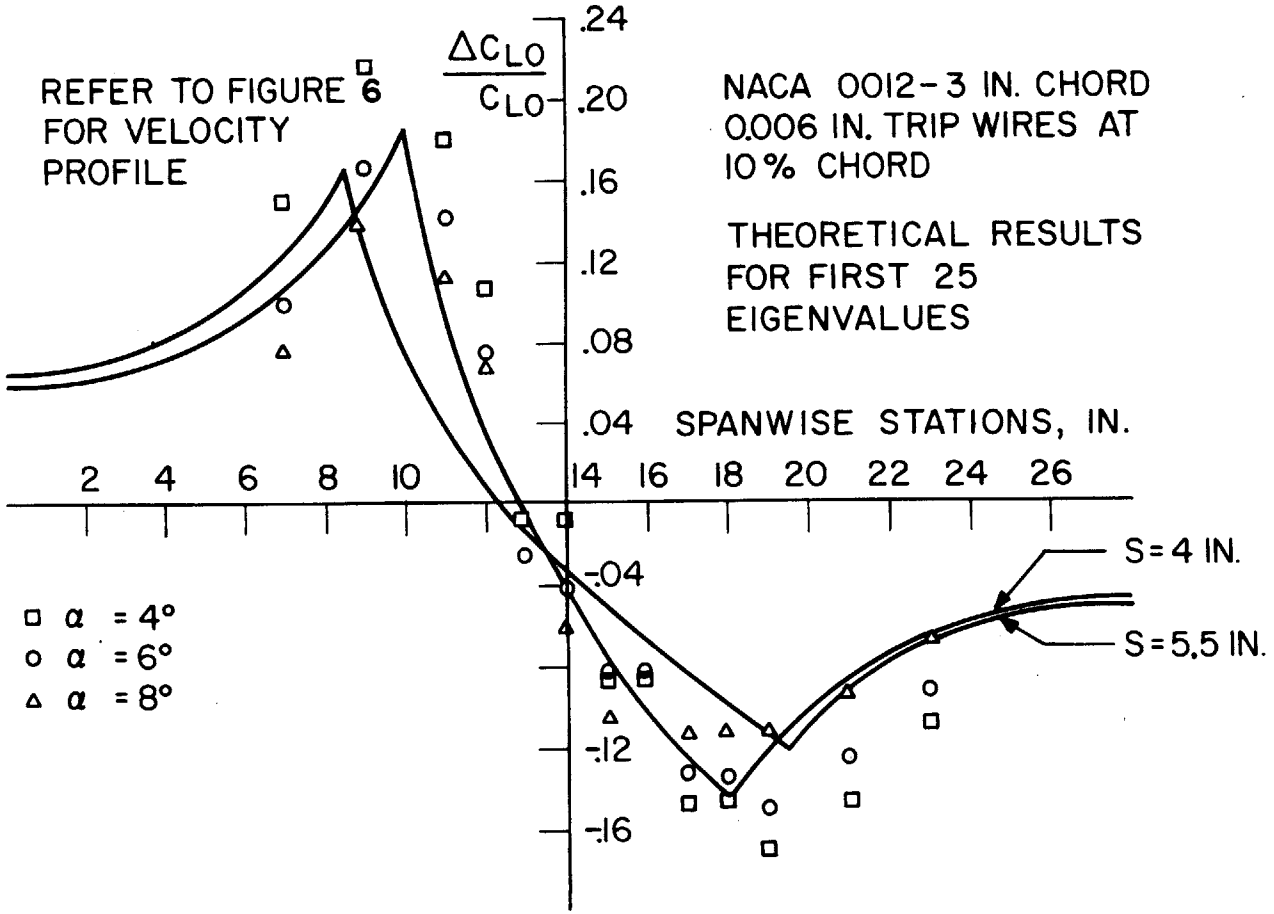

FIGURE 21 COMPARISON OF LINEARIZED THEORY WITH EXPERIMENTAL DATA FOR LARGE SHEAR LATER.

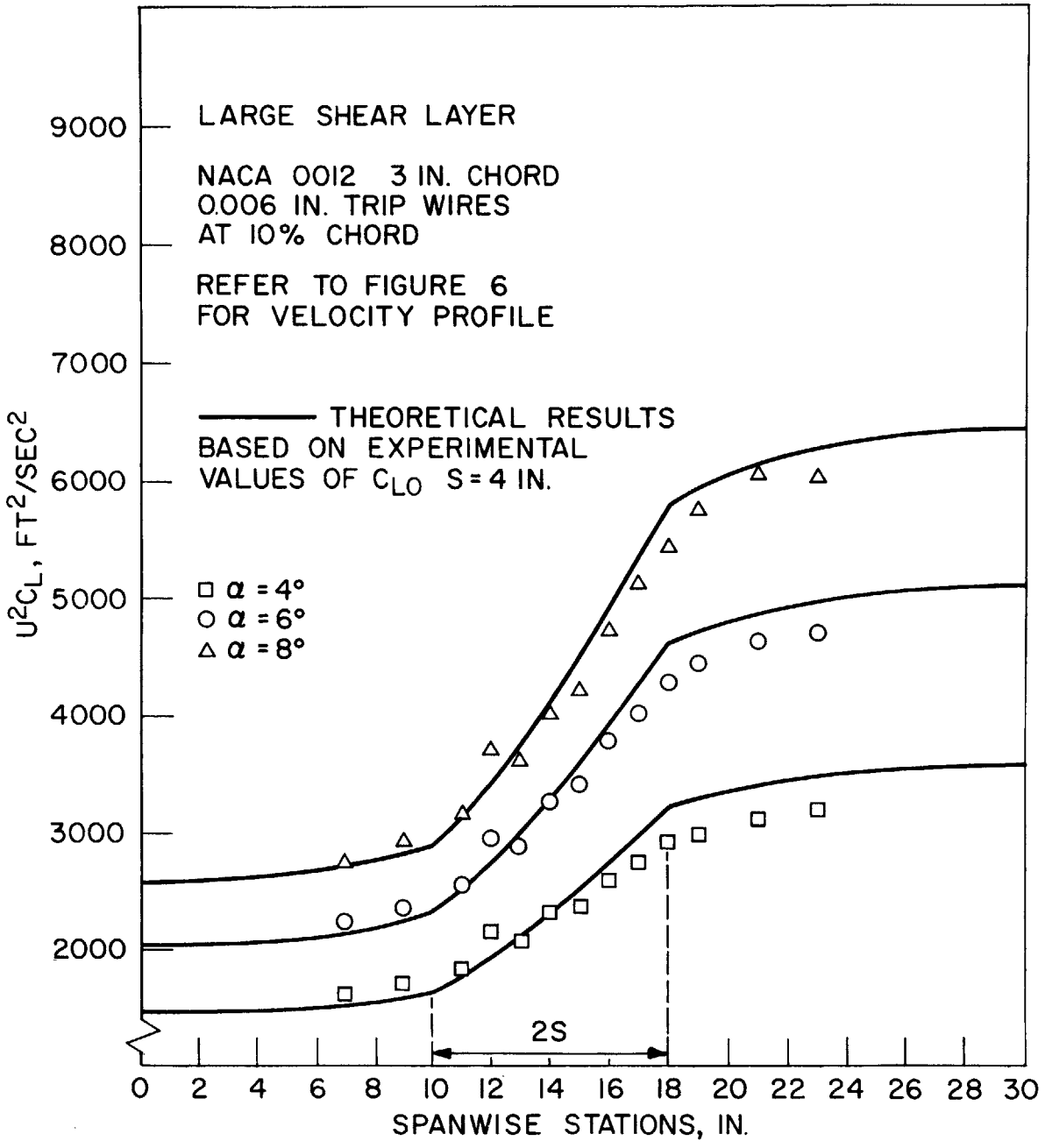

FIGURE 22 COMPARISON OF EXPERIMENTAL AND THEORETICAL DISTRIBUTIONS OF U^2C_L.

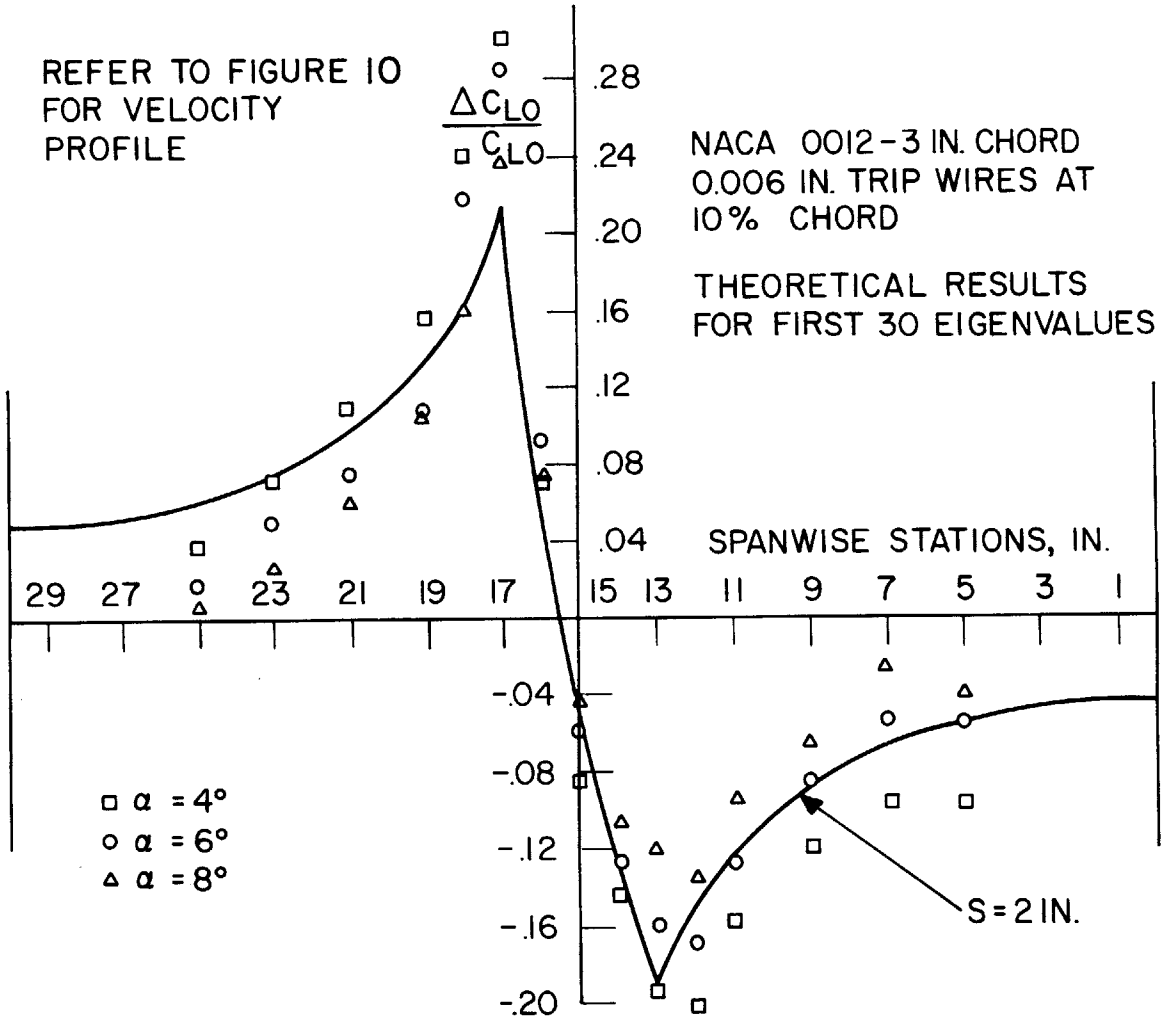

FIGURE 23 COMPARISON OF LINEARIZED THEORY WITH EXPERIMENTAL DATA FOR SMALL SHEAR LAYER.

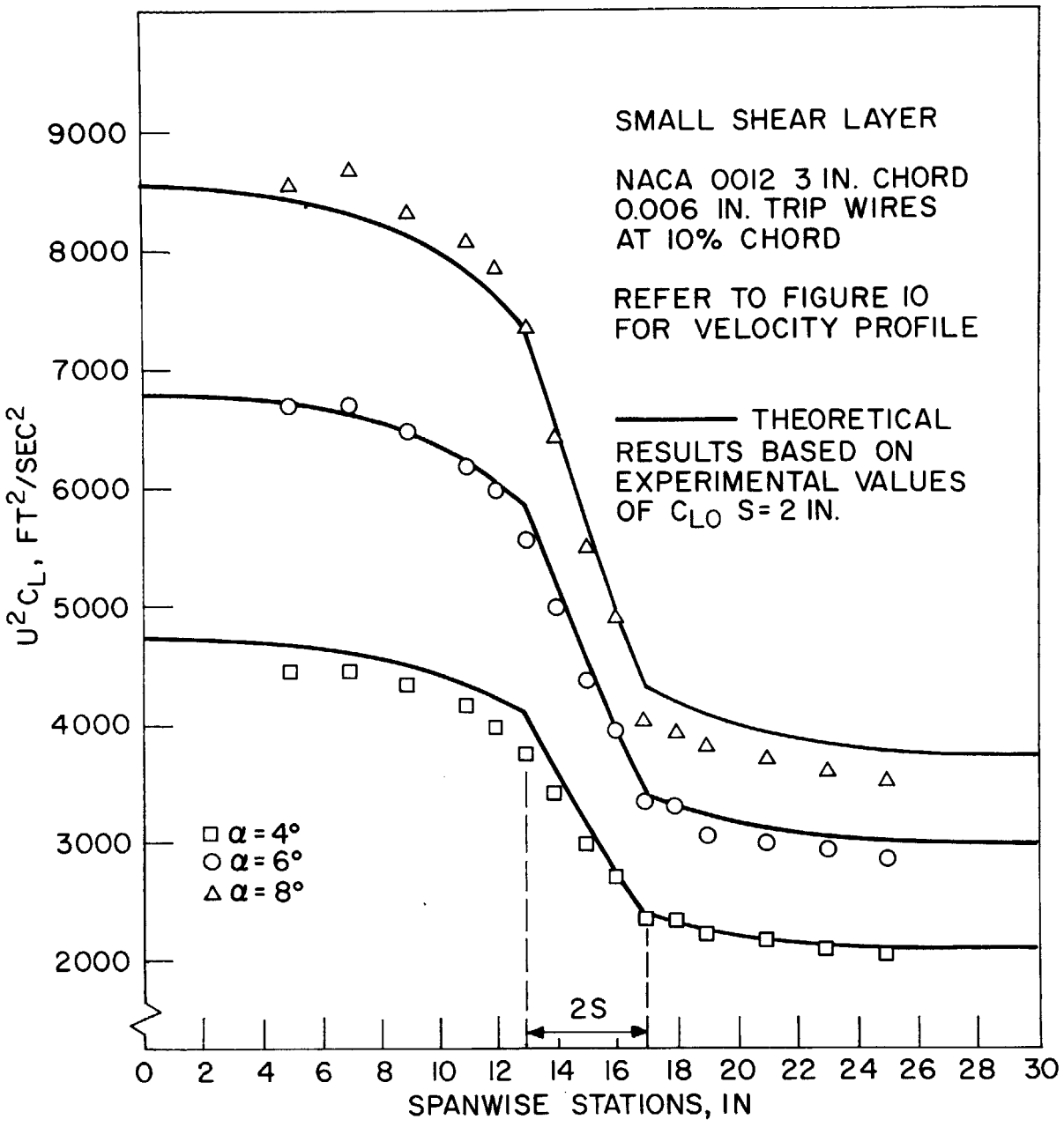

FIGURE 24 COMPARISON OF EXPERIMENTAL AND THEORETICAL DISTRIBUTIONS OF U^2C_L.

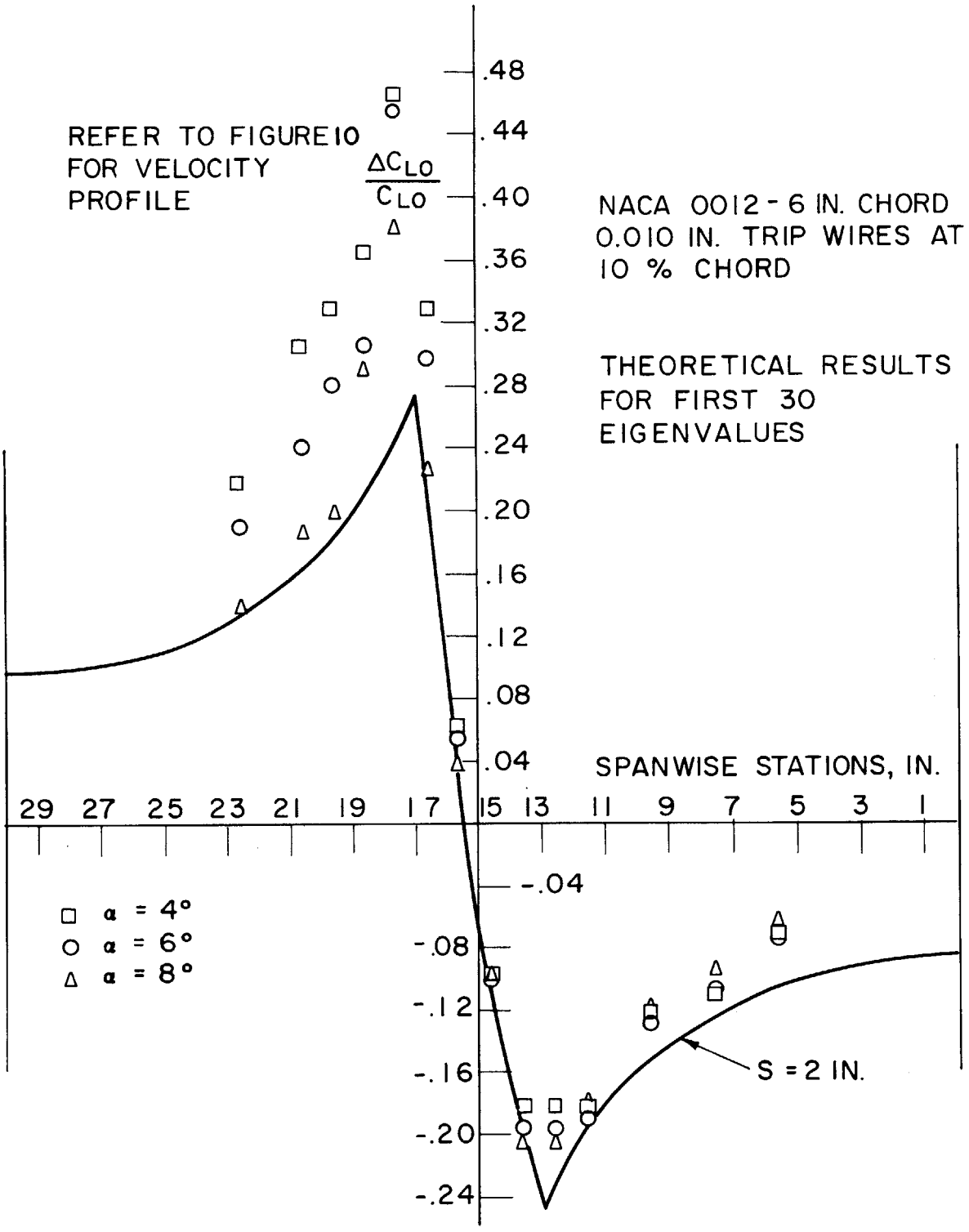

FIGURE 25 COMPARISON OF LINEARIZED THEORY WITH EXPERIMENTAL DATA FOR SMALL SHEAR LAYER

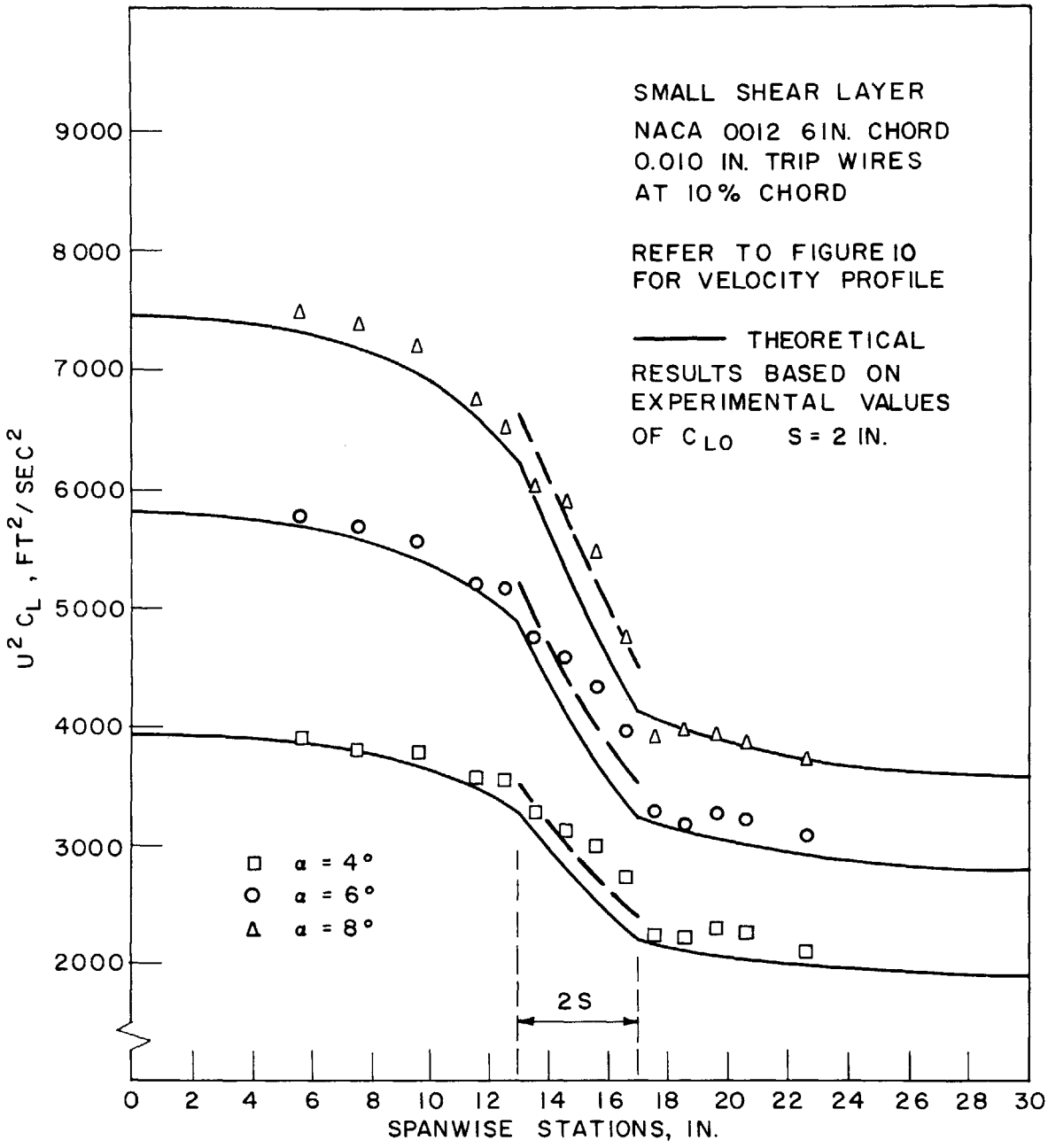

FIGURE 26 COMPARISON OF EXPERIMENTAL AND THEORETICAL DISTRIBUTIONS OF U^2C_L

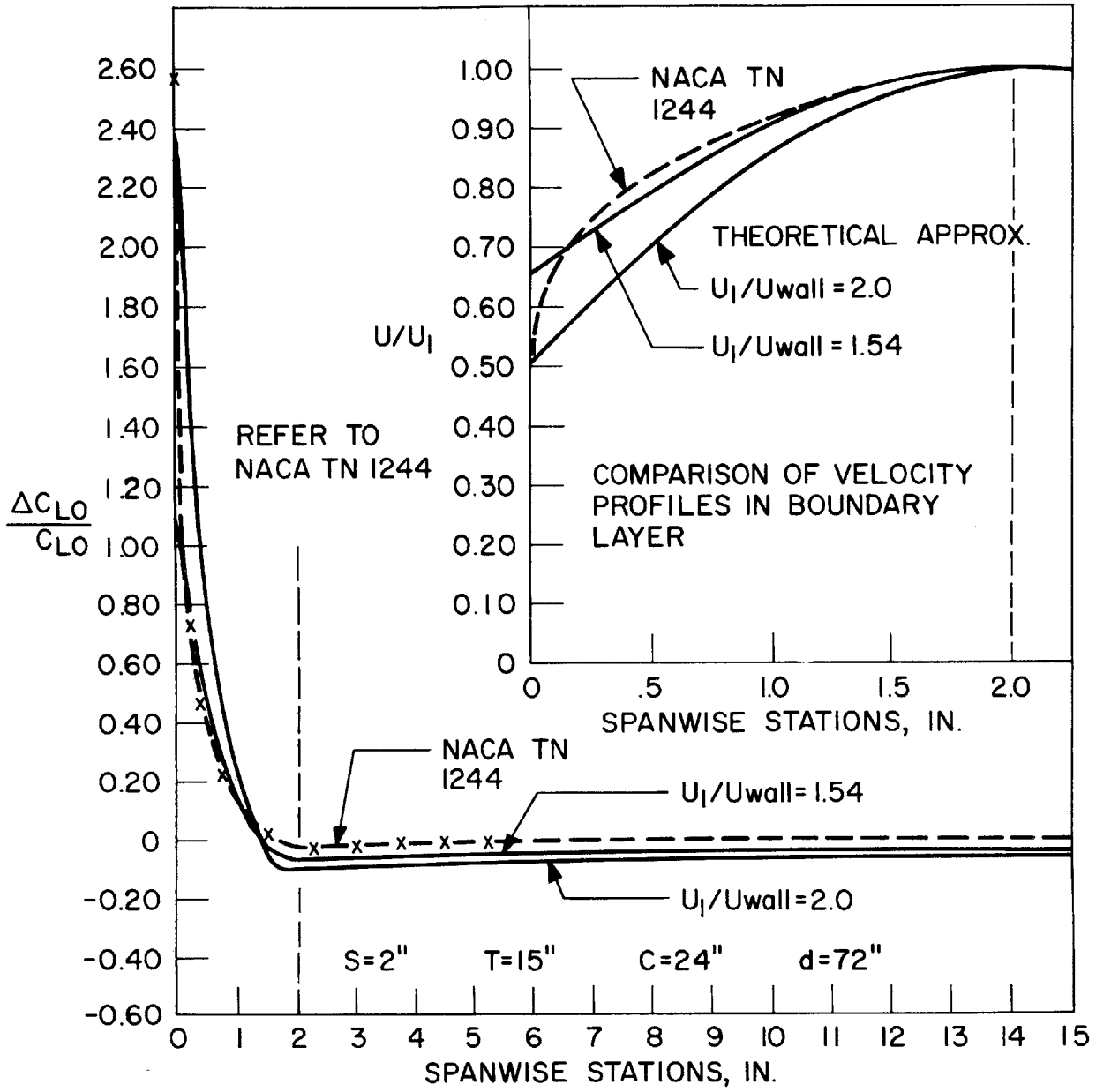

FIGURE 27 COMPARISON OF THEORETICAL RESULTS FOR COSINE UNIFORM PROFILE WITH EXPERIMENTAL DATA OF MENDELSOHN AND POLHAMUS.

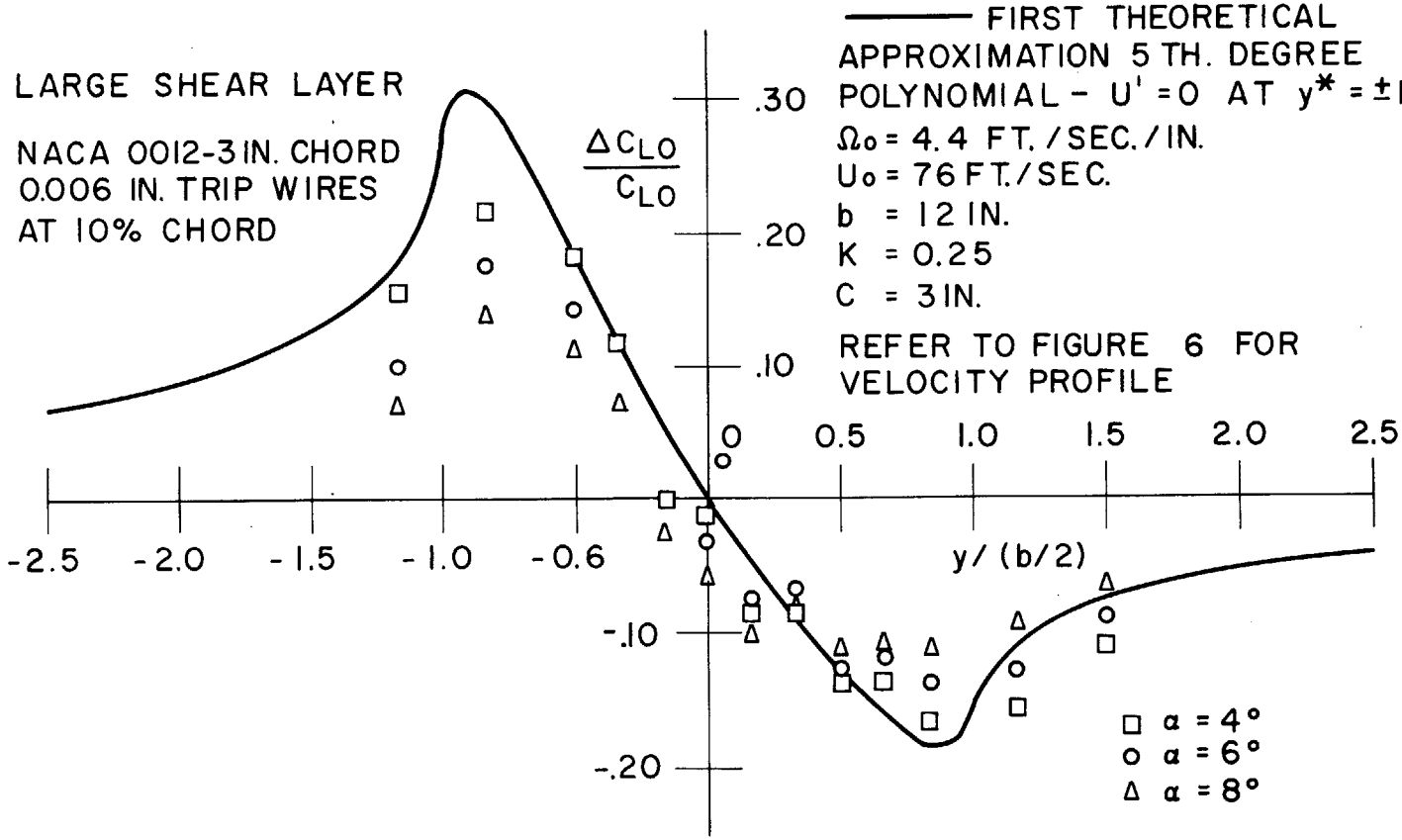

FIGURE 28 COMPARISON OF FIRST THEORETICAL APPROXIMATION WITH EXPERIMENTAL DATA FOR LARGE SHEAR LAYER.

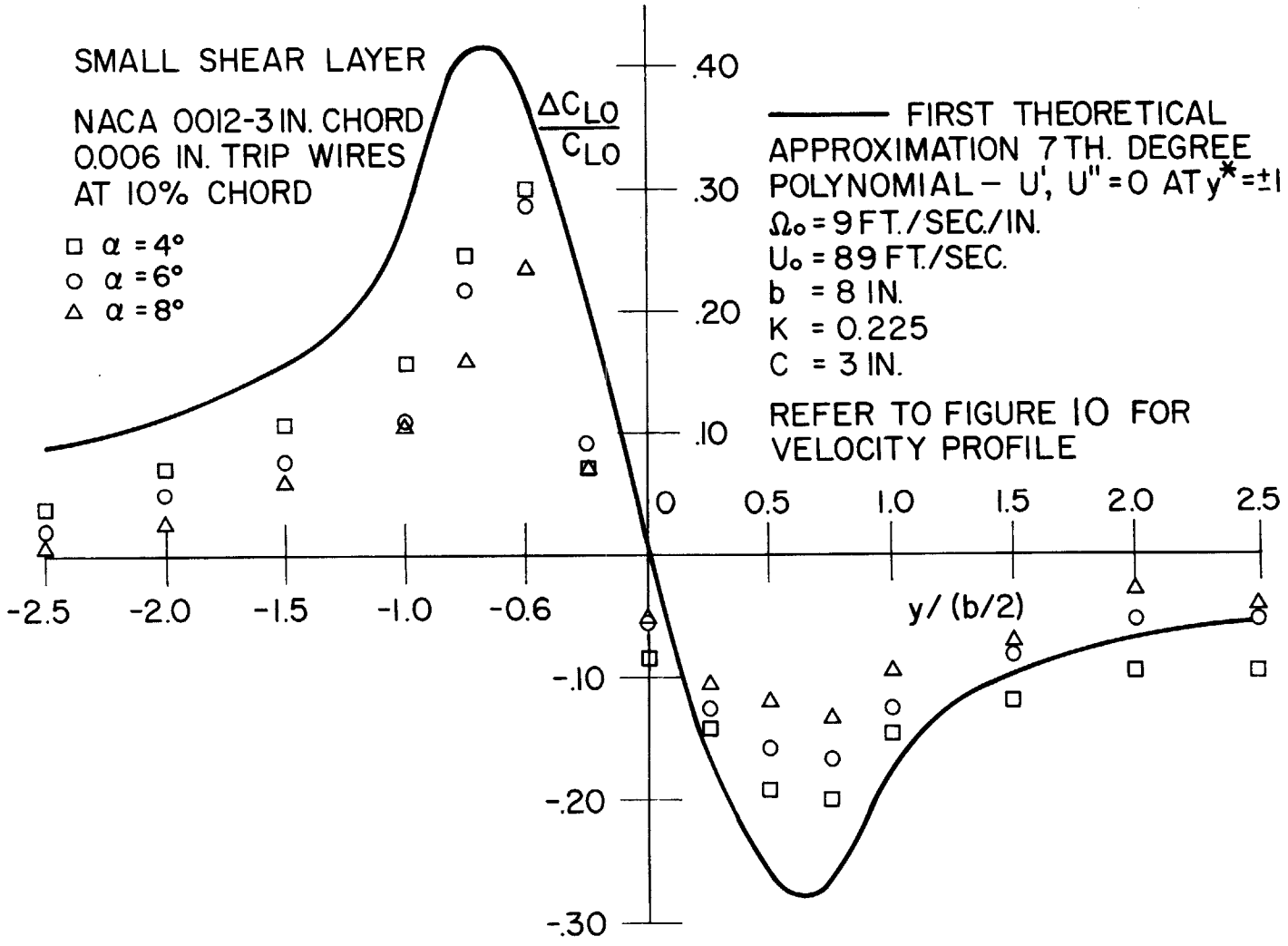

FIGURE 29 COMPARISON OF FIRST THEORETICAL APPROXIMATION WITH EXPERIMENTAL DATA FOR SMALL SHEAR LAYER.

Distortion of Bernoulli Surfaces

The lifting line theory as presented in Sections 2 and 3 does not consider the effects of spanwise displacements of the surfaces of constant stagnation pressure or 'Bernoulli surfaces'. Since there is evidence in the comparison of theory with experiment for the 6" chord airfoil that the limit of the range of applicability of this theoretical approach has been exceeded, a method of correcting the lifting line theory to take this effect into account will now be presented.

The fundamental relationship between the lift on an airfoil and the equations of ideal fluid motion is simply that the lift is the integral of the pressure forces over the chord of the airfoil. Using the sign convention of Figure 3, page 23, we can write

$$L(y) = \int_0^c \left[P(x, y, 0^-) - P(x, y, 0^+) \right] dx \qquad (I-1)$$

From equation (3-10), after integration with respect to x from $(-\infty)$ to (x), we have the following expression for P(x, y, z)

$$P(x, y, z) = - \rho U u - \rho U' \int_{-\infty}^{x} v \, dx \qquad (I-2)$$

where $P(-\infty)$ is taken as zero and $u(-\infty)$ vanishes in accordance with the assumption of undisturbed flow at $x = -\infty$. Substituting equation (I-2) into (I-1) we have the following:

$$L(y) = \rho \int_0^c \left[U(u^+ - u^-) + U' \int_{-\infty}^{x} (v^+ - v^-) \, dx \right]_{z=0} dx \qquad (I-3)$$

The first term in equation (I-3) is simply the lift due to the circulation about the profile at a corrected angle of attack $(\alpha_o + w_{LL}/U)$ in a flow U(y) and represents the contribution of the lifting line theory. Denoting this portion of the total lift by L_{LL} we have the result

$$L(y) = L_{LL}(y) + \rho U' \int_0^c \left[\int_{-\infty}^{x} (v^+ - v^-) \, dx \right]_{z=0} dx \qquad (I-4)$$

Equation (I-4) represents the lift correction due to the distortion of the Bernoulli surfaces. With reference to the sign convention adopted in Figure

3, we note that the 'true' lift is underestimated by the lifting line theory when the effect of displacement of the Bernoulli surfaces becomes significant. Equation (I-4) also indicates that the lift correction is necessarily zero at bounding walls where $v(y) = 0$ and in uniform regions of the flow where $U' = 0$.

Unfortunately, equation (I-4) cannot be evaluated from the lifting line analysis since the Trefftz plane approximation does not consider x dependence in a continuous algebraic sense. However, we can evaluate the equation in an approximate manner by relating the term in the integral to the spanwise gradient of lift through the use of equation (3-63a).

We first assume that the spanwise velocities are zero upstream of the disturbance except very close to the airfoil and that they vary linearly with x along the chord of the airfoil to the magnitude of v_T at the trailing edge. Then for $x < c$

$$\int_{-\infty}^{x} (v^+ - v^-)\, dx \approx \int_0^x (v_T{}^+ - v_T{}^-)\, \frac{x}{c}\, dx = (v_T{}^+ - v_T{}^-)\, \frac{x^2}{2c}$$

Using the above approximation and equation (3-63a) we have from equation (I-4)

$$L(y) \approx L_{LL}(y) + \frac{c^2}{6}\, \frac{U'}{U}\, \frac{d}{dy}\, (L_{LL}(y)) \qquad \text{(I-5)}$$

We note here the dependence on the square of the chord which, in effect, quadrupled the magnitude of the correction between the 3" chord and the 6" chord experiments for the small shear layer in this investigation.

A more useful form of equation (I-5) may be obtained from the use of the relation

$$L_{LL}(y) = \frac{\rho c}{2}\, U^2 C_{Lo} (1 + \Delta C_{Lo}/C_{Lo})$$

$$\frac{L(y)}{L_{LL}(y)} \approx 1 + \frac{c^2}{6}\, \frac{U'}{U} \left[2\, \frac{U'}{U} + \frac{\frac{d}{dy}\, (\Delta C_{Lo}/C_{Lo})}{(1 + \Delta C_{Lo}/C_{Lo})} \right] \qquad \text{(I-6)}$$

Equations (I-6) and (3-81) may then be used to compute the lift correction directly.

The theoretical results as corrected through the use of equation (I-5)

are indicated by the dotted curves in Figure 26 for the 6" chord airfoil.

A difficulty in the application of this correction is apparent for velocity profiles where U'(y) is not continuous. Physically, the corrected lift distribution must be continuous through the requirement of continuity of pressure, therefore, a smoothing of the correction is suggested in regions where U' is not continuous. The lift correction may be applied directly through the use of equations (I-5) or (I-6) for the shear flow solutions presented in Sections 3.7, 3.9, and 3.10 since U'(y) is continuous for all of these velocity profiles.

The order of the lift correction within the shear layer may be estimated from equation (I-6) by the observation that for the matched linear shear profiles investigated here

$$\frac{d}{dy}\left(\Delta C_{Lo}/C_{Lo}\right) \cong - U'/U \qquad |y| < |s|$$

Using this, and neglecting the term $\Delta C_{Lo}/C_{Lo}$ in comparison to 1, equation (I-6) becomes

$$\frac{L(y)}{L_{LL}(y)} = 1 + \frac{1}{6}(cU'/U)^2 \qquad \text{(I-7)}$$

Equation (I-7) indicates the relationship between the Bernoulli surface distortion effects and the parameter (cU'/U).

APPENDIX II

Details of Solution for Matched Linear Profile

The complete solution of the eigenvalue problem for the non-degenerate case requires the evaluation of the integrals in equation (3-81). We write, for convenience, the following form for equation (3-81):

$$\frac{\Delta C_{Lo}}{C_{Lo}} = -2 \sum_{n=1}^{\infty} \frac{C_1(\lambda) \left[F_n(y)/U(y) \right]^2 \sin^2 \lambda(s-t)}{C_2(\lambda) \left[C_3(\lambda) + C_4(\lambda) + C_5(\lambda) \right]} \qquad \text{(II-1)}$$

where

$$C_1(\lambda) = \sin^2 \lambda(s-t) \int_{-s}^{+s} \frac{U_0'}{U_0(y)} \frac{d}{dy} (F_0 U_0)\, dy$$

$$C_2(\lambda) = 1 + \frac{1}{\frac{\pi c \lambda_n}{4} \tanh \lambda_n D} \qquad \text{(II-2)}$$

$$C_3(\lambda) = \sin^6 \lambda(s-t) \int_{-\ell/2}^{-s} \left[\frac{d}{dy} (F_1) \right]^2 dy$$

$$C_4(\lambda) = \sin^6 \lambda(s-t) \int_{-s}^{+s} \left[\frac{\frac{d}{dy} (F_0 U_0)}{U_0} \right]^2 dy$$

$$C_5(\lambda) = \sin^6 \lambda(s-t) \int_{s}^{\ell/2} \left[\frac{d}{dy} (F_2) \right]^2 dy$$

Performing the indicated integration, we have the following results:

$$C_1(\lambda) = U_0' \sin^3 \lambda(s-t) + U_0' \sin^2 \lambda(s-t) \sin \lambda(s+t) + \left[\lambda U_2 + U_0' \sin \lambda(s-t) \cos \lambda(s-t) \right] \left[\cos \lambda(s-t) - \cos \lambda(s+t) \right] \qquad \text{(II-3)}$$

$$C_3(\lambda) = \frac{\lambda}{4} \left[\sin 2\lambda(s-t) - 2\lambda(s-t) \right] \left[\sin \lambda(s-t) \sin 2\lambda s + \frac{\lambda U_2}{U_0'} \sin \lambda(s+t) \right]^2 \qquad \text{(II-4)}$$

$$C_4(\lambda) = \frac{\lambda}{4} \sin^6 \lambda(s-t) \left[4\lambda s + \sin 2\lambda(s-t) + \sin 2\lambda(s+t) \right] - \frac{\lambda}{4} \left[\frac{\lambda U_2}{U_0'} \sin \lambda(s-t) + \sin^2 \lambda(s-t) \cos \lambda(s-t) \right]^2 \left[-4\lambda s + \sin 2\lambda(s-t) + \sin 2\lambda(s+t) \right] - \lambda \left[\frac{\lambda U_2}{U_0'} \sin^4 \lambda(s-t) + \sin^5 \lambda(s-t) \cos \lambda(s-t) \right] \left[\sin^2 \lambda(s-t) - \sin^2 \lambda(s+t) \right] \qquad \text{(II-5)}$$

$$C_5(\lambda) = \frac{\lambda}{4} \left[\frac{\lambda U_2}{U_0'} \sin \lambda(s-t) \right]^2 \left[\sin 2\lambda(s-t) - 2\lambda(s-t) \right] \qquad \text{(II-6)}$$

equations (3-84), (II-1) through (II-6) and the characteristic solutions of equation (3-85a) constitute the complete solution. The number of eigenvalues required for reasonable convergence is dependent on the ratio $\mu = s/t$. For

small values of μ, as many as 30 eigenvalues may be required. The convergence characteristics are indicated for a sample problem in Figure 30 on the following page.

To facilitate the calculation of $\Delta C_{Lo}/C_{Lo}$ the necessary equations were programmed for computation on an IBM 7094 digital computer. The computer program was written in two sections, the first to compute the eigenvalues, λ_n, and the second to compute the desired values of $\Delta C_{Lo}/C_{Lo}$ for various positions along the span of the airfoil. The computer program Fortran Statements are given on the following pages.

We shall now consider the form of the solution for the degenerate case in which $\lambda = \lambda_{(m/\mu)}$ where (m) and $(\frac{m}{\mu})$ are both even or both odd integers. For these degenerate eigenvalues, $\lambda_{(m/\mu)} = \frac{m}{\mu}\frac{\pi}{\ell}$; and $\sin \lambda_{(m/\mu)}(s \pm t) = 0$. As can be seen from equations (II-1) through (II-6), equation (3-81) becomes indeterminate (0/0) when $\sin \lambda(s \pm t) = 0$.

This difficulty may be resolved by rederiving the eigenfunctions $F_n(y)$ taking into account the requirement that $\sin \lambda(s \pm t) = 0$. The degenerate forms of the eigenfunctions in this case then becomes:

$$F_0(y) = \cos \lambda(y - t) - \frac{U_0' \sin \lambda(y - t)}{\lambda U_0(y)} \qquad \text{(II-7a)}$$

$$F_1(y) = \frac{\cos \lambda(s + t)}{\cos \lambda(s - t)} \cos \lambda(y + t) \qquad \text{(II-7b)}$$

$$F_2(y) = \cos \lambda(y - t) \qquad \text{(II-7c)}$$

We can now proceed to evaluate the integrals $K_i(\lambda)$ in equation (3-81) for the degenerate case. Let

$$K_1(\lambda) = \int_{-\ell/2}^{\ell/2} \frac{U'}{U} \frac{d}{dy}(F_n U)\, dy$$

It can then be shown that

$K_1 = 0$ if (m) and $(\frac{m}{\mu})$ are both even

$K_1 = 2U_0' \sin(\frac{m\pi}{2}) \sin(\frac{m}{\mu}\frac{\pi}{2})$ if (m) and $(\frac{m}{\mu})$ are both odd

The coefficient K_2 is simply C_2 given by equation (II-2). We then define

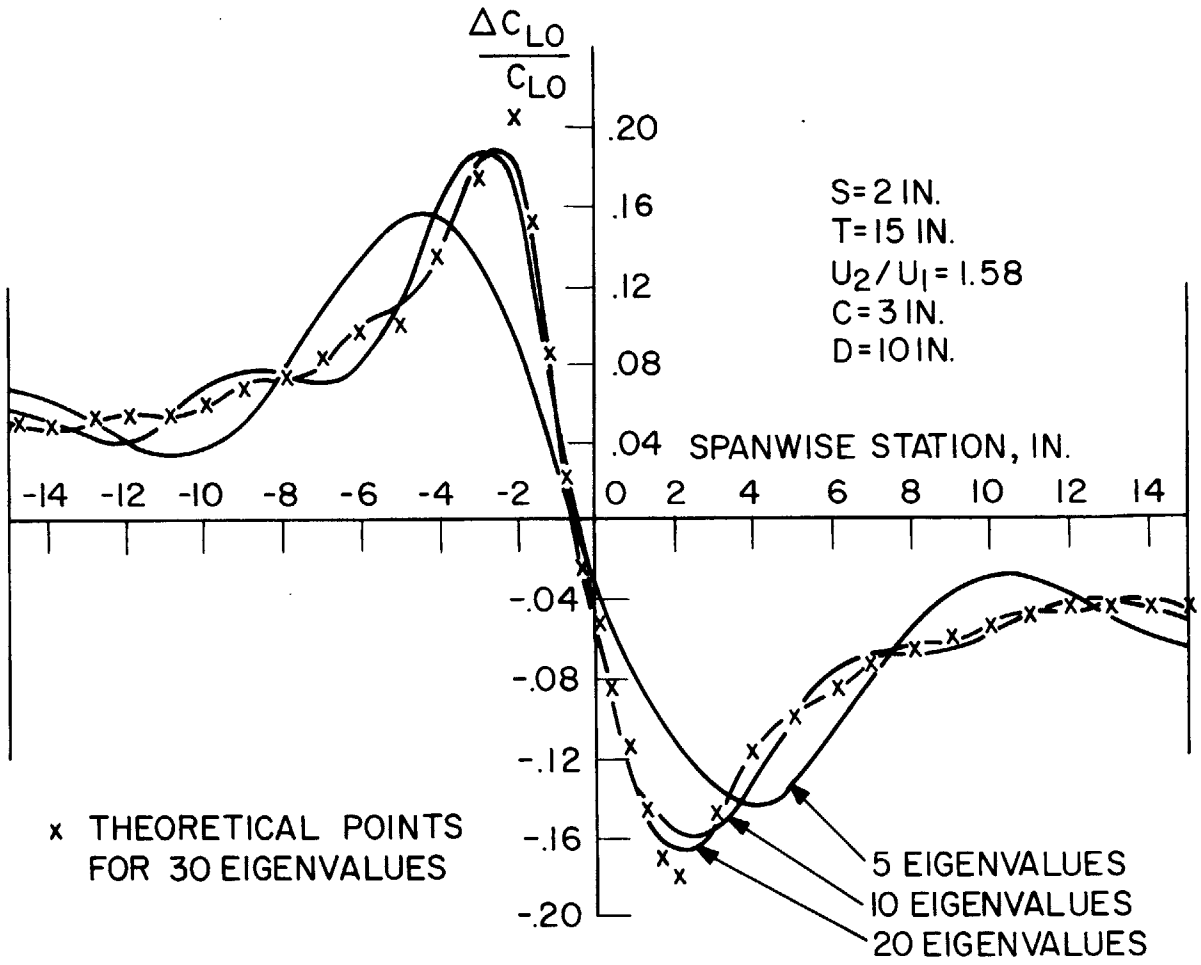

FIGURE 30 CONVERGENCE OF SOLUTION FOR MATCHED LINEAR VELOCITY PROFILE.

```
    LINEARIZED SHEAR FLOW   MATCHED LINEAR PROFILE   EIGENVALUES

    READ 700,M1,L1,L2
700 FORMAT (3I10)
    READ 701,THO,DTH,U1,U2
    READ 701,S,T
701 FORMAT (4F15.7)
    RAT=S/T
    UP=(U2-U1)/(2.0*S)
    UPR=1.0/UP
    DIMENSION EGV(100),TH(2),SIGN(2)
    PRINT 700,M1,L1,L2
    PRINT 701,THO,DTH,U1,U2
    PRINT 701,S,T
    DO 100 I=1,M1
    TH(1)=THO
    TH(2)=THO+DTH
  5 DO 1 K=1,2
  1 SIGN(K)=(TH(K)**2)*SINF(2.0*TH(K)/RAT)-(((U2-U1)**2)/(4.0*U2*U1))*
   1(TH(K)*(COSF(2.0*TH(K)/RAT)-COSF(2.0*TH(K)))+(SINF(2.0*TH(K)))*
   2(SINF((1.0/RAT-1.0)*TH(K)))**2)
    IF(SIGN(1)*SIGN(2)) 3,3,2
  2 TH(1)=TH(2)
    TH(2)=TH(2)+DTH
    GO TO 5
  3 TH(2)=TH(1)+0.1*DTH
  8 DO 4 K=1,2
  4 SIGN(K)=(TH(K)**2)*SINF(2.0*TH(K)/RAT)-(((U2-U1)**2)/(4.0*U2*U1))*
   1(TH(K)*(COSF(2.0*TH(K)/RAT)-COSF(2.0*TH(K)))+(SINF(2.0*TH(K)))*
   2(SINF((1.0/RAT-1.0)*TH(K)))**2)
    IF(SIGN(1)*SIGN(2)) 7,7,6
  6 TH(1)=TH(2)
    TH(2)=TH(2)+0.1*DTH
    GO TO 8
  7 TH(2)=TH(1)+0.01*DTH
 12 DO 9 K=1,2
  9 SIGN(K)=(TH(K)**2)*SINF(2.0*TH(K)/RAT)-(((U2-U1)**2)/(4.0*U2*U1))*
   1(TH(K)*(COSF(2.0*TH(K)/RAT)-COSF(2.0*TH(K)))+(SINF(2.0*TH(K)))*
   2(SINF((1.0/RAT-1.0)*TH(K)))**2)
    IF(SIGN(1)*SIGN(2)) 11,11,10
 10 TH(1)=TH(2)
    TH(2)=TH(2)+0.01*DTH
    GO TO 12
 11 TH(2)=TH(1)+0.001*DTH
 16 DO 13 K=1,2
 13 SIGN(K)=(TH(K)**2)*SINF(2.0*TH(K)/RAT)-(((U2-U1)**2)/(4.0*U2*U1))*
   1(TH(K)*(COSF(2.0*TH(K)/RAT)-COSF(2.0*TH(K)))+(SINF(2.0*TH(K)))*
   2(SINF((1.0/RAT-1.0)*TH(K)))**2)
    IF(SIGN(1)*SIGN(2)) 15,15,14
 14 TH(1)=TH(2)
    TH(2)=TH(2)+0.001*DTH
    GO TO 16
 15 TH(2)=TH(1)+0.0001*DTH
 20 DO 17 K=1,2
 17 SIGN(K)=(TH(K)**2)*SINF(2.0*TH(K)/RAT)-(((U2-U1)**2)/(4.0*U2*U1))*
   1(TH(K)*(COSF(2.0*TH(K)/RAT)-COSF(2.0*TH(K)))+(SINF(2.0*TH(K)))*
   2(SINF((1.0/RAT-1.0)*TH(K)))**2)
```

```
      IF(SIGN(1)*SIGN(2)) 19,19,18
   18 TH(1)=TH(2)
      TH(2)=TH(2)+0.0001*DTH
      GO TO 20
   19 TH(2)=TH(1)+0.00001*DTH
      IF(L1) 27,27,24
   24 DO 21 K=1,2
   21 SIGN(K)=(TH(K)**2)*SINF(2.0*TH(K)/RAT)-(((U2-U1)**2)/(4.0*U2*U1))*
     1(TH(K)*(COSF(2.0*TH(K)/RAT)-COSF(2.0*TH(K)))+(SINF(2.0*TH(K)))*
     2(SINF((1.0/RAT-1.0)*TH(K)))**2)
      IF(SIGN(1)*SIGN(2)) 23,23,22
   22 TH(1)=TH(2)
      TH(2)=TH(2)+0.00001*DTH
      GO TO 24
   23 TH(2)=TH(1)+0.000001*DTH
      IF(L2) 27,27,28
   28 DO 25 K=1,2
   25 SIGN(K)=(TH(K)**2)*SINF(2.0*TH(K)/RAT)-(((U2-U1)**2)/(4.0*U2*U1))*
     1(TH(K)*(COSF(2.0*TH(K)/RAT)-COSF(2.0*TH(K)))+(SINF(2.0*TH(K)))*
     2(SINF((1.0/RAT-1.0)*TH(K)))**2)
      IF(SIGN(1)*SIGN(2)) 27,27,26
   26 TH(1)=TH(2)
      TH(2)=TH(2)+0.000001*DTH
      GO TO 28
   27 EGV(I)=TH(1)/S
      THO=TH(1)+DTH
  100 CONTINUE
      PRINT 750,(EGV(JJ),JJ=1,M1)
  750 FORMAT(4F18.10)
      END
```

EXPLANATION OF INPUT QUANTITIES

M1 = NUMBER OF EIGENVALUES TO BE COMPUTED

L1,L2 = ITERATION DELETION OPTION

IF (L1,L2) POSITIVE, CONTINUE ITERATION

IF (L1,L2) NEGATIVE OR ZERO, DELETE ITERATION

THO = INITIAL VALUE OF THETA

DTH = INCREMENT OF THETA

```
    LINEARIZED SHEAR FLOW   MATCHED LINEAR PROFILE   DELTA CL0 / CL0

    DIMENSION EGV(100),TOP(100),DCLCL1(101),DCLCL0(101),DCLCL2(101),
   1F0(100),F1(100),F2(100),BOT1(100),BOT2(100),BOT3(100),BOTT(100),
   2BOTC(100),Y1(101),Y0(101),Y2(101)
    READ 700,LDATA
    DO 800 L=1,LDATA
    READ 700,M1,N0,N1,N2
700 FORMAT (4I10)
    READ 701,U1,U2
    READ 701,S,T,C,D
701 FORMAT (4F15.7)
    READ 750,(EGV(JJ),JJ=1,M1)
750 FORMAT (4F18.10)
    PRINT 700,M1,N0,N1,N2
    PRINT 701,U1,U2
    PRINT 701,S,T,C,D
    PRINT 750,(EGV(JJ),JJ=1,M1)
    RAT=S/T
    UP=(U2-U1)/(2.0*S)
    UPR=1.0/UP
    DO 150 J=1,M1
    EV=EGV(J)
    S1=SINF(EV*(S-T))
    S2=(SINF(EV*(S-T)))**2
    S3=(SINF(EV*(S-T)))**3
    S4=(SINF(EV*(S-T)))**4
    S5=(SINF(EV*(S-T)))**5
    S6=(SINF(EV*(S-T)))**6
    TOP(J)=S3+S2*SINF(EV*(S+T))+(EV*U2*UPR+S1*COSF(EV*(S-T)))*(COSF(EV
   1*(S-T))-COSF(EV*(S+T)))
    BOT1(J)=0.25*EV*(SINF(2.0*EV*(S-T))-2.0*EV*(S-T))*((S1*SINF(2.0*EV
   1*S)+EV*U2*UPR*SINF(EV*(S+T)))**2)
    BOT2(J)=0.25*EV*S6*(4.0*EV*S+SINF(2.0*EV*(S-T))+SINF(2.0*EV*(S+T))
   1)-0.25*EV*((EV*U2*UPR*S1+S2*COSF(EV*(S-T)))**2)*(-4.0*EV*S+SINF(2.
   20*EV*(S-T))+SINF(2.0*EV*(S+T)))-EV*(EV*U2*UPR*S4+S5*COSF(EV*(S-T))
   3)*(S2-((SINF(EV*(S+T)))**2))
    BOT3(J)=0.25*EV*((EV*U2*UPR*S1)**2)*(SINF(2.0*EV*(S-T))-2.0*EV*(S-
   1T))
    BOTT(J)=BOT1(J)+BOT2(J)+BOT3(J)
150 BOTC(J)=3.14159*C*0.25+1.0/(EGV(J)*TANHF(EGV(J)*D))
    N11=N1+1
    DO 300 K1=1,N11
    AA=K1-1
    AAA=N1
    Y1(K1)=-(T-AA*((T-S)/AAA))
    DO 325 I1=1,M1
    F1(I1)=(((SINF(EGV(I1)*(S-T)))**2)*SINF(2.0*EGV(I1)*S)+EGV(I1)*U2
   1*UPR*SINF(EGV(I1)*(S-T))*SINF(EGV(I1)*(S+T)))*COSF(EGV(I1)*(Y1(K1)
   2+T))
    F1(I1)=(F1(I1)*TOP(I1))/(BOTT(I1)*BOTC(I1))
325 CONTINUE
    SUMF1=0.0
    DO 350 I11=1,M1
350 SUMF1=SUMF1+F1(I11)
300 DCLCL1(K1)=((-3.14159*C*UP)/(2.0*U1))*SUMF1
    N01=N0+1
```

```
      DO 400 K2=1,N01
      BB=K2-1
      BBB=N0
      Y0(K2)=-S+BB*(2.0*S/BBB)
      DO 425 I2=1,M1
      EV=EGV(I2)
      S1=SINF(EV*(S-T))
      S2=(SINF(EV*(S-T)))**2
      S3=(SINF(EV*(S-T)))**3
      S4=(SINF(EV*(S-T)))**4
      F0(I2)=(S3*COSF(EV*(S-T))+EV*U2*UPR*S2+(S4*UP)/(EV*((U2+U1)/2.0+
     1UP*Y0(K2))))*COSF(EV*(Y0(K2)-T))+(S4-(UP/(EV*((U2+U1)/2.0+UP*Y0(K2
     2))))*(EV*U2*UPR*S2+S3*COSF(EV*(S-T))))*SINF(EV*(Y0(K2)-T))
      F0(I2)=(F0(I2)*TOP(I2))/(BOTT(I2)*BOTC(I2))
425   CONTINUE
      SUMF0=0.0
      DO 450 I22=1,M1
450   SUMF0=SUMF0+F0(I22)
400   DCLCL0(K2)=((-3.14159*C*UP)/(2.0*((U2+U1)/2.0+UP*Y0(K2))))*SUMF0
      N21=N2+1
      DO 500 K3=1,N21
      CC=K3-1
      CCC=N2
      Y2(K3)=S+CC*((T-S)/CCC)
      DO 525 I3=1,M1
      F2(I3)=EGV(I3)*U2*UPR*((SINF(EGV(I3)*(S-T)))**2)*COSF(EGV(I3)*
     1(Y2(K3)-T))
      F2(I3)=(F2(I3)*TOP(I3))/(BOTT(I3)*BOTC(I3))
525   CONTINUE
      SUMF2=0.0
      DO 550 I33=1,M1
550   SUMF2=SUMF2+F2(I33)
500   DCLCL2(K3)=((-3.14159*C*UP)/(2.0*U2))*SUMF2
      PRINT 751,(Y1(JJ),DCLCL1(JJ),JJ=1,N11)
      PRINT 751,(Y0(JJ),DCLCL0(JJ),JJ=1,N01)
      PRINT 751,(Y2(JJ),DCLCL2(JJ),JJ=1,N21)
751   FORMAT (6F12.6)
800   CONTINUE
      END
```

EXPLANATION OF INPUT QUANTITIES

- LDATA = NUMBER OF DATA SETS TO BE PROCESSED
- M1 = NUMBER OF EIGENVALUES IN INPUT
- N0 = NUMBER OF INCREMENTS OF Y IN REGION (0)
- N1 = NUMBER OF INCREMENTS OF Y IN REGION (1)
- N2 = NUMBER OF INCREMENTS OF Y IN REGION (2)

K_3 as the following:

$$K_3(\lambda) = \int_{-t}^{-s} \left[\frac{d}{dy} (F_1) \right]^2 dy$$

K_4 and K_5 are defined in a similar manner for Regions (0) and (2). Carrying out the indicated integrations, we have the result

$$K_3 + K_4 + K_5 = \lambda_n^2 t$$

We have now established that the denominator in equation (3-81) is non-zero for the degenerate case, and since the numerator is zero ($K_1 = 0$) when (m) and $(\frac{m}{\mu})$ are both even, we have the result that the eigensolutions corresponding to even degenerate eigenvalues are trivial.

The complete solution for the odd degenerate case must include the degenerate solutions as well as the solution given by equation (II-1). For a given value of μ, the spectrum of eigenvalues may include either or both types of degeneracy. For example, for $\mu = \frac{1}{3}$, $\lambda(3, 6, 9 - - -)$ are degenerate: for $\mu = \frac{2}{15}$, $\lambda(30, 60, 90 - - -)$ are degenerate but trivial.

A Table of Eigenvalues for Three Matched Linear Velocity Profiles is given on the following page. (The corresponding solutions are given in Appendix I.) For a given velocity ratio U_2/U_1, the eigenvalues are relatively insensitive to μ for the first three decimal places, and for purposes of approximation, $\lambda_n = n\pi/\ell$. A number of degenerate eigenvalues, whose exact values are integer multiples of π/ℓ were computed correctly to 7 decimal places as a test of the proper functioning of the eigenvalue computer program.

TABLE: EIGENVALUES FOR MATCHED LINEAR PROFILES

	Case 1 λ_n	Case 2 λ_n	Case 3 λ_n
1	0.105148 in.$^{-1}$	0.105629 in.$^{-1}$	0.105757 in.$^{-1}$
2	0.211899	0.213903	0.213578
3	0.315005	0.314415	0.314228
4	0.422468	0.421304	0.419701
5	0.524085	0.524240	0.525160
6	0.631431	0.628809	0.628452
7	0.733063	0.734586	0.733419
8	0.839709	0.837819	0.838732
9	0.942685	0.943147	0.942669
10	1.048196	1.048077	1.047375
11	1.152753	1.151928	1.152610
12	1.257030	1.257387	1.256875
13	1.362590	1.361757	1.361429
14	1.466125	1.466194	1.466590
15	1.571923	1.571503	1.571069
16	1.675565	1.675632	1.675536
17	1.780978	1.780495	1.780617
18	1.885322	1.885510	1.885249
19	1.990023	1.989682	1.989676
20	2.095096	2.094772	2.094673
21	2.199187	2.199464	2.199417
22	2.304613	2.303855	2.303838
23	2.408563	2.408986	2.408749
24	2.513874	2.513434	2.513571
25	2.618177	2.618095	2.618015
26	2.723040		
27	2.827878		
28	2.932247		
29	3.037450		
30	3.141593		

Case 1: s = 2 in., t = 15 in., U_2 = 109 ft/sec., U_1 = 69 ft/sec.

Case 2: s = 4 in., t = 15 in., U_2 = 95 ft/sec., U_1 = 57 ft/sec.

Case 3: s = 5.5 in., t = 15 in., U_2 = 95 ft/sec., U_1 = 57 ft/sec.

APPENDIX III

Analytical Results for Linear, Cosine, and Matched Cosine-Uniform Velocity Profiles

The results of the solution of equation (3-81) for linear, cosine, and matched cosine-uniform velocity profiles are presented in the Figures following. The intent here is to investigate the magnitudes of the theoretical results for different geometries, and to demonstrate the usefulness and the behavior of the various solutions.

The results for the linear and the cosine velocity profiles are straightforward evaluations of the respective solutions given in equations (3-83) and (3-87). The results for the matched cosine-uniform velocity profiles are obtained through the use of the eigenfunctions given in equations (3-88) and the corresponding characteristic equation (3-89). The algebraic details of the matched cosine-uniform solution are not given, but the Fortran statements in the computer program used to evaluate the solution are presented at the end of this Appendix.

Figures 31, 32, and 33 present the results for the linear velocity profile showing the effects of changes in aspect ratio and other parameters on the solution. Figures 34, 35, and 36 present similar results for the cosine velocity profile. The analytical results for the matched cosine-uniform velocity profiles are shown in Figures 37, 38, and 39 for three values of the ratio of shear layer to bounded flow thickness (s/t). The effects of aspect ratio are indicated also. Because of the small value of s/t for the results shown in Figure 39, the sum of the first 45 eigensolutions was calculated. All calculations were performed on an IBM 7094 digital computer.

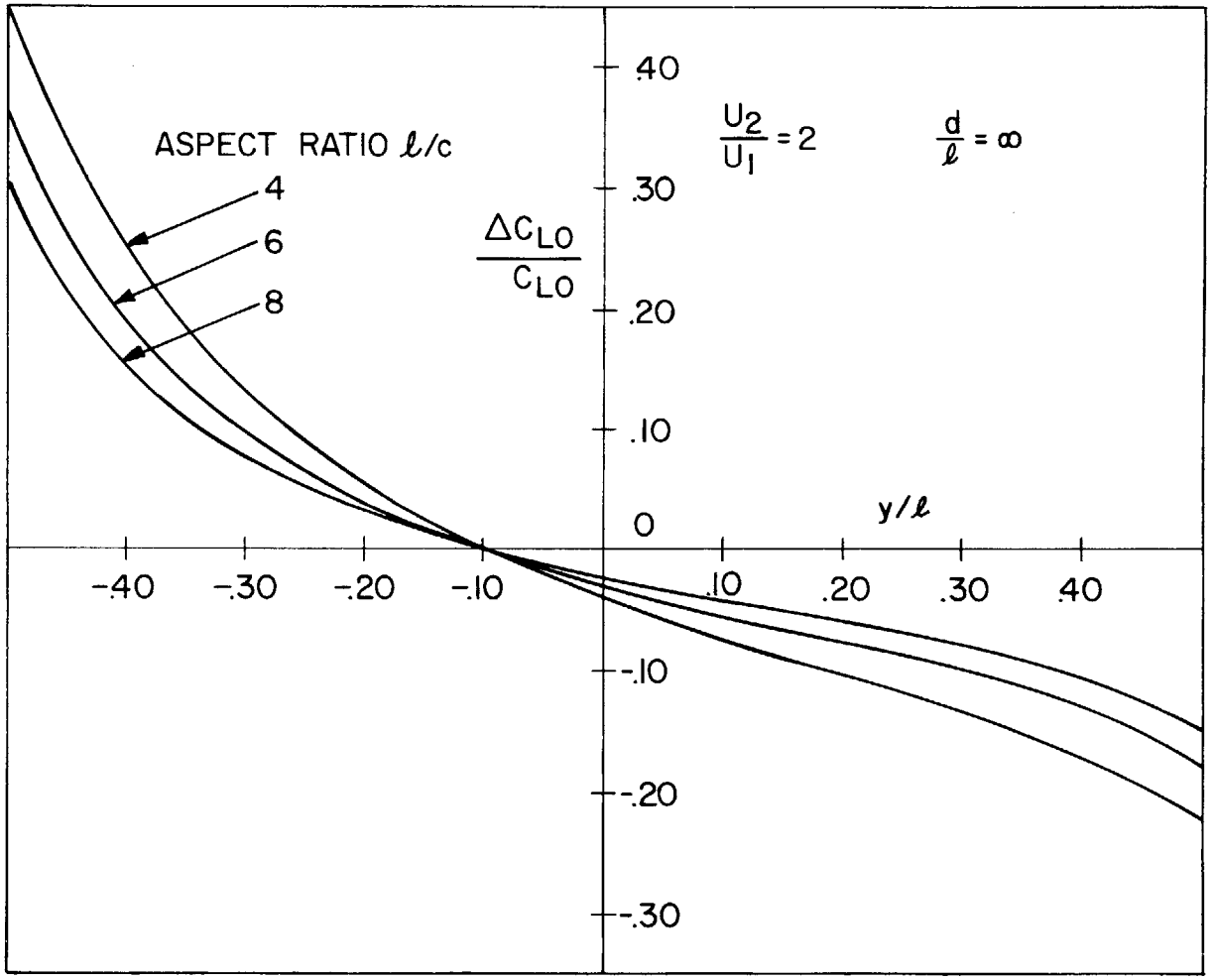

FIGURE 31 CHANGE IN LIFT COEFFICIENT FOR LINEAR VELOCITY PROFILE.

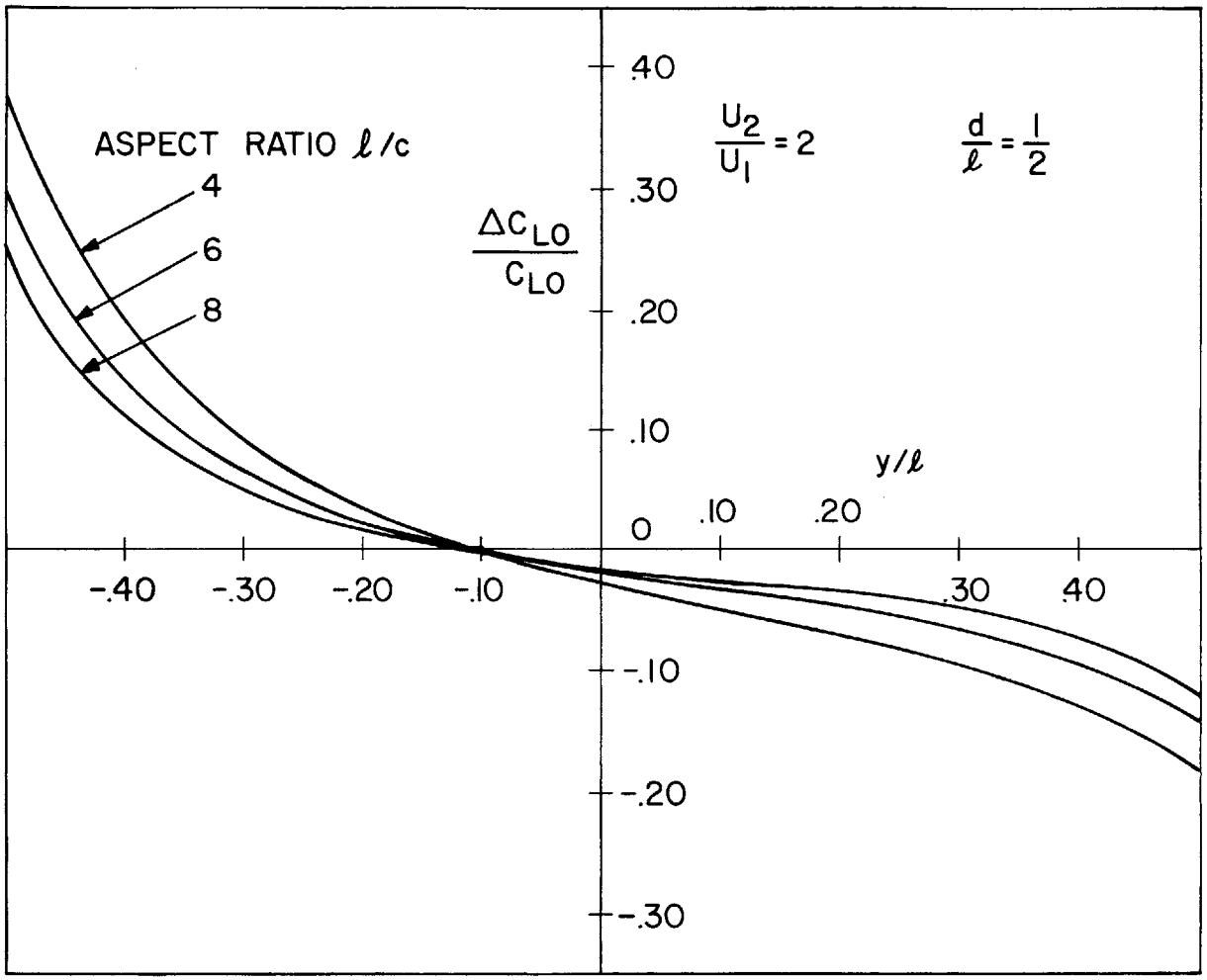

FIGURE 32 CHANGE IN LIFT COEFFICIENT FOR LINEAR VELOCITY PROFILE.

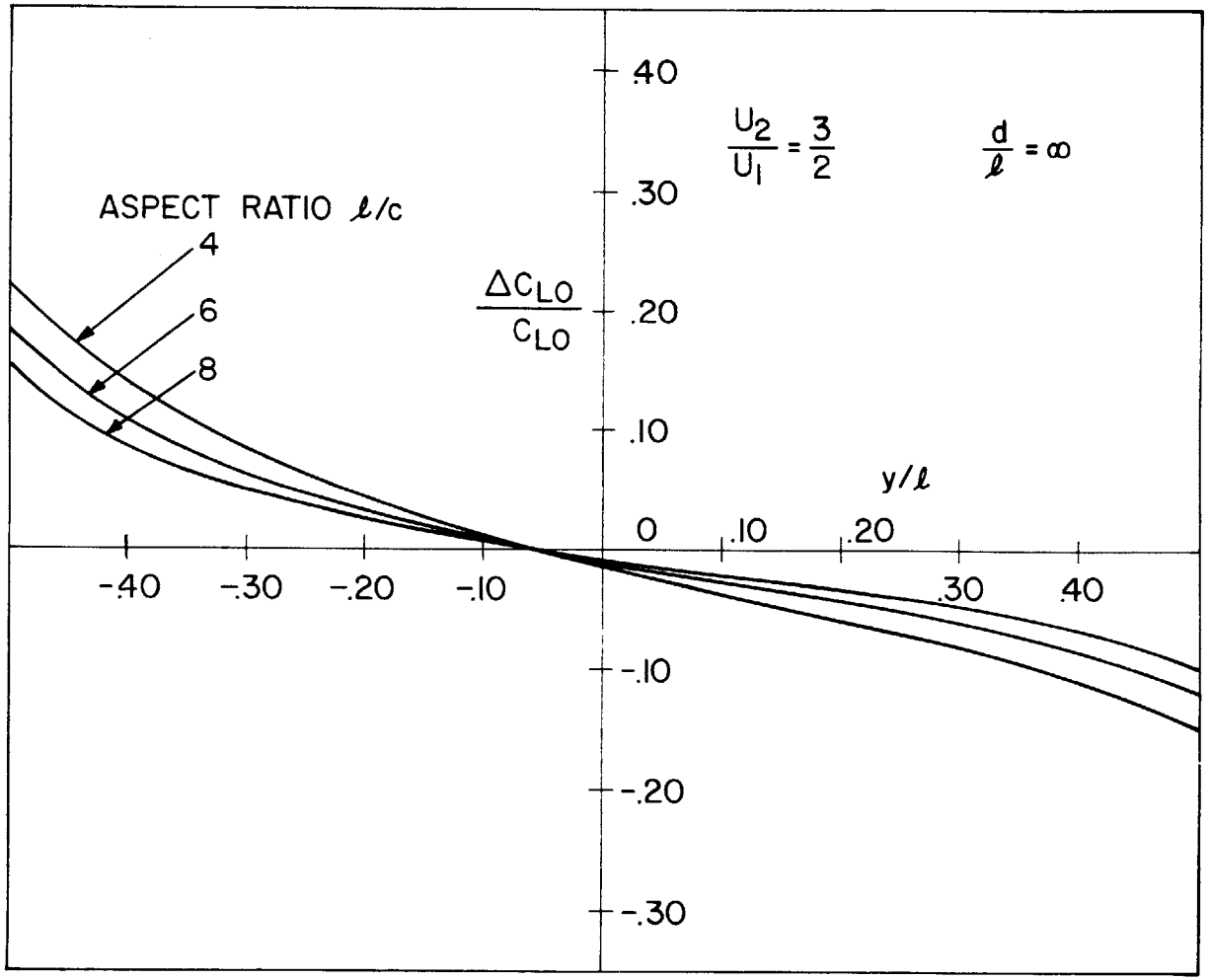

FIGURE 33 CHANGE IN LIFT COEFFICIENT FOR LINEAR VELOCITY PROFILE.

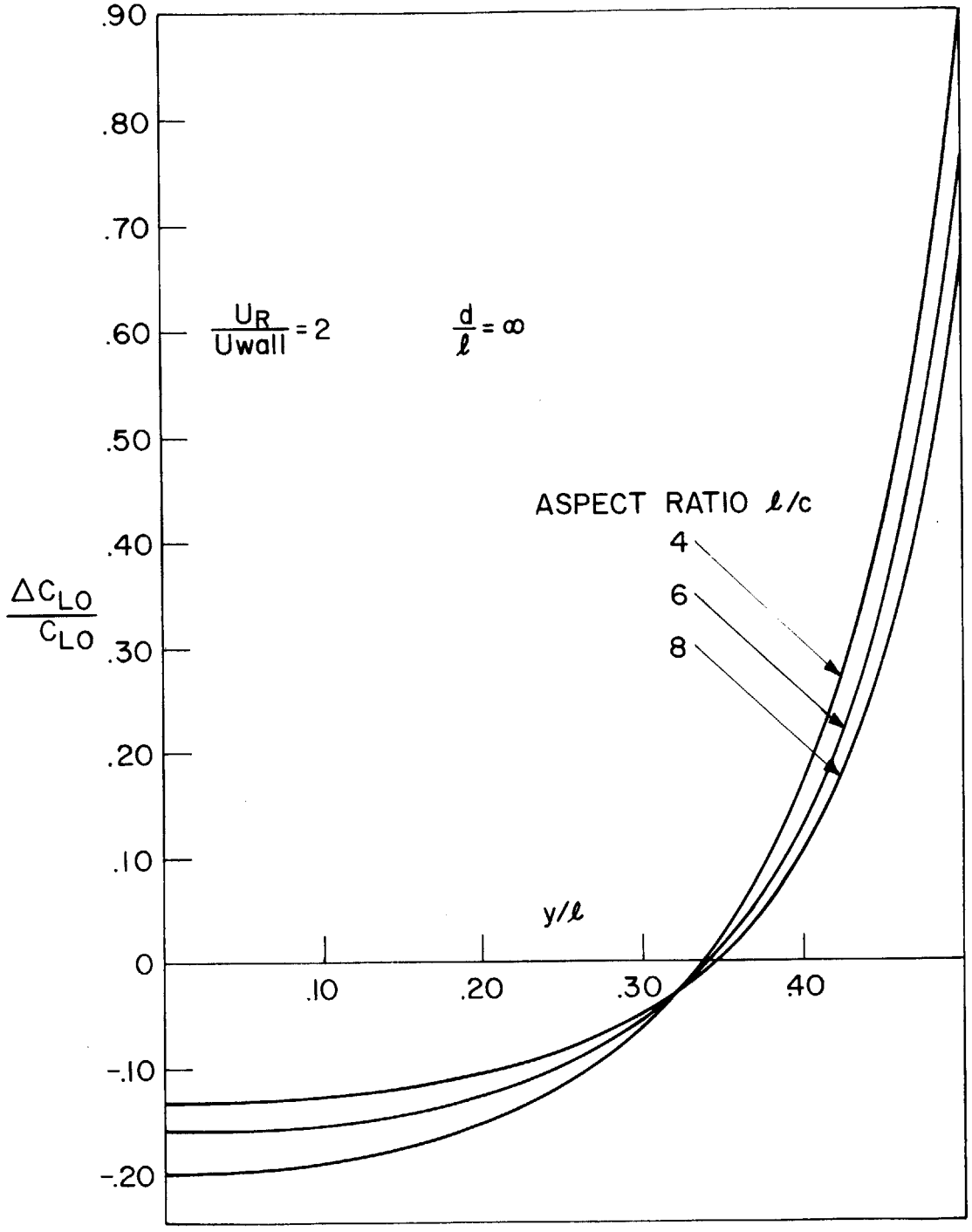

FIGURE 34 CHANGE IN LIFT COEFFICIENT FOR COSINE VELOCITY PROFILE.

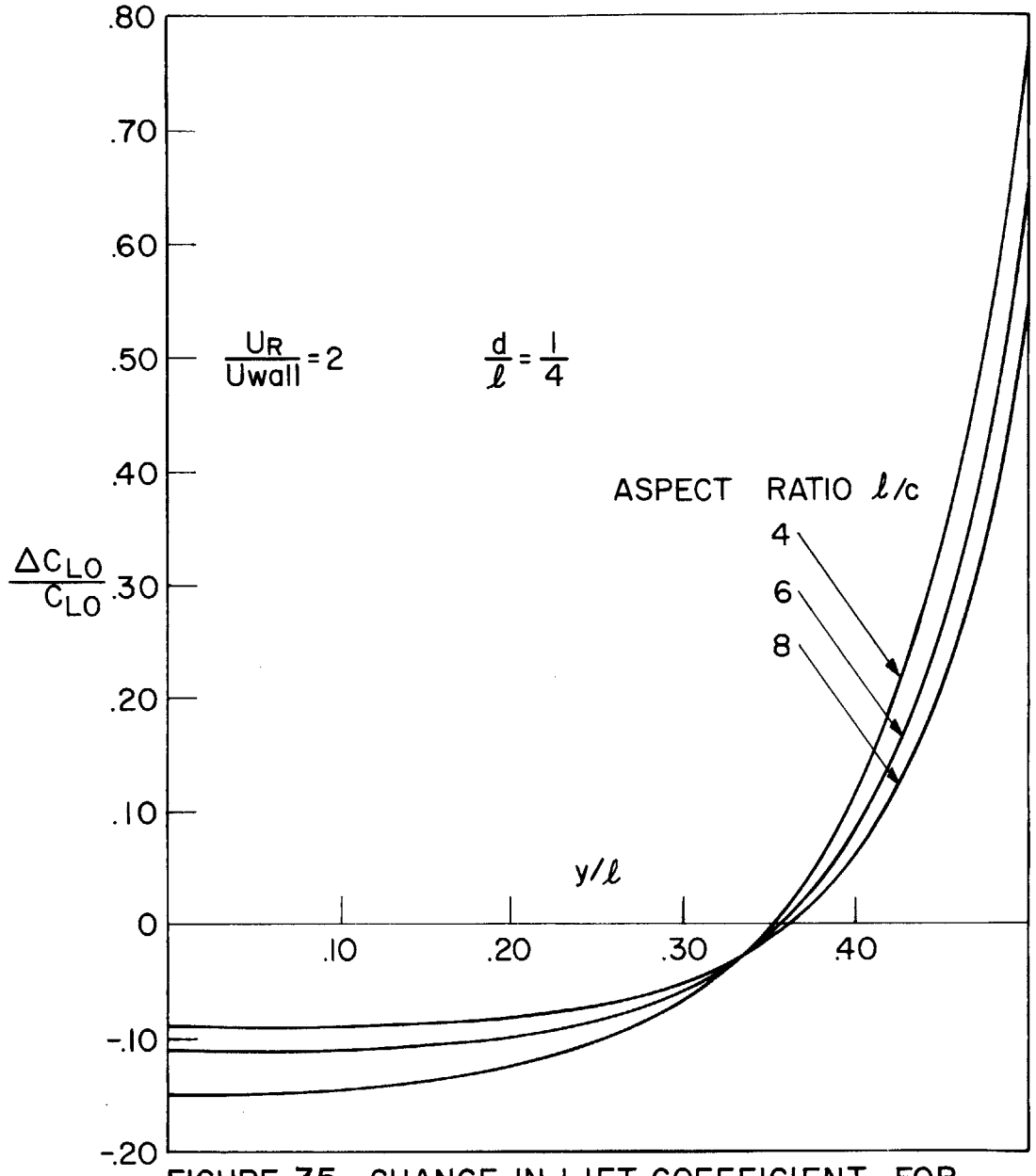

FIGURE 35 CHANGE IN LIFT COEFFICIENT FOR COSINE VELOCITY PROFILE.

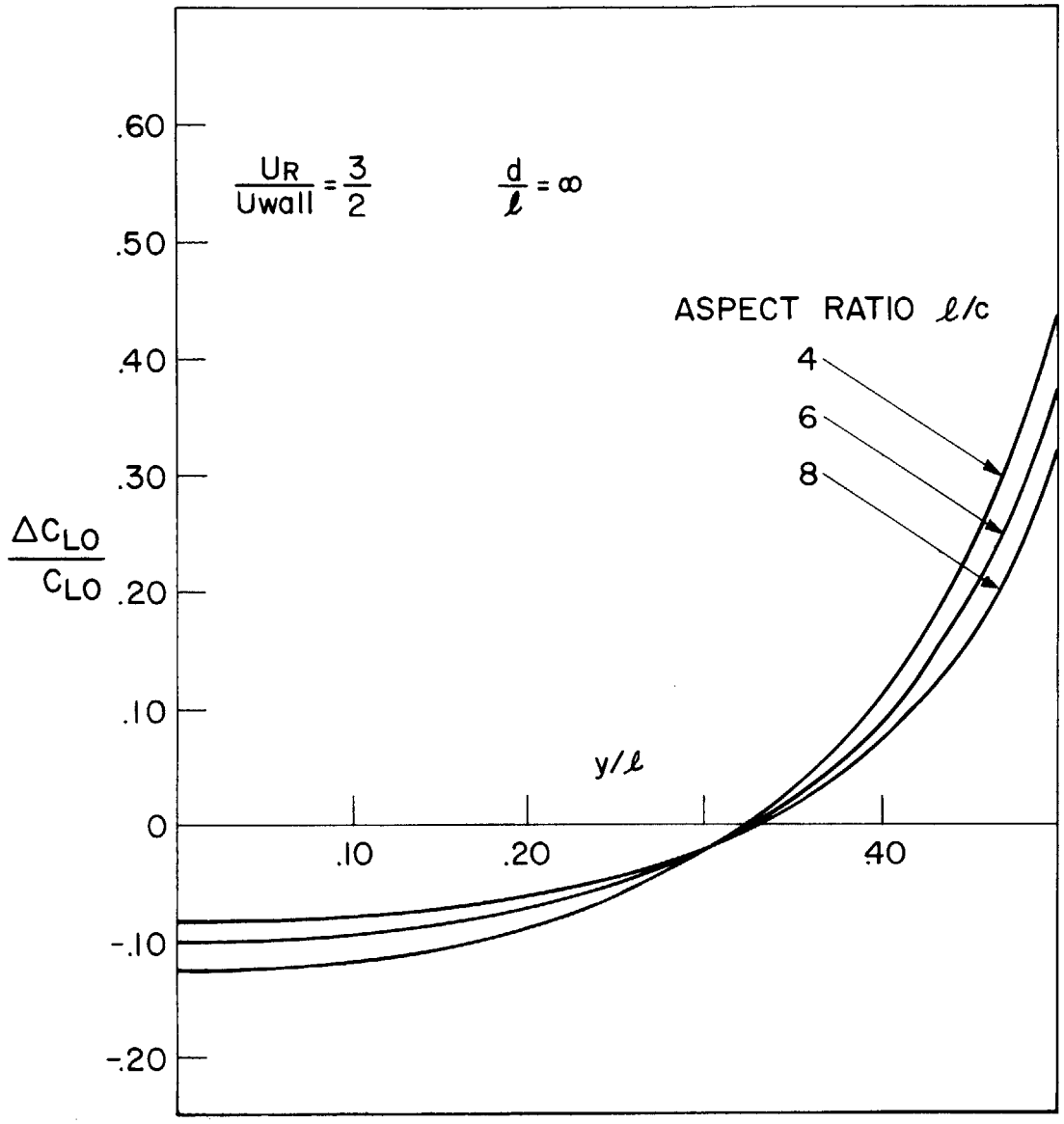

FIGURE 36 CHANGE IN LIFT COEFFICIENT FOR COSINE VELOCITY PROFILE.

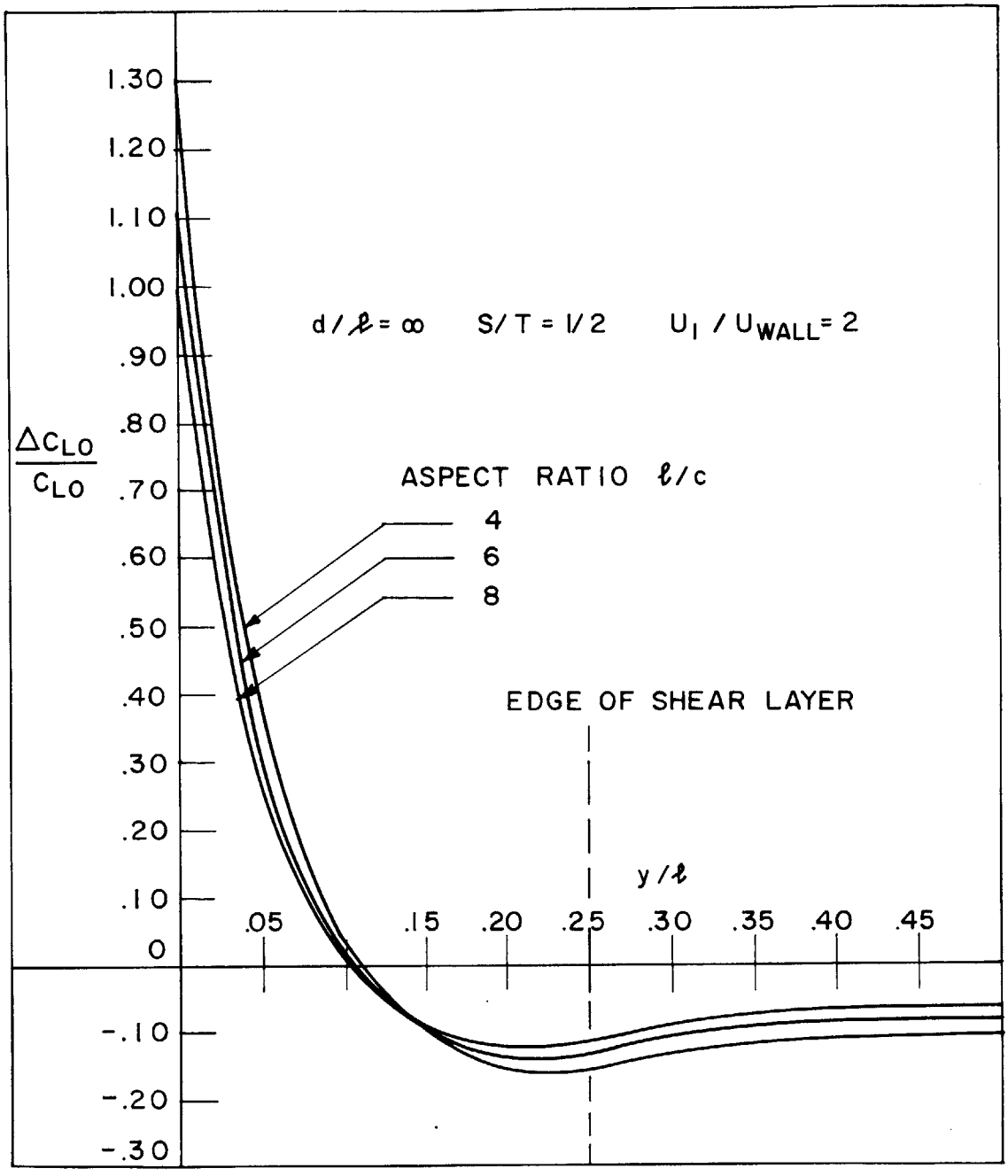

FIGURE 37 THEORETICAL RESULTS FOR MATCHED COSINE - UNIFORM VELOCITY PROFILE

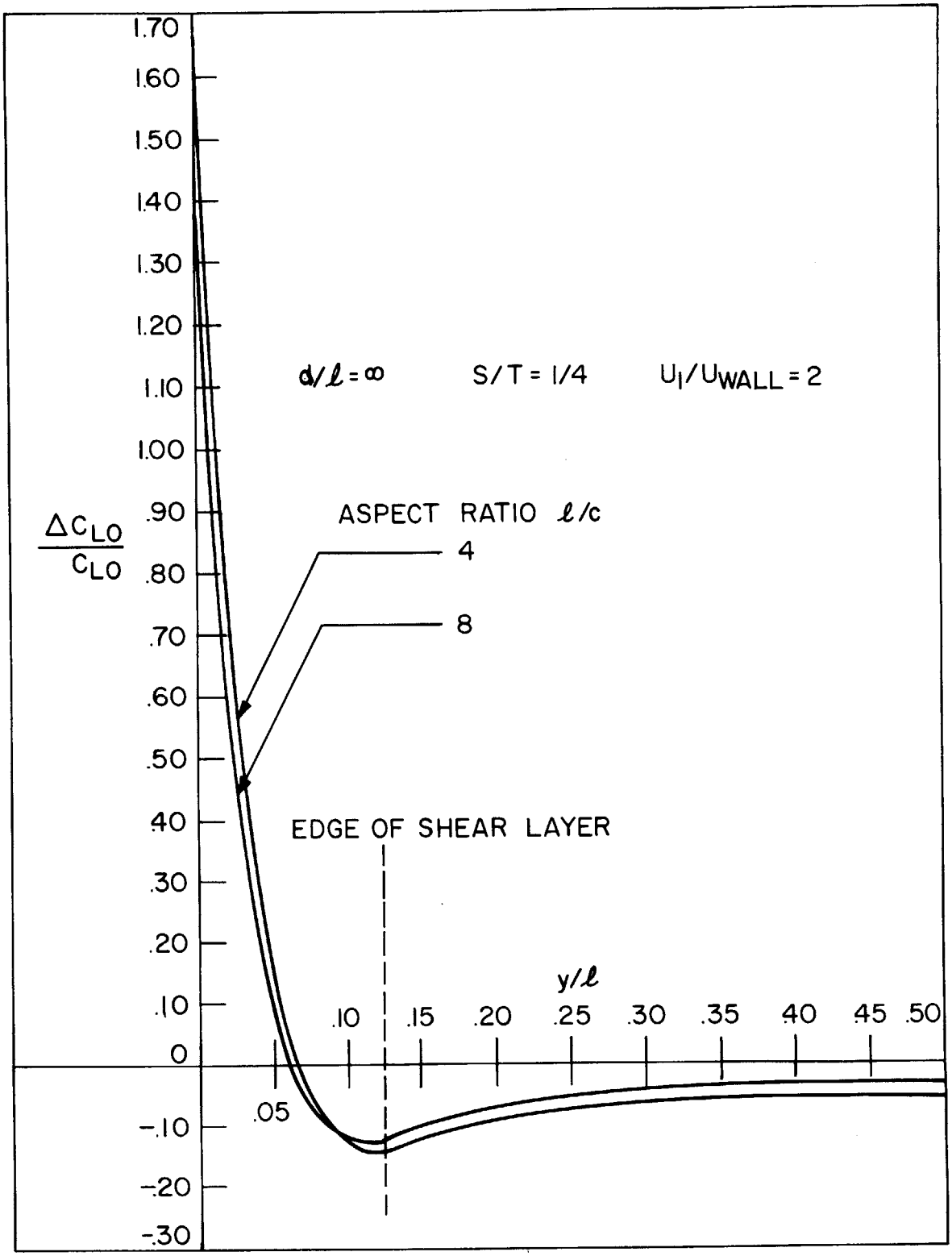

FIGURE 38 THEORETICAL RESULTS FOR MATCHED COSINE-UNIFORM VELOCITY PROFILE.

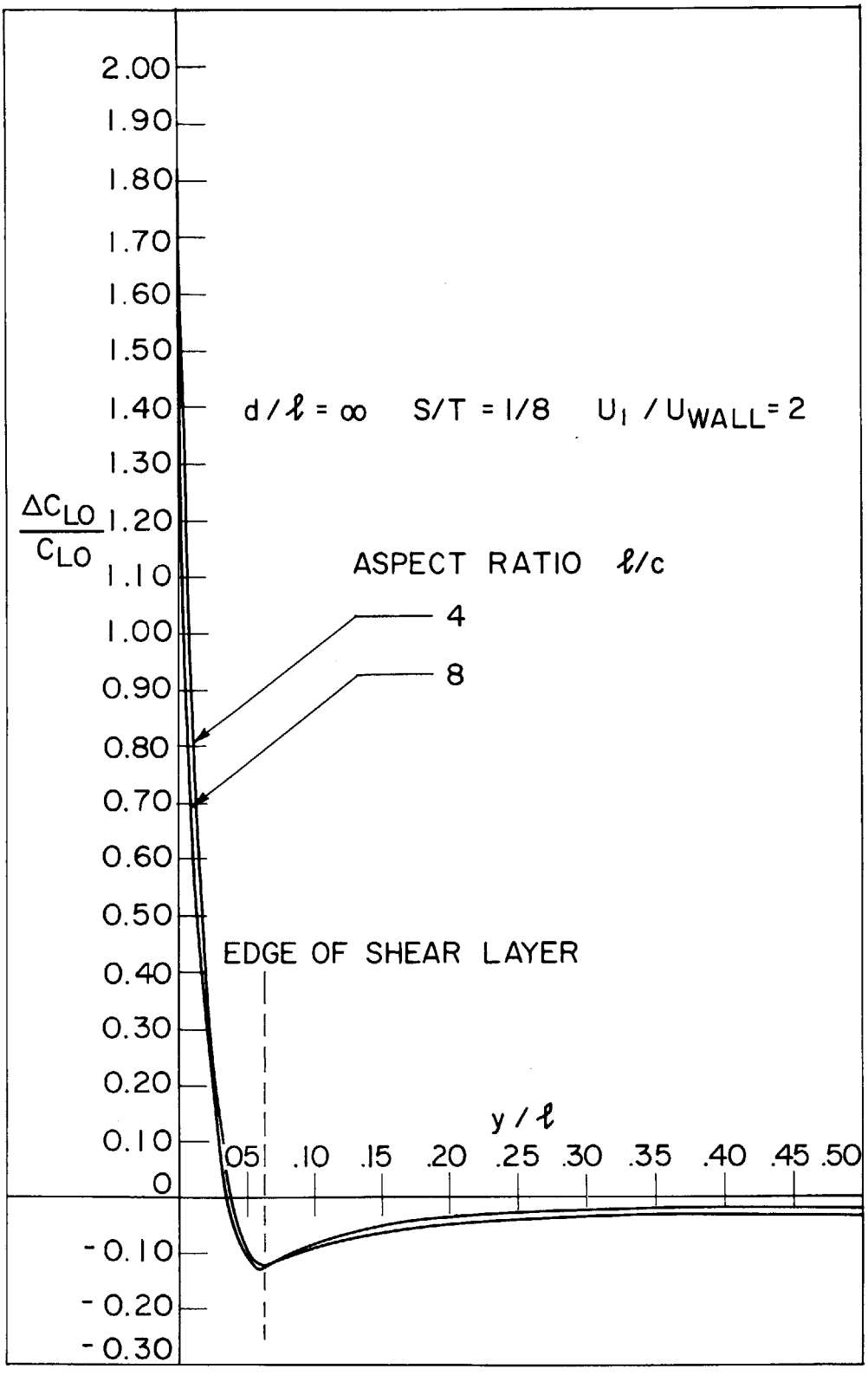

FIGURE 39 THEORETICAL RESULTS FOR MATCHED COSINE-UNIFORM VELOCITY PROFILE

LINEARIZED SHEAR FLOW COSINE-UNIFORM PROFILE EIGENVALUES

```
    READ 700,M1,L1,L2
700 FORMAT (3I10)
    READ 701,THO,DTH,BETA
    READ 701,S,T
701 FORMAT (4F15.7)
    RAT=S/T
    DIMENSION EGV(100),TH(2),SIGN(2),AS(2)
    PRINT 700,M1,L1,L2
    PRINT 701,THO,DTH,BETA
    PRINT 701,S,T
    DO 100 I=1,M1
    TH(1)=THO
    TH(2)=THO+DTH
  5 DO 1 K=1,2
    AS(K)=S*SQRTF((TH(K)/S)**2+BETA**2)
  1 SIGN(K)=TH(K)*COSF(TH(K)*(1.0-1.0/RAT))*SINF(AS(K))
   1-AS(K)*COSF(AS(K))*SINF(TH(K)*(1.0-1.0/RAT))
    IF(SIGN(1)*SIGN(2)) 3,3,2
  2 TH(1)=TH(2)
    TH(2)=TH(2)+DTH
    GO TO 5
  3 TH(2)=TH(1)+0.1*DTH
  8 DO 4 K=1,2
    AS(K)=S*SQRTF((TH(K)/S)**2+BETA**2)
  4 SIGN(K)=TH(K)*COSF(TH(K)*(1.0-1.0/RAT))*SINF(AS(K))
   1-AS(K)*COSF(AS(K))*SINF(TH(K)*(1.0-1.0/RAT))
    IF(SIGN(1)*SIGN(2)) 7,7,6
  6 TH(1)=TH(2)
    TH(2)=TH(2)+0.1*DTH
    GO TO 8
  7 TH(2)=TH(1)+0.01*DTH
 12 DO 9 K=1,2
    AS(K)=S*SQRTF((TH(K)/S)**2+BETA**2)
  9 SIGN(K)=TH(K)*COSF(TH(K)*(1.0-1.0/RAT))*SINF(AS(K))
   1-AS(K)*COSF(AS(K))*SINF(TH(K)*(1.0-1.0/RAT))
    IF(SIGN(1)*SIGN(2)) 11,11,10
 10 TH(1)=TH(2)
    TH(2)=TH(2)+0.01*DTH
    GO TO 12
 11 TH(2)=TH(1)+0.001*DTH
 16 DO 13 K=1,2
    AS(K)=S*SQRTF((TH(K)/S)**2+BETA**2)
 13 SIGN(K)=TH(K)*COSF(TH(K)*(1.0-1.0/RAT))*SINF(AS(K))
   1-AS(K)*COSF(AS(K))*SINF(TH(K)*(1.0-1.0/RAT))
    IF(SIGN(1)*SIGN(2)) 15,15,14
 14 TH(1)=TH(2)
    TH(2)=TH(2)+0.001*DTH
    GO TO 16
 15 TH(2)=TH(1)+0.0001*DTH
 20 DO 17 K=1,2
    AS(K)=S*SQRTF((TH(K)/S)**2+BETA**2)
 17 SIGN(K)=TH(K)*COSF(TH(K)*(1.0-1.0/RAT))*SINF(AS(K))
   1-AS(K)*COSF(AS(K))*SINF(TH(K)*(1.0-1.0/RAT))
    IF(SIGN(1)*SIGN(2)) 19,19,18
 18 TH(1)=TH(2)
```

```
      TH(2)=TH(2)+0.0001*DTH
      GO TO 20
   19 TH(2)=TH(1)+0.00001*DTH
      IF(L1) 27,27,24
   24 DO 21 K=1,2
      AS(K)=S*SQRTF((TH(K)/S)**2+BETA**2)
   21 SIGN(K)=TH(K)*COSF(TH(K)*(1.0-1.0/RAT))*SINF(AS(K))
     1-AS(K)*COSF(AS(K))*SINF(TH(K)*(1.0-1.0/RAT))
      IF(SIGN(1)*SIGN(2)) 23,23,22
   22 TH(1)=TH(2)
      TH(2)=TH(2)+0.00001*DTH
      GO TO 24
   23 TH(2)=TH(1)+0.000001*DTH
      IF(L2) 27,27,28
   28 DO 25 K=1,2
      AS(K)=S*SQRTF((TH(K)/S)**2+BETA**2)
   25 SIGN(K)=TH(K)*COSF(TH(K)*(1.0-1.0/RAT))*SINF(AS(K))
     1-AS(K)*COSF(AS(K))*SINF(TH(K)*(1.0-1.0/RAT))
      IF(SIGN(1)*SIGN(2)) 27,27,26
   26 TH(1)=TH(2)
      TH(2)=TH(2)+0.000001*DTH
      GO TO 28
   27 EGV(I)=TH(1)/S
      THO=TH(1)+DTH
  100 CONTINUE
      PRINT 750,(EGV(JJ),JJ=1,M1)
  750 FORMAT(4F18.10)
      END
```

EXPLANATION OF INPUT QUANTITIES

- M1 = NUMBER OF EIGENVALUES TO BE COMPUTED
- L1,L2 = ITERATION DELETION OPTION
  - IF (L1,L2) POSITIVE, CONTINUE ITERATION
  - IF (L1,L2) NEGATIVE OR ZERO, DELETE ITERATION
- THO = INITIAL VALUE OF THETA
- DTH = INCREMENT OF THETA

```
      LINEARIZED SHEAR FLOW   COSINE-UNIFORM PROFILE   DELTA CLO / CLO

      DIMENSION EGV(100),A(100),C1(100),C2(100),C3(100),C4(100)
      READ 2, LDATA
      DO 100 LL=1,LDATA
      READ 2,M,N0,N1
    2 FORMAT(3I10)
      READ 1,(EGV(JJ),JJ=1,M)
    1 FORMAT(4F18.10)
      READ 3,B,S,T,C,D
    3 FORMAT(5F14.7)
      PRINT 1,(EGV(JJ),JJ=1,M)
      PRINT 2,M,N0,N1
      PRINT 3,B,S,T,C,D
      DO 4 I=1,M
      A(I)=SQRTF((EGV(I)**2)+B**2)
      C1(I)=B*((B**2)/A(I)-A(I))*(COSF(B*S)*(SINF((A(I)-B)*S)/(A(I)-B)-
     1SINF((A(I)+B)*S)/(A(I)+B))-SINF(B*S)*((1.0-COSF((A(I)-B)*S))/(A(I)
     2-B)+(1.0-COSF((A(I)+B)*S))/(A(I)+B)))
      C2(I)=(((B**2)/A(I)-A(I))**2)*(S/2.0-SINF(2.0*S*A(I))/(4.0*A(I)))*
     1((SINF(EGV(I)*(S-T)))**2)
      C3(I)=-((EGV(I)**3)/(2.0*(A(I)**2)))*((SINF(A(I)*S))**2)*(EGV(I)*
     1(S-T)-SINF(2.0*EGV(I)*(S-T))/2.0)
    4 C4(I)=1.0+1.0/(3.141593*C/4.0*EGV(I)*TANHF(EGV(I)*D))
      AA=N0
      N01=N0+1
      DELY0=S/AA
      Y=0.0
      DO 5 K=1,N01
      SUMY=0.0
      DO 6 L=1,M
    6 SUMY=SUMY+(C1(L)/((C2(L)+C3(L))*C4(L)))*(((SINF(EGV(L)*(S-T)))**2
     1)/COSF(B*(Y-S)))*(COSF(A(L)*Y)+B/A(L)*SINF(A(L)*Y)*SINF(B*(Y-S))/
     2COSF(B*(Y-S)))
      PRINT 1,Y,SUMY
    5 Y=Y+DELY0
      BB=N1
      N11=N1+1
      DELY1=(T-S)/BB
      Y=S
      DO 7 K=1,N11
      SUMY=0.0
      DO 8 L=1,M
    8 SUMY=SUMY+(C1(L)/((C2(L)+C3(L))*C4(L)))*EGV(L)/A(L)*SINF(A(L)*S)*
     1SINF(EGV(L)*(S-T))*COSF(EGV(L)*(Y-T))
      PRINT 1,Y,SUMY
    7 Y=Y+DELY1
  100 CONTINUE
      END

      EXPLANATION OF INPUT QUANTITIES
         LDATA = NUMBER OF DATA SETS TO BE PROCESSED
         M = NUMBER OF EIGENVALUES IN INPUT
         N0 = NUMBER OF INCREMENTS OF Y IN REGION (0)
         N1 = NUMBER OF INCREMENTS OF Y IN REGION (1)
```

APPENDIX IV

Design of Honeycomb for Shear Flow Generation

The generation of an artificial shear flow may be accomplished in a number of ways, the most straightforward being the introduction of a disturbance into an otherwise uniform flow. Previous experimenters have used screens[34] and lattices of plates or bars[35] to produce shear profiles. Mair[36] used the wake of a single flat plate to produce a symmetrical shear profile at the center of a uniform flow. The requirements for an artificial shear flow should include the following:

a) steady flow

b) smooth variation of velocity with a minimum of local small scale non-uniformities

c) negligible diffusion of the shear layer through the length of the test section.

The total pressure loss through the device and its effect on the operating characteristics of the wind tunnel and air supply must also be taken into consideration.

For the type of shear flow experiment encountered in this investigation, the use of a honeycomb structure (the type commonly used in aircraft construction) was found to be very satisfactory. The actual material used was 3/16" cell aluminum honeycomb which was supplied by two manufactureres. The use of this material, except for relatively thin sections, eliminates most of the structural and support problems encountered with screens and lattices. The honeycomb may be shaped as desired to provide a wide range of flow geometries, and because of its cellular structure, provides a built-in straightener for the flow if the cells are aligned properly. Because of the uniformity of the disturbance caused by the honeycomb, the structure of the flow downstream is relatively homogeneous compared to that downstream of lattices of plates or bars where local non-uniformities and even separated regions may be found.

The most difficult problem encountered with the use of honeycomb was that of shaping the uncut blocks as supplied by the manufacturer to a predetermined shape to produce the desired shear profile. The recent development of a special band saw blade designed specifically for cutting this type of material greatly simplified the shaping problem. Close-up photographs of the burring of surfaces cut by three different methods are shown in Figure 40 on the following page. The first photograph shows the severe burring as the result of using an ordinary band saw blade. The second and third photographs indicate the improvement obtained through the use of the special honeycomb blade and a newly perfected electrical cutting process respectively. The first and second photographs are of curved surfaces and do not indicate cell distortion. The special saw blade is shown in the fourth photograph. The electrical cutting process, which produces a remarkably smooth cut, is not easily adaptable to the cutting of curved profiles and requires the use of specialized equipment.

Other methods of shaping include machining of the honeycomb before expansion if it is of the expandable type, and machining of block honeycomb which has been filled with low melting point filler material. The most economical and flexible method is that of the use of the special honeycomb band saw blade which yields an acceptable cut with a minimum of effort. Of the two types of honeycomb obtained from manufacturers, that which is fabricated by gluing corrogated sheets together is less satisfactory than the expanded type because of the non-uniform accumulation of glue within the cells. The use of stacked thicknesses of honeycomb sheets to build up a desired profile is not recommended because cell misalignment will result in poor velocity profiles unless local non-uniformities can be allowed to smooth through diffusion.

The calculation of the honeycomb profile to produce a desired shear flow profile was based largely on measured values of the friction coefficient

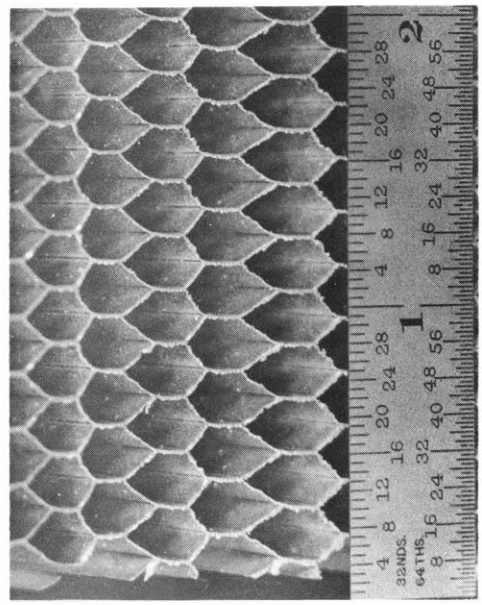

HONEYCOMB BLADE CUT

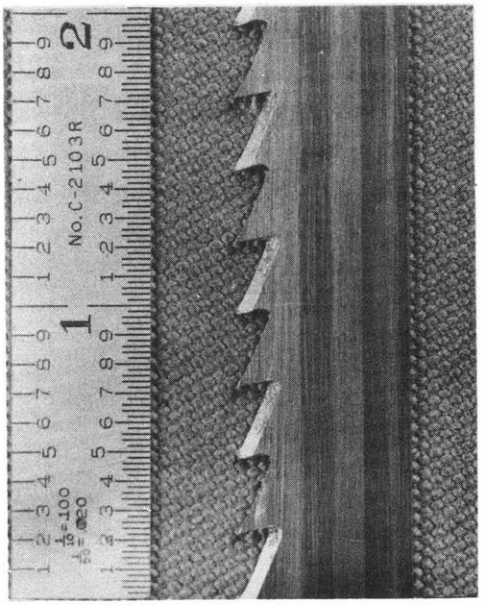

SPECIAL HONEYCOMB BLADE

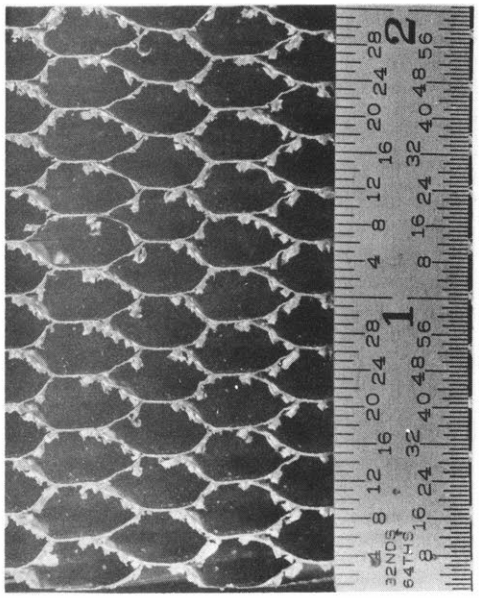

BAND SAW CUT

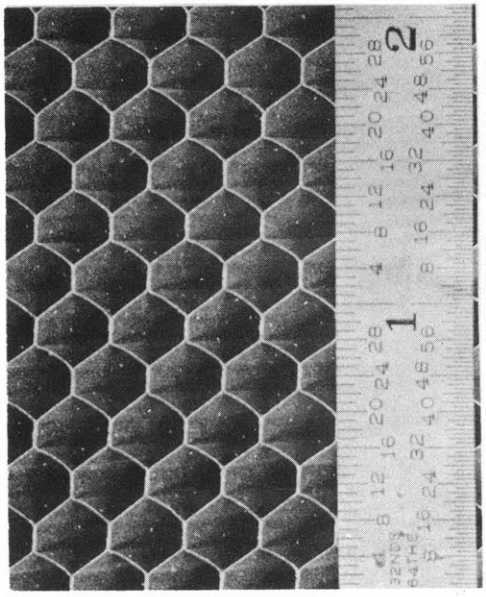

ELECTRICAL CUTTING PROCESS

FIGURE 40 HONEYCOMB CUT SURFACES

defined as follows:

$$4fL / D = \Delta P / \frac{1}{2} \rho U^2$$

The experimental values of friction coefficient for Reynolds numbers in the range of from 6000 to 8000 were f = 0.012 for the glued material and f = 0.008 for the relatively clean expanded material. To simplify the calculation, the flow in the honeycomb cells was assumed to be fully developed, and therefore f was taken as constant for the range of Reynolds numbers considered. In addition to the 'pipe' friction loss, additional losses are encountered at the entrance region of the honeycomb because of the angle of the incident streamlines with respect to the axes of the honeycomb cells. We can estimate this loss as the loss of the component of velocity head normal to the cell axes. Since, in most wind tunnels, a uniform velocity profile is desired at the test section, the flow upstream of the honeycomb, excluding wall boundary layers, may be taken as potential. The two-dimensional flow upstream of the honeycomb may be calculated from potential flow theory with the boundary conditions of undisturbed parallel flow upstream at infinity, a prescribed component of axial velocity at the honeycomb, and the condition of no flow normal to the boundary walls of the channel. The geometry of such a flow is given in the following sketch. We assume that the rotational flow downstream of the honeycomb is parallel and that $\nabla P = 0$.

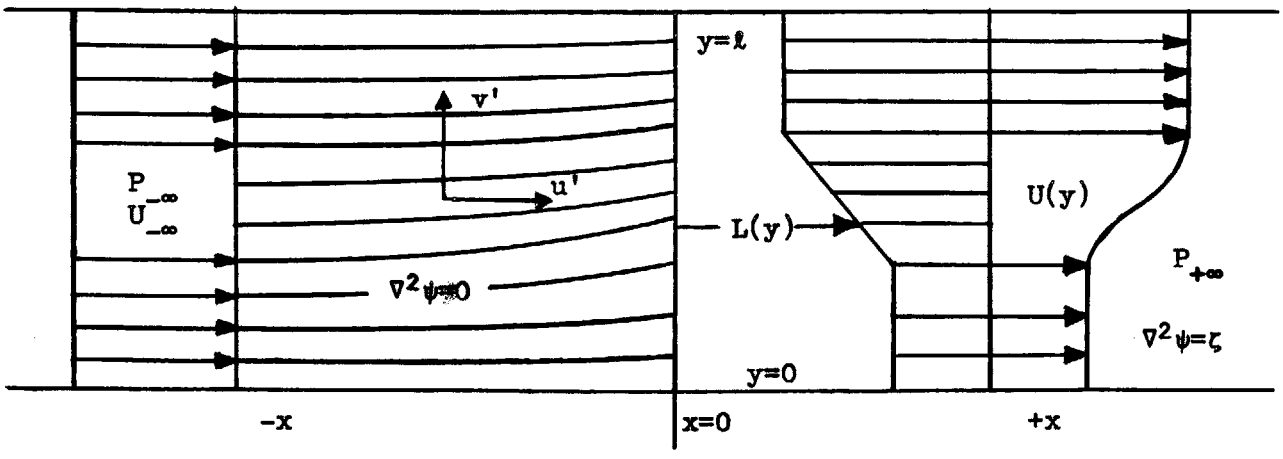

We have, from potential flow theory, $\nabla^2\psi = 0$ where ψ is the familiar two-dimensional stream function.

Also $$u' = \frac{\partial\psi}{\partial y} \qquad v' = -\frac{\partial\psi}{\partial x} \tag{IV-1}$$

We select for $\psi(x, y)$ the solution

$$\psi = c_1 y + (a_1 \sin ky + a_2 \cos ky)(b_1 \exp kx + b_2 \exp -kx)$$

Through consideration of the imposed boundary conditions at the walls $y = 0, \ell$ and at $x = -\infty$ we have the result:

$$\psi(x, y) = U_{-\infty}\, y + \sum_{n=1}^{\infty} a_n \sin \frac{n\pi y}{\ell} \exp \frac{n\pi x}{\ell} \tag{IV-2}$$

At the entrance to the honeycomb ($x = 0$) we have the condition

$$u' = U(y) = \frac{\partial\psi}{\partial y} = U_{-\infty} + \sum_{n=1}^{\infty} a_n \frac{n\pi}{\ell} \cos \frac{n\pi y}{\ell}$$

or

$$\sum_{n=1}^{\infty} a_n \frac{n\pi}{\ell} \cos \frac{n\pi y}{\ell} = U(y) - U_{-\infty} \tag{IV-3a}$$

We then solve equation (IV-3a) through the usual Fourier methods with the result

$$a_n = \frac{2}{n\pi} \int_0^{\ell} \cos \frac{n\pi y}{\ell} \left[U(y) - U_{-\infty} \right] dy \tag{IV-3b}$$

The pressure drop through the honeycomb may be written

$$P(0,y) - P_{+\infty} = \Delta P(y) = \frac{4fL(y)}{D} \frac{1}{2} \rho U^2(y) \tag{IV-4}$$

from the Bernoulli equation in the potential flow region, we have the result:

$$P(0, y) = P_{-\infty} + \frac{1}{2} \rho U_{-\infty}^2 - \frac{1}{2} \rho U^2(y) - \frac{1}{2} \rho v'^2 (0, y) \tag{IV-5}$$

Combining equations (IV-4) and (IV-5)

$$U^2(y) \left[1 + \frac{4fL(y)}{D} + \frac{v'^2(y)}{U^2(y)} \right]_{x=0} = \text{constant} \tag{IV-6}$$

For a given velocity distribution downstream of the honeycomb ($U(y)$) equations (IV-1) through (IV-3) may be solved for $v'(0, y)$, and the honeycomb thickness $L(y)$ may be obtained from (IV-6).

It is of interest to determine the angle of incidence at the entrance to the honeycomb

$$\theta = \tan^{-1} (v'/u') \tag{IV-7}$$

To illustrate the order of the incidence effect consider the shear velocity profile

$$U(y) = U_{-\infty} - \frac{U_{-\infty}}{3} \cos \frac{\pi y}{\ell}$$

For this velocity profile, we have the result

$$\frac{v'}{u'} = \tan \theta = \frac{\sin \frac{\pi y}{\ell}}{3 - \cos \frac{\pi y}{\ell}}$$

The maximum value of v'/u' is approximately 0.35 with a corresponding θ of about 19°. If we consider the relative magnitudes of the friction and incidence terms from equation (IV-6), for the geometries considered in this investigation, the incidence term is of the order of 10% of the friction term. This is, of course, dependent on the particular flow geometry selected.

The above analysis could be refined further to include an incidence loss coefficient (assumed here to be 1) which could be related to the angle of incidence θ and variable friction factor $f = f(y)$ for $L/D < 20$[37]. The incidence effects should be taken into account, at least in this approximate manner, if the cut surface of the honeycomb is clean and uniform, but for relatively rough and burred surfaces, non-uniformities resulting from the poor surface condition may outweigh the incidence effects.

APPENDIX V

Note on the Solution of Certain Sturm-Liouville Equations

From the results of Section 3.3, differential equations of the form

$$F'' + F\left[\lambda^2 + \frac{U''}{U} - 2\left(\frac{U'}{U}\right)^2\right] = 0 \qquad \text{(V-1)}$$

and

$$Y'' - 2\frac{U'}{U}Y' + \lambda^2 Y = 0 \qquad \text{(V-2)}$$

may be reduced to the higher order equation

$$\left(\frac{\psi}{U}\right)'' + \left(\frac{\psi}{U}\right)\left[\lambda^2 - \frac{U''}{U}\right] = 0 \qquad \text{(V-3)}$$

by the substitution

$$\psi = Y' = (FU)' \qquad \text{(V-4)}$$

The corresponding solutions of (V-1) and (V-2) when $U''/U = \beta^2$ are the following (taking y as the independent variable)

$$F(y) = \frac{C_1 \int U \sin \sigma y \, dy}{U} + \frac{C_2 \int U \cos \sigma y \, dy}{U} \qquad \text{(V-5)}$$

and

$$Y(y) = C_1 \int U \sin \sigma y \, dy + C_2 \int U \cos \sigma y \, dy \qquad \text{(V-6)}$$

where $\sigma = \sqrt{\lambda^2 - \beta^2}$

For example, particular forms of equation (V-1) that may be solved by this method are the following:

for $U = a + b y$

$$F'' + F\left[\lambda^2 - 2b^2/(a + b y)^2\right] = 0$$

for $U = \cosh \beta(y - h)$

$$F'' + F\left[\lambda^2 + \beta^2(1 - 2 \tanh^2 \beta(y - h))\right] = 0$$

for $U = \cos \beta(y - h)$

$$F'' + F\left[\lambda^2 - \beta^2(1 + 2 \tan^2 \beta(y - h))\right] = 0$$

To the above, the corresponding forms of equation (V-1) for $U = \sinh\beta(y-h)$ and $U = \sin\beta(y-h)$ may be added.

APPENDIX VI

Photographs

Figures 41 through 48

SMOKE FLOW APPARATUS

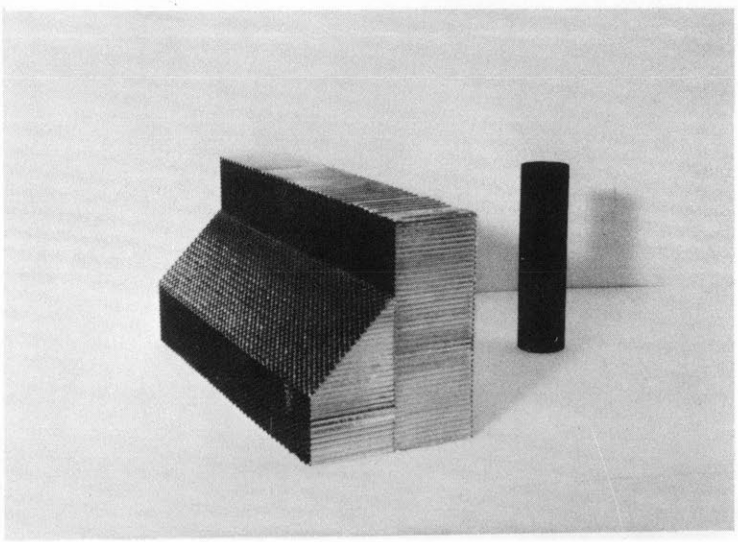

HONEYCOMB AND CYLINDER

FIGURE 41 SMOKE FLOW
EXPERIMENTAL EQUIPMENT

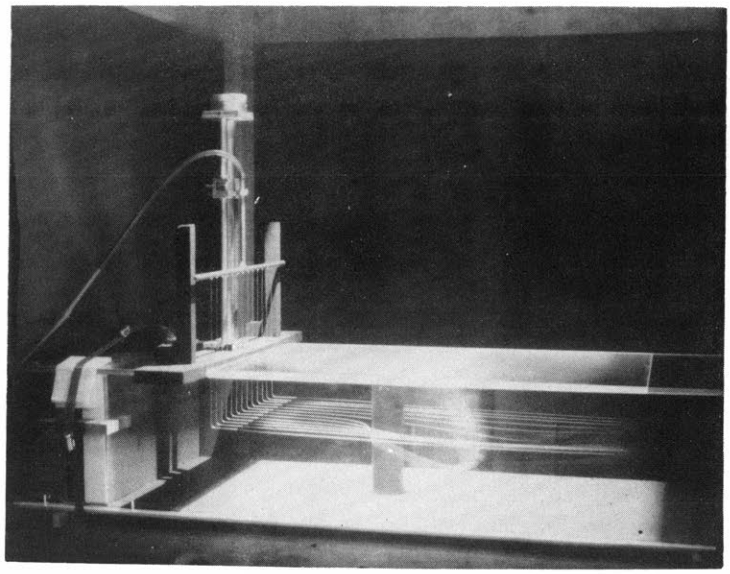

HORIZONTAL SMOKE RAKE

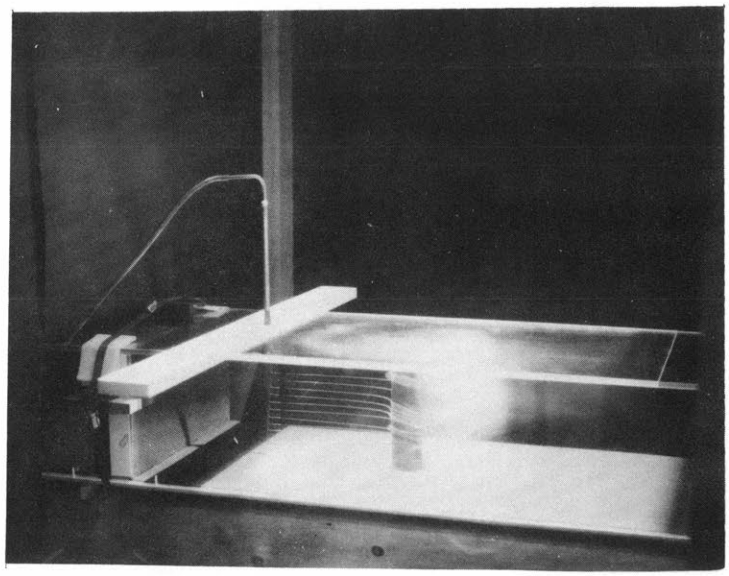

VERTICAL SMOKE RAKE

FIGURE 42 SMOKE FLOW
TEST SECTION

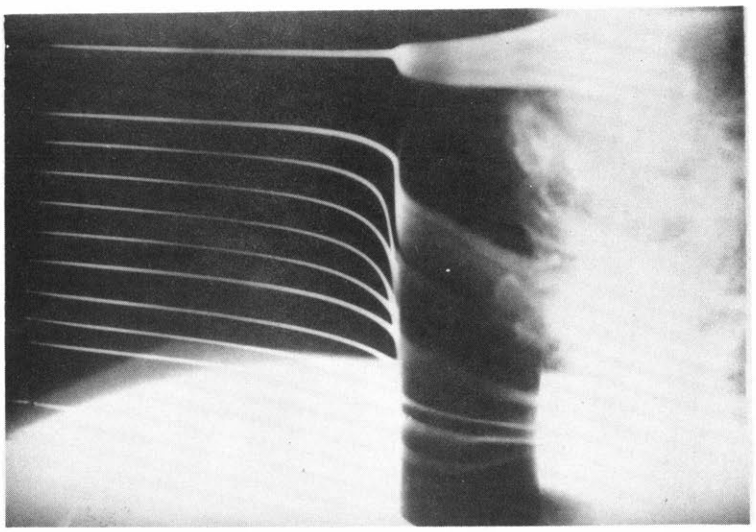

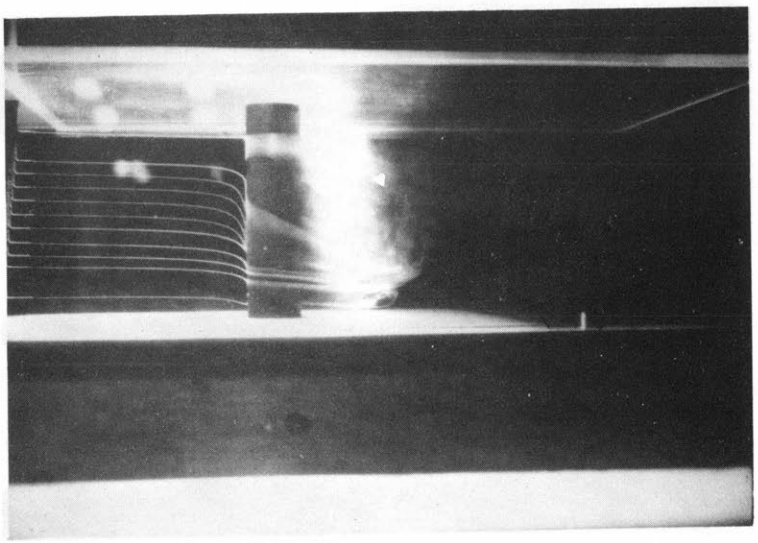

FIGURE 43 SMOKE FLOW VERTICAL
RAKE CLOSE - UPS

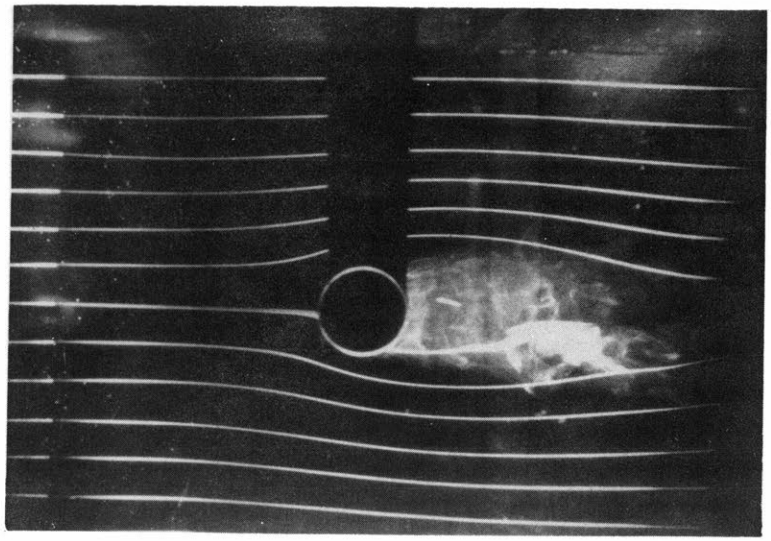

HIGH VELOCITY REGION

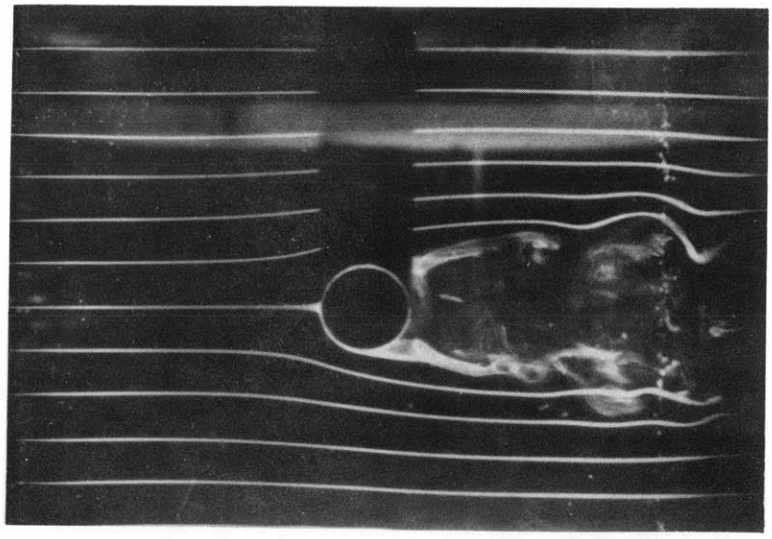

LOW VELOCITY REGION

FIGURE 44 SMOKE FLOW HORIZONTAL RAKE CLOSE-UPS

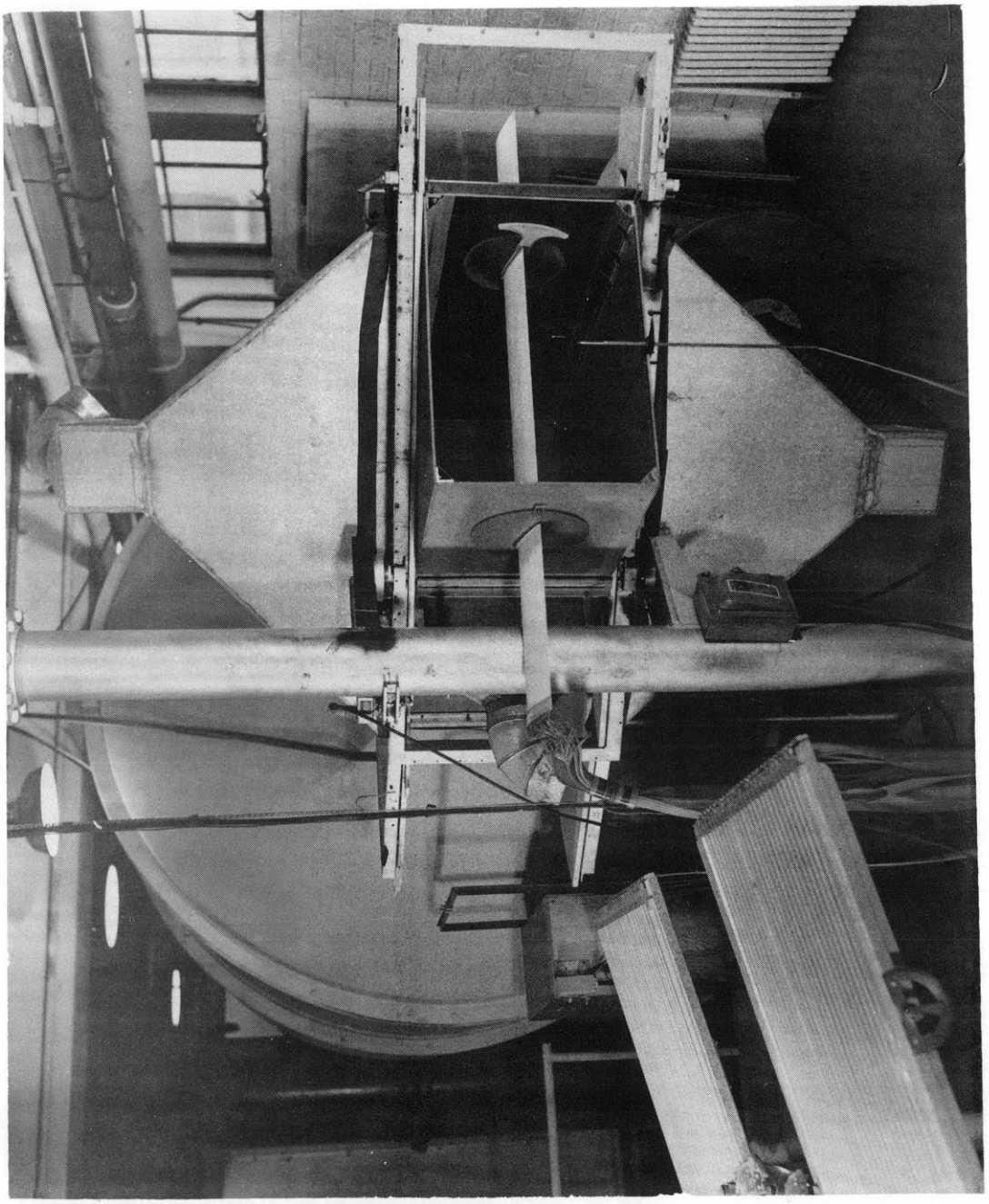

SHEAR FLOW EXPERIMENTAL APPARATUS

FIGURE 45

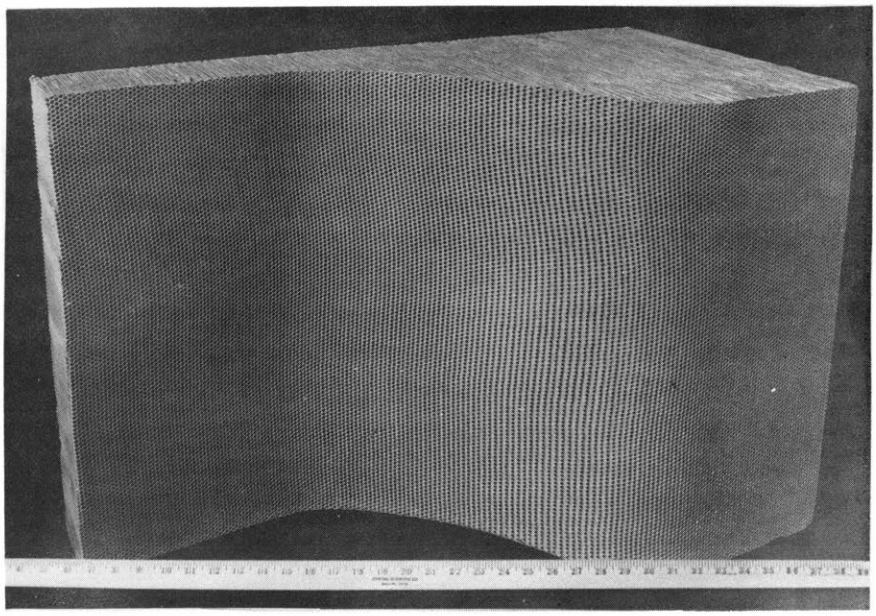

LARGE SHEAR LAYER

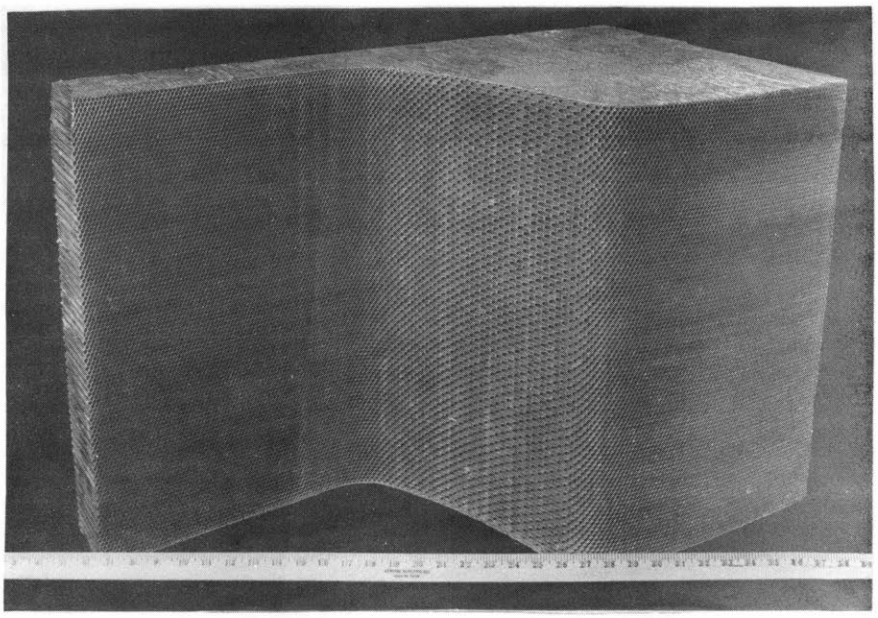

SMALL SHEAR LAYER

FIGURE 46 HONEYCOMBS FOR SHEAR FLOW GENERATION

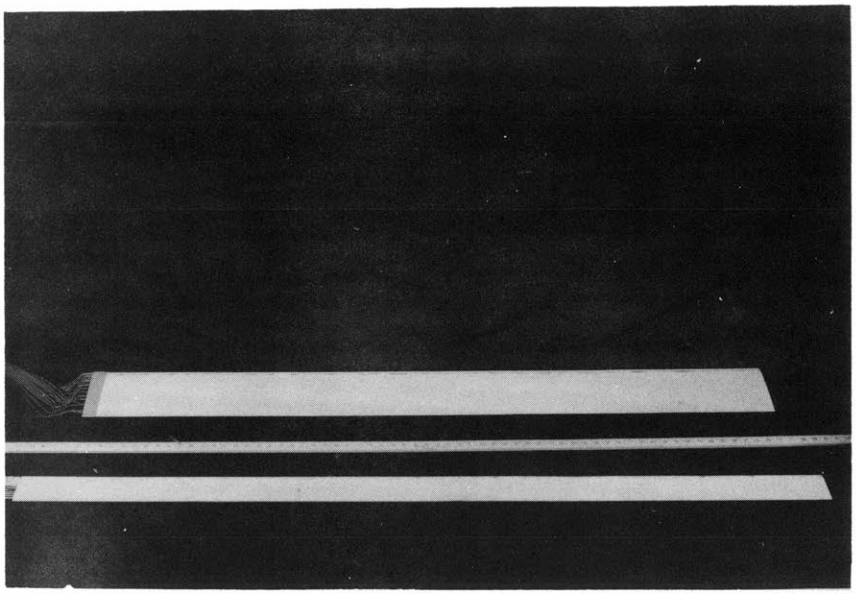

AIRFOILS

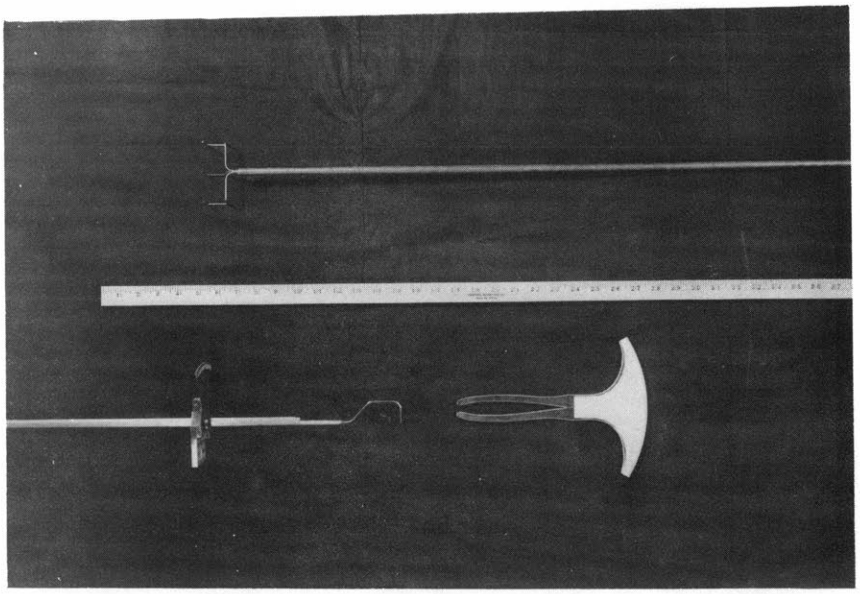

PROBES

FIGURE 47

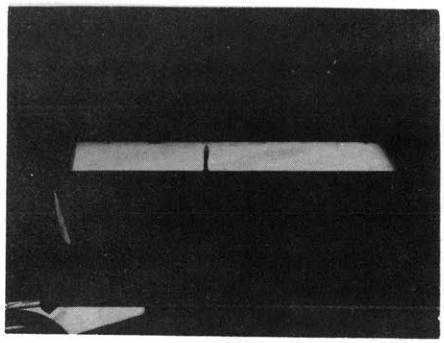

19" FROM WALL

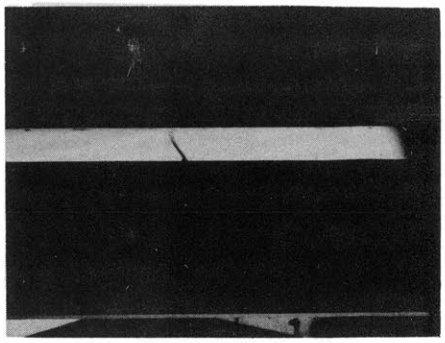

17" FROM WALL

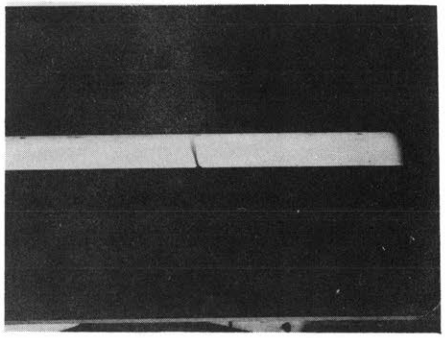

15" FROM WALL

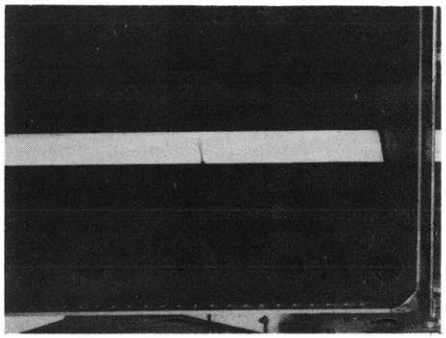

13" FROM WALL

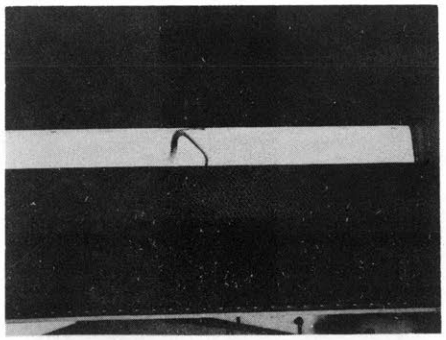

BACK FLOW REGION

FIGURE 48 OIL TRACES ON 3 IN. CHORD AIRFOIL